RICE UNIVERSITY

Wave function theories for finite-temperature electronic structure

By

Gaurav Harsha

A THESIS SUBMITTED
IN PARTIAL FULFILLMENT OF THE
REQUIREMENTS FOR THE DEGREE

Doctor of Philosophy

APPROVED, THESIS COMMITTEE

Gustavo Scuseria
Gustavo Scuseria (Oct 19, 2021 08:07 CDT)

Gustavo E. Scuseria
Robert A. Welch Professor of Chemistry,
Professor of Physics and Astronomy, and
Professor of Materials Science and Nano Engineering

Andriy Nevidomskyy
Associate Professor of Physics and
Astronomy

Anatoly Kolomeisky (Oct 19, 2021 07:21 CDT)

Anatoly Kolomeisky
Professor of Chemistry,
Professor of Chemical and Biomolecular
Engineering, and
Center for Theoretical Biological Physics

HOUSTON, TEXAS

October 2021

RICE UNIVERSITY

Wave function theories for finite-temperature electronic structure

by

Gaurav Harsha

A Thesis Submitted
in Partial Fulfillment of the
Requirements for the Degree

Doctor of Philosophy

Approved, Thesis Committee:

Gustavo E. Scuseria, Chair
Robert A. Welch Professor of Chemistry,
Professor of Physics and Astronomy, and
Professor of Materials Science and Nano Engineering

Andriy Nevidomskyy
Associate Professor of Physics and Astronomy

Anatoly Kolomeisky
Professor of Chemistry,
Department of Chemical and Biomolecular Engineering, and
Center for Theoretical Biogical Physics

Houston, Texas

October, 2021

ABSTRACT

Wave function theories for finite-temperature electronic structure

by

Gaurav Harsha

Wave function methods have offered a robust, systematically improvable means to study the ground-state properties in quantum many-body systems. Theories like coupled cluster and their derivatives provide highly accurate approximations to the energy landscape at a reasonable computational cost. Analogs of such methods to study thermal properties, though highly desirable, have been lacking because evaluating thermal properties involve a trace over the entire Hilbert space. Approximating every state in the Hilbert space is an impossible task. Besides, excited-state theories are not as well studied as ground-state ones.

In this thesis, we overcome these difficulties by employing thermofield dynamics, a theory that allows the purification of the ensemble density matrix and constructs a pure wave function that encodes the equilibrium thermal behavior of the system. Ensemble averages become expectation values over this so-called thermal state. Around this thermal state, we develop a framework to extend ground-state wave function theories to non-zero temperatures.

We discuss explicit formulations of mean-field, configuration interaction, and coupled cluster theories for thermal properties of fermions in the grand canonical ensemble. For fermions in the canonical ensemble, we present mean-field, configuration interaction, and perturbation theories. We also discuss thermal mean-field, configu-

ration interaction, and coupled cluster formalisms for SU(2) systems.

To assess the quality of these approximations, we study both model and small atomic and molecular as benchmark electronic problems while comparing against exact results. For spins, we use the Lipkin-Meshkov-Glick and the one-dimensional transverse field Ising models as our reference systems. Indeed, the thermal methods perform reasonably well while merely adding a prefactor to the computational cost. They also inherit all the properties, good or bad, from their ground-state counterparts, signifying the robustness of our formalism.

Acknowledgments

First and foremost, I would like to thank my mentor and supervisor, Professor Gustavo E. Scuseria. He showed a tremendous amount of confidence and belief in me, even in my first year as a graduate student, which allowed me to enjoy the scientific process without worrying about the end result. His enthusiasm towards science has been a source of inspiration.

Along with Gus, my colleagues and fellow group members have always been considerate and helpful. I am indebted to the support extended by Dr. Thomas M. Henderson for sharing his expertise in science, coding, and academic writing through numerous discussions. I am also thankful to Drs. Yiheng Qiu and Jin-Mo Zhao for their assistance with *drudge*, the computer algebra system which has been indispensable in my research. Discussions with Rishab Dutta, Ruiheng Song, Armin Khamoshi, and Dr. Guo Chen have also helped me grow as a researcher.

Despite being thousands of miles away in India, my family and my parents, to whom I dedicate this thesis, have been a constant source of inspiration and driving force that pushes me to keep improving at everything in life. Without their support, I cannot imagine even starting my Ph.D., let alone complete it.

During my life as a graduate student, I faced many hurdles, in research or otherwise, most of which I overcame triumphantly. But I was able to do so only with the help and support of my mentors, colleagues, family, and friends. While the complete list of people to whom I am thankful is far too long to give here, my supportive friends and the GSA Soccer Club deserve a special mention for providing a vibrant life outside the office.

Dedicated to my caring parents.

Contents

Illustrations

Chapter 1

Introduction

New materials with exotic properties have fuelled the technological revolution that we have experienced since the early twentieth century. The evolution of desktop computers alone presents us with numerous examples: magnetic and optical hard-drives got replaced by spintronic technology as computer memory, which, in turn, has been upgraded to the state-of-the-art solid-state technology; display devices have similarly evolved from bulky cathode-ray screens and liquid crystal displays to light-emitting-diode technology. What is astonishing is that all of these developments happened within thirty years. The development of photovoltaic materials, graphene, and superconductors, all of which find themselves in a wide range of applications, are other examples of significant breakthroughs. On the other hand, the synthesis of new chemical compounds and reaction pathways has similarly impacted almost every aspect of human lives. It is difficult to imagine a sustainable modern world without efficient drug discovery, polymers and plastic devices for day-to-day use, wastewater treatment, fertilizers and pesticides to maintain large agricultural farms, and long-lived batteries for our mobile phones and laptops.

The properties of macroscopic systems can be traced back to the collective behavior of their constituent particles, electrons and nuclei, which are governed by the laws of quantum mechanics and obey the Schrödinger equation. Naturally, the ability to understand any phenomenon from its microscopic quantum origins is essential to explain scientific discoveries, as well as to design new materials and molecules with

desired properties. While the principles of quantum mechanics were discovered and perfected nearly 90 years ago, their application to realistic, large systems of interacting electrons remains a challenge. In fact, in 1929, Paul A. M. Dirac [1] stated that

> *The fundamental laws necessary for the mathematical treatment of a large part of physics and the whole of chemistry are thus completely known, and the difficulty lies only in the fact that application of these laws leads to equations that are too complex to be solved.*

The Schrödinger equation is formally complete, i.e. one can, in principle, obtain the wave function ψ, the most fundamental quantity in quantum mechanics, by solving the time-dependent Schrödinger equation (TDSE)

$$i\hbar\frac{\partial\psi}{\partial t} = H\psi, \tag{1.1}$$

or its stationary state formulation, the time-independent Schrödinger equation (TISE),

$$H\psi = E\psi. \tag{1.2}$$

The TISE is, in fact, a linear eigenvalue problem where the wave function ψ is the eigenfunction of the Hamiltonian matrix H and the energy E is the corresponding eigenvalue. Once we obtain the complete set of eigenstates ψ_n along with their corresponding energies E_n, we can compute everything there is to know about the quantum system. What makes the real-world application of quantum mechanics challenging is that the dimensionality of the Hilbert space in which ψ resides, and therefore the computational resources required to solve Eq. 1.2, grows exponentially with the number of particles. And the number of electrons in a typical application is enormous, ranging from a few dozens in small molecules to Avogadro number of electrons in

materials. Even with the largest supercomputers, we can find the exact ground state wave function for only tens of electrons. This is known as the *many-body problem* in computational quantum physics and chemistry.

While an exact solution is still out of reach for most applications, computers have certainly revolutionized the field of quantum chemistry in the pursuit of approximate, computationally feasible solutions to the Schrödinger equation for real systems. A wide variety of such approximate methods, deterministic and stochastic, have been proposed to obtain an approximation to the grounds-state of many-electron systems, e.g. Hartree-Fock, [2–4] density functional theory, [5, 6] perturbation theory, [7] configuration interaction (CI), coupled cluster (CC), [8, 9] quantum Monte Carlo (QMC), [10–15], density matrix renormalization group (DMRG), [16, 17] embedding theories, [18–21] etc. Application of artificial neural networks towards this problem has also gathered significant interest in recent years. [22,23] Generalization of many of these ground state theories to excited states have also been explored. [24–26]

1.1 Problems at finite temperature

For many conventional chemical systems (such as organic molecules) as well as insulating solids, the energy gap between the electronic ground state and the first excited state, also known as the optical gap, is of the order of a few electron volts, which is equivalent to thousands of kelvins in temperature scale. Therefore, for most applications at room temperature ($T = 300K$), the properties are purely governed by the ground state and it is not necessary to compute and study thermal corrections to ground-state properties.

There are many other systems where the optical gap is very small ($\sim 1meV$), e.g. transition metal complexes, strongly-correlated systems including high-Tc supercon-

ductors, [27] ultracold chemistry, [28,29] etc., and there are even more problems where quantum systems are studied at very high temperatures ($\sim 1000K$) such as geochemical processes in the cores of planets. [30] In these problems, we can no longer make do with a few electronic states and must evaluate properties as thermal averages weighted over an appropriate ensemble of states. For a system in thermal equilibrium at inverse temperature β, the ensemble of choice is generally canonical or grand canonical and the expectation value of an observable A is defined as

$$\langle A \rangle_\beta = \frac{1}{\mathcal{Z}} \mathrm{Tr}(A\rho), \tag{1.3}$$

where ρ is the thermal density matrix, and $\mathcal{Z}$ is the partition function, which are defined as

$$\rho = e^{-\beta H}, \quad \mathcal{Z} = \mathrm{Tr}(\rho). \tag{1.4}$$

For grand-canonical ensemble, the Hamiltonian H is defined to include the chemical potential term, i.e., $H \to H - \mu N$, which acts as a Lagrange multiplier to fix the desired number of particles.

Determining ρ and $\mathcal{Z}$ exactly requires information about the entire spectrum of the Hamiltonian, which, as we have already noted, is far from feasible. The many-body problem at finite temperatures is far more severe than the ground state because the sheer number of states in the spectrum of the Hamiltonian is enormous. Besides, there are fewer accurate excited-state theories than ground-state. Therefore, just as for zero temperature, approximate methods to study thermal properties are required. Several methods have been proposed to address study quantum systems at finite temperatures, e.g., thermal Hartree-Fock, [31,32] perturbation theories, [33–36] path integral and Green's function methods, [37] finite-temperature QMC, [38–47] extensions of DMRG, [48–53] and the recently explored thermal generalizations of

coupled cluster. [54–62]

1.2 Motivation for this work

Of the finite-temperature methods mentioned above, only a few work directly with wave functions, e.g., Ancilla DMRG, [48, 49] finite-temperature perturbation theories, [34, 63] and finite-temperature CC theories. [54–62] Wave function theories are popular for ground-state properties, particularly in finite-sized systems, as they have undergone significant development for over half a century and offer controllable features that make their thermal generalizations highly desirable. Constructing thermal methods is, however, challenging because

1. the thermal density matrix ρ is an ensemble density matrix, and it cannot be represented using a single wave function,

2. computing approximations to every single ground and excited state is an impossible task as the number of states in the Hilbert space grows exponentially with the system size.

In this work, we develop a wave function framework to study the thermal behavior of quantum mechanical systems by leveraging the principles of thermofield dynamics (TFD), [64–67] This wave function framework provides a recipe to generalize any ground-state wave function method to finite temperatures. We have developed a thermal version of coupled cluster and configuration interaction theories that allow us to study both canonical and grand-canonical ensemble properties in correlated fermionic systems. We have also worked out a similar framework for SU(2) systems. These results are reported in the following articles:

1. G. Harsha, T. M. Henderson, and G. E. Scuseria, "Thermofield theory for finite-temperature quantum chemistry," *J. Chem. Phys.*, vol. 150, p. 154109, Apr. 2019,

2. G. Harsha, T. M. Henderson, and G. E. Scuseria, "Thermofield theory for finite-temperature coupled cluster," *J. Chem. Theory Comput.*, vol. 15, pp. 6127–6136, Nov. 2019,

3. G. Harsha, T. M. Henderson, and G. E. Scuseria, "Wave function methods for canonical ensemble thermal averages in correlated many-fermion systems," *J. Chem. Phys.*, vol. 153, p. 124115, Sept. 2020,

4. G. Harsha, Y. Xu, T. M. Henderson, and G. E. Scuseria, "Thermal coupled cluster theory for SU(2) systems," *arXiv:2107.07922 [cond-mat, physics:physics]*, July 2021.

1.3 Outline

The purpose of this thesis is to report a detailed derivation, discussion, and application of the aforementioned thermal wave function theories. In Chapter 2, we introduce the theoretical background upon which our thermal methods are constructed, namely, the general many-body Hamiltonian for *ab-initio* and model electronic systems, ground-state wave function theories, and thermofield dynamics. Chapter 3 presents the thermal wave function framework in the grand-canonical ensemble and the derivation of thermal CI and CC theories within this framework. Benchmark applications for thermal CI and CC are also presented in Chapter 3. We then turn our attention to wave function theories for the canonical ensemble in Chapter 4, and

SU(2) systems in Chapter 5. Finally, we make concluding remarks in Chapter 6 and comment on the future prospects of our work.

Chapter 2

Theoretical Background

If I have seen further, it is by standing on the shoulders of Giants

-Sir Issac Newton

This quote by Sir Issac Newton beautifully sums up modern-day research. New theoretical and experimental developments rely on years of research and established results. This work is no exception; we use various concepts from quantum chemistry, quantum field theory, statistical mechanics, etc., and construct a framework for finite-temperature wave function theories. In this chapter, we provide a brief introduction to some of the elementary concepts that will both aid the understanding and provide a foundation for the subsequent chapters. We start with a brief description of the general *ab-initio* electronic Hamiltonian and how it can be used to derive various model Hamiltonians, both of which we use as benchmark problems to assess the performance of new theories. We follow this with an introduction to conventional ground-state wave function methods, namely Hartree-Fock, configuration interaction, and coupled cluster whose finite-temperature equivalents constitute the key findings reported here. Finally, we also introduce thermofield dynamics, the theory central to the thermal wave function framework reported in this thesis.

2.1 *Ab-initio* Hamiltonian

The Hamiltonian is the fundamental object that describes a quantum mechanical system. Before we dive into ways to efficiently solve the Schrödinger equation for atoms and molecules, it is necessary to construct an accurate Hamiltonian for the system with minimal approximations. In the first quantization, working with atomic units, the Hamiltonian for a non-relativistic system of electrons and nuclei is defined as

$$H = -\sum_{A} \frac{1}{2M_A}\nabla_A^2 - \sum_{i} \frac{1}{2}\nabla_i^2 + \sum_{A<B} \frac{Z_A Z_B}{r_{AB}} - \sum_{Ai} \frac{Z_A}{r_{iA}} + \sum_{i<j} \frac{1}{r_{ij}}, \tag{2.1}$$

where the uppercase indices A, B label the atomic nuclei and the lowercase indices i, j label the electrons. The symbols Z_A and M_A denote the charge and mass of the A^{th} nucleus, while r_{ij}, r_{AB} and r_{iA} denote the distance between the labelled entities.

The mass of an atomic nucleus is three orders of magnitude larger than that of an electron. Therefore, for most applications, where we are interested in the electronic properties of the system, we can use the Born-Oppenheimer approximation, i.e., the atomic nuclei can be considered stationary, classical objects. After invoking this approximation, the full *ab-initio* Hamiltonian reduces to the general electronic Hamiltonian

$$H_{el} = E_{nn} - \sum_{i} \frac{1}{2}\nabla_i^2 - \sum_{Ai} \frac{Z_A}{r_{iA}} + \sum_{i<j} \frac{1}{r_{ij}}, \tag{2.2}$$

where E_{nn} is the classical nuclear repulsion energy. By introducing an appropriate basis set of single-electron wave functions $\{\phi_\mu(\vec{r})\}$, such as atomic or molecular orbitals, the Hamiltonian H_{el} can be transformed into its second quantized form,

$$H_{el} = E_{nn} + \sum_{pq} h_{pq} c_p^\dagger c_q + \frac{1}{4}\sum_{pqrs} v_{pqrs} c_p^\dagger c_q^\dagger c_s c_r. \tag{2.3}$$

Here, the matrix elements h_{pq} and v_{pqrs} are defined as

$$h_{pq} = \langle p|\hat{h}|q\rangle = \int d\vec{r}\,\phi_p^*(\vec{r})\left(-\frac{1}{2}\nabla^2 - \sum_A \frac{Z_A}{r_A}\right)\phi_q(\vec{r}), \tag{2.4a}$$

$$v_{pqrs} = \langle pq|\hat{v}|rs\rangle - \langle qp|\hat{v}|rs\rangle\,, \tag{2.4b}$$

$$\langle pq|\hat{v}|rs\rangle = \int\int d\vec{r}_1 d\vec{r}_2\,\phi_p^*(\vec{r}_1)\phi_q^*(\vec{r}_2)\left(\frac{1}{r_{12}}\right)\phi_r(\vec{r}_1)\phi_s(\vec{r}_2), \tag{2.4c}$$

and are also known as one- and two-body interaction terms, or one- and two-electron integrals. By definition, the two-electron integrals have a four-fold anti-symmetry,

$$v_{pqrs} = -v_{qprs} = -v_{pqsr} = v_{qpsr}. \tag{2.5}$$

In addition, the one-electron basis functions $\{\phi_p\}$ can be chosen to be real, and in doing so, we can introduce an extra symmetry in the two-electron integrals, $v_{pqrs} = v_{rspq}$. The operators c_p ($c_p^\dagger$) annihilate (create) an electron in the p^{th} orbital (or basis function). For an orthonormal set of single-electron states $\{\phi_p\}$, the fermion operators obey canonical the following anti-commutation relation:

$$[c_p, c_q^\dagger]_- = c_p c_q^\dagger + c_q^\dagger c_p = \delta_{pq}, \tag{2.6a}$$

$$[c_p, c_q]_- = c_p c_q + c_q c_p = 0, \tag{2.6b}$$

$$[c_p^\dagger, c_q^\dagger]_- = c_p^\dagger c_q^\dagger + c_q c_p^\dagger = 0, \tag{2.6c}$$

where $[A, B]_-$ gives the anti-commutator of the operators A and B. We will work with orthonormal single-particle states for the remainder of this thesis. The indices p, q, r, s label the spin-orbitals here, but we can use them for other labels such as spin-orbitals (composite orbital and spin index), lattice sites, etc.

2.1.1 Symmetries

Symmetries are transformations through which the system (and, therefore, its Hamiltonian) remains invariant. Mathematically, these are quantum mechanical operators

that commute with the Hamiltonian, i.e.

$$[H, \mathcal{O}_{\text{symm.}}] = H\mathcal{O}_{\text{symm.}} - \mathcal{O}_{\text{symm.}}H = 0, \tag{2.7}$$

where $\mathcal{O}_{\text{symm.}}$ is the generator of symmetry transformation, and $[A, B]$ defines the commutator of operators A and B. Since mutually commuting operators can be diagonalized simultaneously, the wave functions for the eigenstates of the Hamiltonian should also be constructed as symmetry eigenfunctions. The Hamiltonian and the symmetry operator $\mathcal{O}_{\text{symm.}}$ can be diagonalized simultaneously. These ideas can be extended to the maximal set of mutually commuting symmetry operators, which form a mathematical *group*, also known as a symmetry group. Eigenvalues of the symmetry group operators are generally called quantum numbers and can be used to label the eigenstates of the Hamiltonian.

Physical systems generally have several symmetries. For example, the kinetic and Coulomb operators in the general electronic Hamiltonian (Eq. 2.2) depend only on the position of the electrons in the real space, and not on their spins. As a result, the total electronic spin is a symmetry of the Hamiltonian. Mathematically, this means that the quantum mechanical operators, $\mathbf{S}^2_{\text{Total}}$ and S^z_{Total}, along with the Hamiltonian, form a set of mutually commuting operators, i.e.

$$[H, \mathbf{S}^2_{\text{Total}}] = 0 = [H, S^z_{\text{Total}}] = [\mathbf{S}^2_{\text{Total}}, S^z_{\text{Total}}], \tag{2.8}$$

where $\mathbf{S}_{\text{Total}} = \mathbf{S}_1 + \mathbf{S}_2 + \cdots$, and $\mathbf{S}_i = \hat{x}S^x_i + \hat{y}S^y_i + \hat{z}S^z_i$. As a result, the spin quantum numbers $|s, m_s\rangle$ can be used to label the eigenstates. Similarly, lattice structures with periodic boundary conditions (e.g., rings, cylinders, etc.) have discrete translational symmetry, which allows us to label the wave functions using momentum quantum numbers. The list of symmetries varies from one system to another. We will introduce any new relevant symmetry as and when needed.

2.1.2 Model Hamiltonians

Starting with the general description in Eq. 2.3, we can describe any electronic system, with at most two-body interactions, by assigning appropriate definitions to matrix elements h_{pq} and v_{pqrs}. For example, for the Hubbard model [72] on a lattice, we have

$$H_{\text{Hubbard}} = -t \sum_{\langle i,j\rangle,\sigma} (c^\dagger_{i\sigma} c_{j\sigma} + c^\dagger_{j\sigma} c_{i\sigma}) + U \sum_i c^\dagger_{i\uparrow} c^\dagger_{j\downarrow} c_{j\downarrow} c_{i\downarrow}, \tag{2.9}$$

where $\langle i,j\rangle$ means the summation is performed over nearest-neighbor lattice sites i and j, while σ labels the spin of electron. The parameter t quantifies the probability of an electron to hop from one lattice site to a neighboring site, and U quantifies the on-site Coulomb repulsion. By definition, both t and U are positive real. The Hubbard model can explain a wide variety of physics: for weak Coulomb repulsion, i.e. when U/t is small, the ground-state for half-filling (i.e. one electron per site) is metallic, whereas for large U/t, the ground-state is a Mott insulator. As we go away from half-filling, Hubbard model exhibits an even richer variety of physics, particularly useful in understanding high-Tc superconductivity. [73]

We can also define the reduced Bardeen-Cooper-Schaefer (BCS) Hamiltonian [74–76] by modifying Eq. 2.3 into

$$H_{\text{BCS}} = \sum_p \epsilon_p \left(c^\dagger_{p\uparrow} c_{p\uparrow} + c^\dagger_{p\downarrow} c_{p\downarrow} \right) - G \sum_{pq} c^\dagger_{p\uparrow} c^\dagger_{p\downarrow} c_{q\downarrow} c_{q\uparrow}, \tag{2.10}$$

where ϵ_p denotes the energy for an electron to occupy p^{th} level, and G quantifies the amount by which energy is lowered when a pair of electrons in the q^{th} level hops to p^{th} level. The reduced BCS Hamiltonian explains BCS superconductivity for large, positive value of the pair interaction G, and is also useful in describing low-energy nuclear structure.

Model systems such as the Hubbard and reduced-BCS are built heuristically in order to explain specific physical mechanisms. Their ability to capture a wide variety

of physics by tuning a relatively small number of parameters also makes model systems excellent test-beds to benchmark new wave function theories in quantum chemistry. Furthermore, exact analytical solutions are often available for these systems, e.g., the exact energy spectrum for the reduced-BCS model as well as the Hubbard model on a 1D lattice can be obtained exactly using the Bethe ansatz. [77] In the following chapters, we will use these model systems and standard benchmark molecular systems to assess the performance of our thermal wave function theories.

2.2 Ground-state methods

The motivation behind this work, as discussed in Section 1.2, is to leverage ground-state wave function theories, and their years of accumulated advances, to study many-body quantum systems at finite temperatures. Therefore, a discussion about such wave function methods and their salient features is warranted. Here, we provide a brief account of Hartree-Fock, configuration interaction, and coupled cluster theories, some of the most used zero-temperature wave function methods in quantum chemistry.

2.2.1 Hartree-Fock

Hartree-Fock (HF) is one of the simplest ways to approximately solve Eq. 1.2, the ground-state time-independent Schrödinger equation (TISE). The electrons are treated as independent particles in the presence of an effective background potential, which captures the averaged Coulomb interaction due to other electrons. Therefore, HF is also known as the mean-field theory. The wave function is approximated as a single Slater determinant,

$$|\Phi\rangle = a_1^\dagger a_2^\dagger \dots a_N^\dagger |-\rangle \,, \tag{2.11}$$

where $|-\rangle$ is the physical vacuum state with no electrons, N is the number of electrons, and $\{a_p^\dagger\}$ are constructed as linear combinations of the fermion creation operators $\{c_p^\dagger\}$,

$$a_p^\dagger = \sum_q c_q^\dagger \Lambda_{qp}. \tag{2.12}$$

Equation 2.12 describes a transformation of the fermion operators $\{c_p^\dagger\}$, generally from atomic orbitals, to a new basis $\{a_p^\dagger\}$, the molecular orbitals (MO), in which the Slater determinant $|\Phi\rangle$ is built. The HF energy can be calculated as

$$E_{HF}[\Lambda] = \frac{\langle\Phi|H|\Phi\rangle}{\langle\Phi|\Phi\rangle} = E_{nn} + \sum_{pq} h_{pq}\rho_{pq} + \frac{1}{2}\sum_{pqrs} v_{pqrs}\rho_{pr}\rho_{qs}, \tag{2.13}$$

where $\rho_{pq} = \langle\Phi|c_p^\dagger c_q|\Phi\rangle \,/\, \langle\Phi|\Phi\rangle$ is the HF density matrix. The density matrix, and therefore the HF energy, depend on the MO-coefficients Λ_{qp}. The variational principle ensures that the HF energy is an upper bound to the exact ground-state energy and can, therefore, be minimized in order to determine the optimal MO-coefficients.

Symmetry considerations

The molecular orbitals are generally constructed in a way such that the new basis respects the symmetries of the Hamiltonian. In the context of spin-symmetry, this is known as restricted Hartree-Fock (RHF). The RHF MO-coefficients do not depend on the spin, i.e.,

$$a_{p\sigma}^\dagger = \sum_q c_{q\sigma}^\dagger \Lambda_{qp}. \tag{2.14}$$

For weak correlation, i.e., when the two-body interaction is small as compared to the one-body part of the Hamiltonian, RHF provides a qualitatively accurate result, which can then be used as a starting point to add correlation effects via, for instance, CI or CC. On the other hand, in the presence of strong correlation, i.e., when the Coulomb repulsion becomes dominant, e.g., for large values of U/t in Hubbard,

symmetry-adapted HF provides a very bad approximation to the true ground-state. However, we can get energetically better results by admitting lower symmetry in the wave function than the system, usually known as symmetry breaking. For instance, allowing different MO-coefficients for alpha (up) and beta (down) spins breaks the S^2-symmetry, i.e. a Slater determinant constructed out of $\{a^\dagger_{p\sigma}\}$ that are defined as

$$a^\dagger_{p\sigma} = \sum_q c^\dagger_{q\sigma} \Lambda_{qp,\sigma}, \tag{2.15}$$

is no longer an eigenstate of the $\mathbf{S}^2_{\text{Total}}$ operator. This is known as the unrestricted Hartree-Fock (UHF). Additionally, we can also relax the S^z_{Total} symmetry and build the MO's by mixing the alpha and beta orbitals, i.e.,

$$a^\dagger_{p} = \sum_{q,\sigma} c^\dagger_{q\sigma} \Lambda_{q\sigma,p}. \tag{2.16}$$

This is known as generalized Hartree-Fock (GHF). It is clear from Eqs. 2.15 and 2.16 that UHF increases the dimensionality of the variational parameter space, and GHF even more so, and provide potentially better approximations to the ground-state energy than RHF, albeit at the loss of symmetries.

The ideas of symmetry breaking can be generalized to any other symmetry of interest. For example, electron number symmetry can be broken artificially to obtain an energetically better mean-field wave function, the BCS state, in the large G regime of the reduced-BCS Hamiltonian. The BCS state is defined as,

$$|BCS\rangle = \bigotimes_p \left(u_p + v_p c^\dagger_{p\uparrow} c^\dagger_{p\downarrow}\right) |-\rangle\,, \tag{2.17}$$

where u_p and v_p are complex numbers that parameterize the mean-field state, with $|u_p|^2 + |v_p|^2 = 1$. For the remainder of this thesis, we will consider symmetry breaking as an option in any wave function ansatz, and not concern ourselves too much with the associated benefits or consequences.

2.2.2 Configuration Interaction

Mean-field theory or HF generally provides a good qualitative description of the underlying physical phenomena but is insufficient in making accurate quantitative predictions of physical properties. This is because of the averaged consideration of electron-electron interactions. Correlated wave function ansätze overcome this problem and provide a better treatment of the Coulomb interaction.

Configuration interaction (CI) is a correlated theory in which, starting with HF, the wave function is expanded as a linear combination of all possible linearly independent Slater determinants,

$$|\Psi_{CI}\rangle = |\Phi\rangle + \sum_{ia} C_i^a \, |\Phi_i^a\rangle + \frac{1}{(2!)^2} \sum_{ijab} C_{ij}^{ab} \, |\Phi_{ij}^{ab}\rangle + \frac{1}{(3!)^2} \sum_{ijkabc} C_{ijk}^{abc} \, |\Phi_{ijk}^{abc}\rangle + \cdots , \quad (2.18)$$

where $|\Phi\rangle$ is the Hartree-Fock reference, the indices $i, j, k, l, \ldots$ and $a, b, c, d, \ldots$ label occupied and unoccupied (or virtual) molecular orbitals, respectively, in the HF state $|\Phi\rangle$, and the state $|\Phi_{ijk\ldots}^{abc\cdots}\rangle$ refers to a Slater determinant constructed by exciting electrons from the occupied orbitals $\{i, j, k, \ldots\}$ to the unoccupied orbitals $\{a, b, c, \ldots\}$. The coefficients $C_{ijk\ldots}^{abc\cdots}$ parameterize the CI wave function, and can be found either by solving the TISE,

$$H \, |\Psi_{CI}\rangle = E \, |\Psi_{CI}\rangle \, , \quad (2.19)$$

or by variational minimization of the CI energy,

$$E_{CI} = \frac{\langle \Psi_{CI}|H|\Psi_{CI}\rangle}{\langle \Psi_{CI}|\Psi_{CI}\rangle}. \quad (2.20)$$

The full CI expansion of an exact ground- (or excited-) state wave function for a general many-body Hamiltonian goes to all possible orders in excitation rank, making it unfeasible to store and compute. Therefore, it is practical to use a CI expansion truncated at some finite-order as an approximation to the ground state. For problems

with weak electron correlation, a CI ansatz truncated at the level of single- and double-excitations (CISD) provides a good balance between accuracy and computational cost. Higher-order CI theories provide a systematic way to improve the quality of approximations. Finally, CI theories can be based either on symmetry-adapted or symmetry-broken HF states.

2.2.3 Coupled Cluster

The CI theory, though better than HF, is not size-extensive, i.e., for systems of different sizes, e.g., 1D Hubbard models or Hydrogen chains with different sizes, the CI energy does not scale linearly with the system size, which is the correct scaling for the exact energy in the thermodynamic limit. Therefore, CI is ill-suited for real-world applications. Coupled cluster (CC) theory overcomes this hurdle by introducing an exponential parameterization in place of the linear expansion in CI, i.e.,

$$|\Psi_{CC}\rangle = e^{T} |\Phi\rangle , \tag{2.21}$$

where $|\Phi\rangle$ is again the HF reference and T, known as the cluster operator, is defined as

$$T = T_1 + T_2 + \ldots , \tag{2.22a}$$

$$T_1 = \sum_{ia} t_i^a a_a^\dagger a_i , \tag{2.22b}$$

$$T_2 = \frac{1}{(2!)^2} \sum_{ia} t_{ij}^{ab} a_a^\dagger a_b^\dagger a_j a_i , \tag{2.22c}$$

and so on. Here, T_1 creates single excitations on the HF Slater determinant $|\Phi\rangle$, T_2 creates double excitations, etc. The particle-hole index notation is the same as that for CI. The amplitudes $\{t_i^a, t_{ij}^{ab}, \ldots\}$ parametrize the CC wave function. Inserting the

CC ansatz into the TISE (Eq. 1.2), we get

$$H\left|\Psi_{CC}\right\rangle = E_{CC}\left|\Psi_{CC}\right\rangle \quad \Rightarrow \quad e^{-T}He^{T}\left|\Phi\right\rangle = E_{CC}\left|\Phi\right\rangle . \tag{2.23}$$

The CC energy and amplitudes can then be computed by projecting Eq. 2.23 against various ground and excited HF Slater determinants, i.e.,

$$E_{CC} = \langle\Phi|e^{-T}He^{T}|\Phi\rangle\,, \tag{2.24a}$$

$$0 = \langle\Phi|a_i^\dagger a_a \bar{H}|\Phi\rangle \qquad \forall\{i \in O; a \in V\}, \tag{2.24b}$$

$$0 = \langle\Phi|a_i^\dagger a_j^\dagger a_b a_a \bar{H}|\Phi\rangle \qquad \forall\{i,j \in O; a,b \in V\}, \tag{2.24c}$$

where $\bar{H} = e^{-T}He^{T}$ is the similarity transformed Hamiltonian. Using the Baker-Campbell-Hausdorff (BCH) expansion, we can simplify $\bar{H}$ as

$$\bar{H} = H + [H,T] + \frac{1}{2}[[H,T],T] + \frac{1}{3!}[[[H,T],T],T] + \ldots \tag{2.25}$$

For a general two-body electronic Hamiltonian, this similarity transformation truncates at the fourth-order nested commutator due to the pure excitation nature of the cluster operator T. In order to have a computationally feasible theory, it is necessary to truncate the cluster operator to a finite order in excitation rank. For most applications, CC with single and double excitations (CCSD) performs well, with a computational scaling of $\mathcal{O}(N^6)$, where N is a measure of the system size (e.g. number of orbitals in the basis set, or number of lattice sites).

Expectation values in coupled cluster

As introduced so far, CC describes a correlated ansatz for the *ket* wave function. To compute expectation values of observables other than the Hamiltonian, one also needs a correlated *bra* state. A linear response wave function is generally employed

for this purpose, [78, 79] i.e. one makes the energy functional

$$E = \langle \Phi | (1 + Z) e^{-T} H e^{T} | \Phi \rangle \tag{2.26}$$

stationary with respect to T and Z, where

$$Z = Z_1 + Z_2 + \ldots, \tag{2.27a}$$

$$Z_1 = \sum_{i,a} z_i^a c_i^\dagger c_a, \tag{2.27b}$$

$$Z_2 = \frac{1}{4} \sum_{i,a} z_{ij}^{ab} c_i^\dagger c_j^\dagger c_b c_a. \tag{2.27c}$$

Stationarity of the energy functional (Eq. 2.26) stationary with respect to Z results in the familiar set of equations in Eq. 2.24. The expectation value of any physical observable $\mathcal{O}$ can then be computed as

$$\langle \mathcal{O} \rangle_{CC} = \langle \Phi | (1 + Z) e^{-T} \mathcal{O} e^{T} | \Phi \rangle = \langle \Psi_{CI} | \mathcal{O} | \Psi_{CC} \rangle \,. \tag{2.28}$$

By realizing that the cluster operator T and the CI operator Z are composed of particle-hole excitation and de-excitation operators respectively, the *bra* state can be re-written as an explicit CI wave function

$$\langle \Psi' | = \langle \Phi | (1 + Z) e^{-T} = \langle \Phi | (1 + W) e^{w_0}, \tag{2.29}$$

where w_0 is a constant and W has the same operator-form as Z.

2.2.4 Comparison of different methods

Before moving ahead and exploring finite-temperature wave function theories, it is useful to highlight the merits and shortcomings of the different ground-state methods discussed above with the help of a simple benchmark example. Figure 2.1 plots the error in ground-state energies for HF, CISD, and CCSD with respect to the exact results

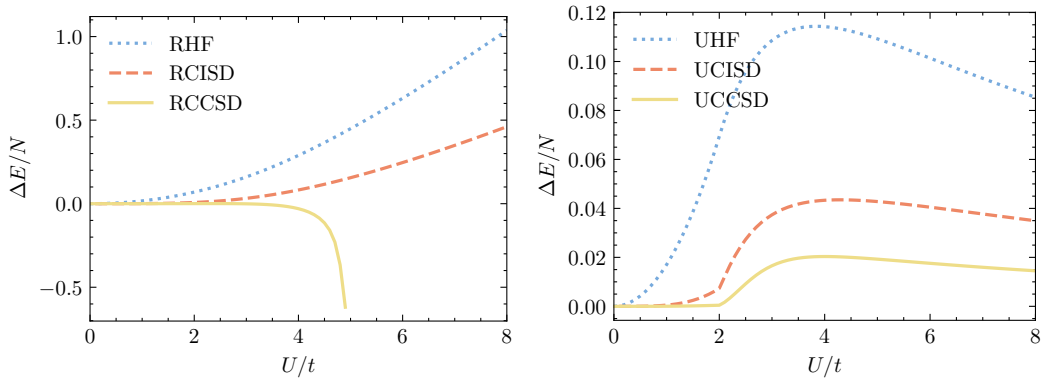

Figure 2.1 : Comparison of symmetry-adapted (left panel) and symmetry-broken (right panel) Hartree Fock, CISD and CCSD theories for predicting the ground-state energy for different values of U/t in a 10-site 1D Hubbard model with periodic boundary conditions.

for the 10-site Hubbard model. Our system is a one-dimensional lattice with periodic boundary conditions (making it equivalent to a ring) at half-filling. The energy error is plotted as a function of the correlation strength U/t. The panel on the left shows symmetry-adapted results, i.e., the methods that conserve the S^2 and S^z symmetries, whereas the results in the right panel are based on UHF, i.e., the theories break S^2 while still preserving the S^z symmetry. It is apparent that symmetry-restricted methods perform very well for small U/t but break down disastrously beyond $U/t \simeq 4$. On the other hand, UHF-derived results perform reasonably well for the entire range of correlation strengths. To provide an idea about the extent of symmetry breaking, we also plot the expectation value of the $\mathbf{S}^2_{\text{Total}}$ operator in Fig. 2.2. We can see that symmetry breaking occurs for $U/t \gtrsim 2$, where a UHF Slater determinant yields lower energy than RHF. All the results presented in Figs. 2.1 and 2.2 were computed with PySCF. [80, 81]

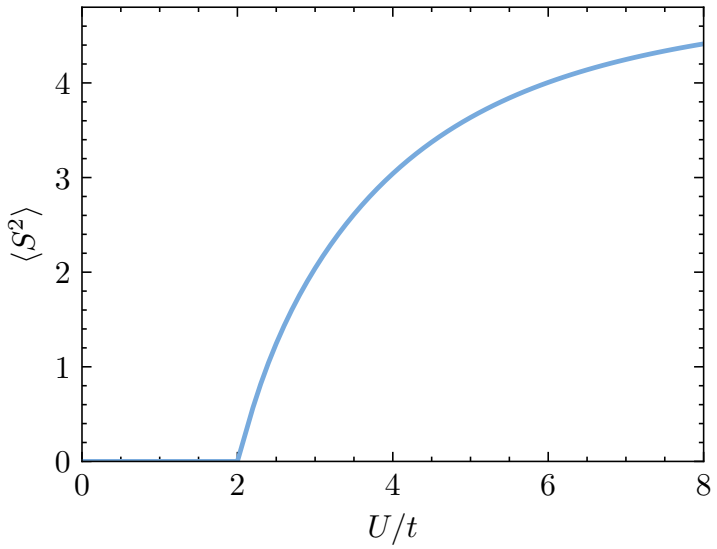

Figure 2.2 : Expectation value of $\mathbf{S}^2_{\text{Total}}$ operator as a function of the interaction strength U/t, computed over UHF Slater determinant for the half-filled 10-site Hubbard model with periodic boundary conditions.

2.3 Thermofield dynamics

Equilibrium thermal properties of quantum systems are calculated as ensemble averages, as described in Eq. 1.3. Specifically, for a quantum system at an inverse temperature β (or temperature $T = 1/\beta$), the thermal expectation value of an observable $\mathcal{O}$ is given by,

$$\langle \mathcal{O} \rangle_\beta = \frac{1}{\mathcal{Z}} \text{Tr}(\mathcal{O}\rho) = \frac{1}{\mathcal{Z}} \sum_m \langle m|\mathcal{O}\rho|m\rangle \,, \tag{2.30}$$

where $\rho = e^{-\beta(H-\mu N)}$ is the thermal density matrix, constructed in the appropriate choice of ensemble spanned by $\{|m\rangle\}$, and $\mathcal{Z} = \text{Tr}(\rho)$ is the partition function. In Sections 1.1 and 1.2, we highlighted that the wave function methods, at least in their conventional formulation, are ill-suited to study thermal properties in correlated quantum many-body systems. This is due to the enormous number of eigenstates that

need to be determined in a realistic system, which is beyond the reach of imaginable computational capabilities, combined with the fact that there are fewer accurate and efficient methods for excited states.

Thermofield dynamics [64–67] (TFD) contains a way to overcome this hurdle. It provides a prescription for purification of the finite-temperature ensemble density matrix and constructs a single wave function, often known as the *thermal* or the *thermofield double* state, that can exactly capture the thermal behavior of quantum systems. This is achieved by working in an enlarged space made up of the original Hilbert space and its conjugate copy. The ensemble thermal average in the physical space becomes as an expectation value over the purified thermal state in the doubled space,

$$\langle \mathcal{O} \rangle_\beta = \frac{1}{\mathcal{Z}} \mathrm{Tr}\left(e^{-\beta H}\mathcal{O}\right) = \frac{\langle \Psi(\beta)| \mathcal{O} |\Psi(\beta)\rangle}{\langle \Psi(\beta)|\Psi(\beta)\rangle}, \tag{2.31}$$

where, once again, β is the inverse temperature, and H is the Hamiltonian. The purification of the ensemble density matrix by introducing an auxiliary or tilde-conjugate space $\tilde{\mathcal{H}}$, conjugate to the physical space $\mathcal{H}$, requires $\tilde{\mathcal{H}}$ to have the following structure:

1. The dimensionality of $\tilde{\mathcal{H}}$ is the same as $\mathcal{H}$, i.e. for every state $|\psi\rangle$ in $\mathcal{H}$, there is a corresponding $|\tilde{\psi}\rangle$ in $\tilde{\mathcal{H}}$ and likewise for operators.

2. The *tilde* operators obey similar (anti-) commutation rules as their physical counterparts. For instance, for a bosonic (fermionic) spin-orbital p, we have the extended set of field operators $\{c_p, c_p^\dagger; \tilde{c}_p, \tilde{c}_p^\dagger\}$, which obey the canonical commutation (anti-commutation) rules,

$$[c_p, c_p^\dagger]_\mp = 1 = [\tilde{c}_p, \tilde{c}_p^\dagger]_\mp, \tag{2.32a}$$

$$[c_p, \tilde{c}_p]_\mp = 0 = [c_p, \tilde{c}_p^\dagger]_\mp, \tag{2.32b}$$

where the convention for commutator / anti-commutator is defined as

$$[A, B]_{-\eta} = AB - \eta BA, \tag{2.33}$$

such that $\eta = -1$ in Eq. 2.32 produces the anti-commutation rules for fermions, and $\eta = +1$ produces the commutation rules for bosons.

3. A tilde conjugation operation transforms operators between $\mathcal{H}$ and $\tilde{\mathcal{H}}$ with the following general rules:

$$\widetilde{(\tilde{c}_k)} = \eta c_k, \tag{2.34a}$$

$$\widetilde{\left(\alpha c_k + \delta c_q^\dagger\right)} = \alpha^\star \tilde{c}_k + \delta^\star \tilde{c}_q^\dagger, \tag{2.34b}$$

$$\widetilde{\left(c_k c_q^\dagger\right)} = \tilde{c}_k \tilde{c}_q^\dagger, \tag{2.34c}$$

where $\alpha^\star, \delta^\star$ are complex conjugates of α, δ respectively, and $\eta = \pm 1$ for bosons / fermions. With these conjugation rules, a Hamiltonian for the *tilde* system can be defined, generally denoted by $\tilde{H}$.

4. The time-dependent Schrödinger equation in $\tilde{\mathcal{H}}$ becomes ($\hbar = 1$)

$$-i\frac{\partial}{\partial t}\left|\psi\right\rangle = \tilde{H}\left|\psi\right\rangle. \tag{2.35}$$

5. Operators in the physical space do not act on states in the tilde space, and *vice versa*.

The complex conjugate nature of the tilde space is not important while studying equilibrium properties, but becomes necessary when working with time-dependent phenomena at finite temperatures, which is what the thermofield theory was originally developed for. However, the conjugation and doubling of the Hilbert space also

has well-justified connections with Hopf algebra. [82, 83] In the expanded space, the thermal state is expressed as

$$|\Psi(\beta)\rangle = e^{-\beta H/2} \sum_m |m\rangle \otimes |\tilde{m}\rangle \,, \tag{2.36}$$

where, as already mentioned above, the orthonormal bases $\{|m\rangle\}$ and $\{|\tilde{m}\rangle\}$ span the canonical or grand-canonical ensemble Hilbert spaces $\mathcal{H}$ and $\tilde{\mathcal{H}}$ respectively, β is the inverse temperature and H is the Hamiltonian of the system. The norm of the thermal state gives the partition function

$$\mathcal{Z} = \langle \Psi(\beta)|\Psi(\beta)\rangle \,. \tag{2.37}$$

2.3.1 The identity state

At infinite temperature, or $\beta = 0$, the thermal state becomes an equal superposition of all possible states in the physical space, paired with their tilde counterparts, i.e.,

$$|\Psi(\beta = 0)\rangle = |\mathbb{I}\rangle = \sum_m |m\rangle \otimes |\tilde{m}\rangle = \sum_m |m; \tilde{m}\rangle \,. \tag{2.38}$$

This reflects the fact that at $\beta = 0$, the Hamiltonian and the associated interactions are all washed out. In fact, the infinite temperature density matrix is just an identity matrix. Therefore, we introduce the notation, $|\Psi(\beta = 0)\rangle = |\mathbb{I}\rangle$, and call the infinite temperature state, which exhibits maximal entanglement between the physical and auxiliary spaces, as the identity state. The identity state is invariant under any basis transformation.

Depending on the choice of thermal ensemble and the underlying algebra of the quantum system, e.g. fermionic, bosonic, $su(2)$, etc., the identity state can be defined in different ways. For fermions in grand-canonical ensemble, we can define the identity state as

$$|\mathbb{I}\rangle_{\text{grand canonical}} = \prod_{p=1}^{L} \left(1 + c_p^\dagger \tilde{c}_p^\dagger\right) |-;-\rangle \,, \tag{2.39}$$

where p is a general spin-orbital index labelling all the single-electron levels in the system, L is the total number of spin-orbitals and $|-;-\rangle$ is the combined vacuum state for physical and auxiliary space. The canonical ensemble equivalent of the identity state can be constructed by projecting the grand-canonical state against the desired number sector. For a system with N_0 electrons, we get

$$|\mathbb{I}\rangle_{\text{canonical}} = \mathcal{P}_{N_0} \prod_{p=1}^{L} \left(1 + c_p^\dagger \tilde{c}_p^\dagger\right) |-;-\rangle\,, \tag{2.40a}$$

$$= \frac{1}{N_0!} \left(\sum_{p=1}^{L} c_p^\dagger \tilde{c}_p^\dagger\right)^{N_0} |-;-\rangle\,, \tag{2.40b}$$

where $\mathcal{P}_{N_0}$ is the number-projection operator which selects only those terms in the wave function that has N_0 particles. We will introduce the identity state for SU(2) systems in Chapter 5. The basis independence of the identity state is a consequence of the fact that the auxiliary space is complex-conjugate space, i.e., for a unitary rotation of the physical fermion operators given by

$$c_p^\dagger = \sum_q a_q^\dagger U_{qp}, \tag{2.41}$$

we have a corresponding transformation for the tilde-space operators,

$$\tilde{c}_p^\dagger = \sum_q \tilde{a}_q^\dagger U_{qp}^*. \tag{2.42}$$

Therefore, the identity state for, say, the canonical ensemble becomes

$$|\mathbb{I}\rangle_{\text{canonical}} = \frac{1}{N_0!} \left(\sum_p \sum_{qr} a_q^\dagger \tilde{a}_r^\dagger U_{qp} U_{rp}^*\right)^{N_0} |-;-\rangle\,, \tag{2.43a}$$

$$= \frac{1}{N_0!} \left(\sum_{qr} a_q^\dagger \tilde{a}_r^\dagger \delta_{qr}\right)^{N_0} |-;-\rangle\,, \tag{2.43b}$$

$$= \frac{1}{N_0!} \left(\sum_{p=1}^{L} a_p^\dagger \tilde{a}_p^\dagger\right)^{N_0} |-;-\rangle\,. \tag{2.43c}$$

which has the same form as the original canonical ensemble identity state. Here, we have used the unitarity of the transformation, i.e., $\sum_p U_{qp} U^*_{rp} = \delta_{qr}$, to simplify the expression.

2.3.2 How does thermofield theory work?

The finite-temperature ensemble average of any physical observable $\mathcal{O}$ can be computed as an expectation value over the thermofield double state, as pointed out in Eq. 2.30. Since $\mathcal{O}$ acts only on the physical part of the thermal state, the auxiliary states in Eq. 2.36 provide a means to transform the expectation value into trace. Written explicitly, the expectation value simplifies in the following manner:

$$\langle \mathcal{O} \rangle_\beta = \frac{\langle \Psi(\beta) | \mathcal{O} | \Psi(\beta) \rangle}{\langle \Psi(\beta) | \Psi(\beta) \rangle}, \tag{2.44a}$$

$$= \frac{1}{\mathcal{Z}} \sum_{m,n} \langle m, \tilde{m} | \, e^{-\beta H/2} \mathcal{O} e^{-\beta H/2} \, | n, \tilde{n} \rangle \,, \tag{2.44b}$$

$$= \frac{1}{\mathcal{Z}} \sum_{m,n} \langle m | \, e^{-\beta H/2} \mathcal{O} e^{-\beta H/2} \, | n \rangle \otimes \langle \tilde{m} | \tilde{n} \rangle \,, \tag{2.44c}$$

$$= \frac{1}{\mathcal{Z}} \sum_{m} \langle m | \, e^{-\beta H/2} \mathcal{O} e^{-\beta H/2} \, | m \rangle \,, \tag{2.44d}$$

$$= \frac{1}{\mathcal{Z}} \mathrm{Tr} \left(e^{-\beta H/2} \mathcal{O} e^{-\beta H/2} \right), \tag{2.44e}$$

$$= \frac{1}{\mathcal{Z}} \mathrm{Tr} \left(e^{-\beta H} \mathcal{O} \right). \tag{2.44f}$$

In going from Eq. 2.44c to Eq. 2.44d, we have used the fact that $\langle \tilde{m} | \tilde{n} \rangle = \langle m | n \rangle = \delta_{mn}$, were as from Eq. 2.44e to Eq. 2.44f, we have invoked the cyclic property of trace.

2.3.3 Imaginary-time evolution

By its construction, the thermal state obeys an imaginary-time evolution equation,

$$\frac{\partial}{\partial \beta} | \Psi(\beta) \rangle = -\frac{1}{2} H \, | \Psi(\beta) \rangle \,, \tag{2.45}$$

which, combined with an appropriate initial condition, can be integrated to yield the thermal state at any other β. While working explicitly with the grand-canonical ensemble, the thermal state can be defined as

$$|\Psi(\beta,\mu)\rangle = e^{-\beta(H-\mu N)/2}\,|\mathbb{I}\rangle\,, \tag{2.46}$$

where μ is the chemical potential. Assuming that the Hamiltonian preserves the particle number, i.e. $[H,N]=0$, which is the case for most physical systems, the imaginary-time evolution equation (Eq. 2.45) gets modified as

$$\frac{\partial}{\partial\beta}\,|\Psi(\beta,\mu)\rangle = -\frac{1}{2}(H-\mu N)\,|\Psi(\beta,\mu)\rangle\,. \tag{2.47}$$

Similarly, we can derive an evolution equation along the chemical potential direction:

$$\frac{\partial}{\partial\mu}\,|\Psi(\beta,\mu)\rangle = \frac{\beta}{2}N\,|\Psi(\beta,\mu)\rangle\,. \tag{2.48}$$

Starting from some inverse temperature β_0 and chemical potential μ_0, we can integrate Eqs. 2.47 and 2.48 to obtain the thermal state for any desired β and μ. The exact integration of these equations for a general electronic Hamiltonian naturally suffers from the same exponential computational barrier as the ground-state theories. Developing approximate wave function theories is the objective of the work reported in the following chapters.

2.3.4 Real-time evolution

TFD was originally developed as a framework to study quantum dynamical problems at finite temperatures. The finite-temperature time-dependent expectation value of an observable can be computed as

$$\langle\mathcal{O}\rangle_\beta(t) = \mathrm{Tr}\left(e^{-\beta H}\mathcal{U}(0,t)\mathcal{O}\mathcal{U}(t,0)\right), \tag{2.49}$$

where $\mathcal{U}(t_2, t_1)$ is the real-time evolution operator from t_1 to t_2. From the perspective of a path integral, the expectation value $\langle \mathcal{O} \rangle_\beta (t)$ involves a forward and a backward propagation along the real-time axis in addition to a propagation along the imaginary-time direction. The auxiliary space in TFD is defined to be a complex conjugate space precisely to handle the backward propagation. Specifically, the real-time evolution of the thermal state is governed by a modified TDSE,

$$i\frac{\partial}{\partial t}|\Psi(\beta, t)\rangle = H_{TFD}(t)|\Psi(\beta, t)\rangle, \tag{2.50}$$

where H_{TFD} is known as the thermofield Hamiltonian, and is defined as

$$H_{TFD} = H(t) - \tilde{H}(t). \tag{2.51}$$

The Hamiltonian for the tilde-space, $\tilde{H}(t)$, is defined by taking the tilde-conjugate of the physical Hamiltonian.

2.3.5 Physical interpretation

It is worthwhile to provide a physical intuition behind the auxiliary system in TFD. Here, we present a brief discussion on two interpretations that we find interesting.

Ad hoc interpretation

In terms of the energy eigenvalues $\{E_m\}$ and eigenstates $\{|m\rangle\}$, the thermal density matrix at inverse temperature β becomes

$$\rho = \sum_m e^{-\beta E_m} |m\rangle \langle m| . \tag{2.52}$$

Loosely speaking, we can map the *bra* state $\langle m|$ to a *ket* in a new space, $|\tilde{m}\rangle$, such that $|\tilde{m}\rangle$ has the same properties as $\langle m|$. In other words, a tilde-space wave function

should obey the same TDSE as a generic *bra* state, i.e.,

$$i\frac{\partial}{\partial t}\langle\psi| = -\langle\psi| H \quad \Rightarrow \quad i\frac{\partial}{\partial t}|\tilde{\psi}\rangle = -\tilde{H}|\tilde{\psi}\rangle\,. \tag{2.53}$$

This also justifies the form of the driving Hamiltonian, H_{TFD} in the real-time evolution equation (Eq. 2.50) for the thermofield double state.

Schmidt decomposition

The temperature of a system quantifies its entanglement with the environment or the thermal bath. In that sense, the universe or the super system, which comprises the physical system and the environment, is essentially at zero temperature. As a consequence, we can use a single wave function $|\Psi_{\text{super}}\rangle$ to study any property of the super system.

Naturally, the super wave function lives in a tensor product space of the system and bath Hilbert spaces, i.e. $\mathcal{H}_{\text{super}} = \mathcal{H}_S \otimes \mathcal{H}_B$. Expanding the super wave function in terms of orthonormal basis states $\{|S_m\rangle\}$ and $\{|B_m\rangle\}$ of the system and bath respectively, we get

$$|\Psi_{\text{super}}\rangle = \sum_{\mu=1}^{L_S}\sum_{\nu=1}^{L_B}\psi_{\mu\nu}|S_\mu\rangle \otimes |B_\nu\rangle\,, \tag{2.54}$$

where L_S and L_B are the dimensionality of the system and bath Hilbert spaces. Using the singular value decomposition for the coefficients $\psi_{\mu\nu}$, we get

$$|\Psi_{\text{super}}\rangle = \sum_{\mu=1}^{L_S}\sum_{\nu=1}^{L_B}\sum_{\alpha=1}^{\min(L_S,L_B)} U_{\mu\alpha}\lambda_\alpha V^*_{\nu\alpha}|S_\mu\rangle \otimes |B_\nu\rangle\,. \tag{2.55}$$

By introducing basis transformations for both physical and bath states,

$$|\alpha\rangle = \sum_{\mu=1}^{L_S} U_{\mu\alpha}|S_\mu\rangle\,, \tag{2.56a}$$

$$|\tilde{\alpha}\rangle = \sum_{\nu=1}^{L_B} V^*_{\nu\alpha}|B_\nu\rangle\,, \tag{2.56b}$$

and combining it with the fact that the dimensionality of the bath Hilbert space is much larger than that of the system's, we can re-write the super wave function as

$$|\Psi_{\text{super}}\rangle = \sum_{\alpha=1}^{L_S} \lambda_\alpha |\alpha\rangle \otimes |\tilde{\alpha}\rangle \,. \tag{2.57}$$

By choosing $\{|\alpha\rangle\}$ to be the eigenstates of the physical Hamiltonian and $\lambda_\alpha = e^{-\beta E_\alpha/2}$, where $\{E_\alpha\}$ are the corresponding energy eigenvalues, we can recover the thermal state defined in Eq. 2.36.

2.3.6 Asymmetric thermofield theories

We have seen how TFD performs the purification of the thermal density matrix into a thermal state $|\Psi(\beta)\rangle$ such that thermal traces can be expressed as expectation value over the latter,

$$\langle \mathcal{O} \rangle_\beta = \frac{\langle \Psi(\beta)|\mathcal{O}|\Psi(\beta)\rangle}{\langle \Psi(\beta)|\Psi(\beta)\rangle} = \frac{\langle \mathbb{I}|e^{-\beta H/2}\mathcal{O}e^{-\beta H/2}|\mathbb{I}\rangle}{\langle \mathbb{I}|e^{-\beta H}|\mathbb{I}\rangle}. \tag{2.58}$$

By re-examining this expression, we can clearly see that computing expectation value over the identity state $|\mathbb{I}\rangle$ is equivalent to computing the trace. Using the cyclic property of the trace, we can then derive an equally valid expression for thermal averages, given by

$$\langle \mathcal{O} \rangle_\beta = \frac{1}{\mathcal{Z}} \langle \mathbb{I}|e^{-(1-\sigma)\beta H}\mathcal{O}e^{-\sigma\beta H}|\mathbb{I}\rangle \,, \tag{2.59}$$

where $0 \leq \sigma \leq 1$. Consequently, the imaginary-time evolution equations for the *bra* and the *ket* become

$$\frac{\partial}{\partial\beta} |\Psi_\sigma(\beta)\rangle = -\sigma H |\Psi_\sigma(\beta)\rangle \,, \tag{2.60a}$$

$$\frac{\partial}{\partial\beta} \langle \Psi_\sigma(\beta)| = -(1-\sigma) \langle \Psi_\sigma(\beta)| H. \tag{2.60b}$$

For $\sigma = 1/2$, we recover the conventional, symmetric thermofield dynamics presented in the preceding subsections. We adhere to this convention for most of the developments presented in this thesis, but also discuss an example of asymmetric thermal CI theory. An asymmetric formulation of thermal CC has also been explored by Shushkov et al. [61] On the other hand, for $\sigma \neq 1/2$, we would require two different thermal states, one each for the *bra* and the *ket*. This freedom in the choice of contour used in the imaginary-time path integral has been explored in Refs. 64, 84.

Chapter 3

Thermal wave function theories for the grand canonical ensemble

The explicit wave function formulation of the thermal density matrix in TFD, along with the associated imaginary-time evolution equation, provides a framework to generalize standard ground-state ansätze to finite temperatures. In this chapter, we focus our attention on wave function theories to study the finite-temperature properties of fermionic many-body systems in the grand canonical ensemble. The thermal state at inverse temperature β and chemical potential $\mu = \alpha/\beta$ is defined as

$$|\Psi(\alpha,\beta)\rangle = e^{(\alpha N - \beta H)/2}\,|\mathbb{I}\rangle\,, \tag{3.1}$$

where the identity state is given by Eq. 2.39. We introduce a change in the definition of the chemical potential from μ to $\alpha = \beta\mu$. For a Hamiltonian that preserves the total particle number, the modified parametrization of the chemical potential simplifies both the number dependence and the associated evolution equations for the thermal state, and we get,

$$\frac{\partial}{\partial\alpha}\,|\Psi(\alpha,\beta)\rangle = \frac{N}{2}\,|\Psi(\alpha,\beta)\rangle\,, \tag{3.2a}$$

$$\frac{\partial}{\partial\beta}\,|\Psi(\alpha,\beta)\rangle = -\frac{H}{2}\,|\Psi(\alpha,\beta)\rangle\,. \tag{3.2b}$$

As we mentioned in the previous chapter, an exact integration of these equations scales exponentially with the system size and can be performed only for relatively small systems with just a few orbitals. In the following sections, we will explore

thermal generalization of approximate ground-state wave function theories, namely mean-field, CI, and CC. To assess the performance of these methods, we study small Hubbard, reduced BCS as well as molecular systems, while comparing with exact benchmark results.

3.1 Mean-field theory

The simplest approximation that can be used to construct the thermal state is the mean-field approach, where an effective one-body Hamiltonian H_0 is used to evolve the thermal state, and results in

$$|\Psi(\alpha,\beta)\rangle_{\text{mean field}} = e^{(\alpha N-\beta H_0)/2}\,|\mathbb{I}\rangle\,. \tag{3.3}$$

Working in a basis where H_0 is diagonal, i.e. $H_0 = \sum_p \epsilon_p c_p^\dagger c_p$, and using the basis-invariance of $|\mathbb{I}\rangle$, we get the following expression for the mean-field thermal state,

$$|\Psi(\alpha,\beta)\rangle_{\text{mean field}} = \prod_p \left(1 + e^{(\alpha-\beta\epsilon_p)/2} c_p^\dagger \tilde{c}_p^\dagger\right)|-;-\rangle\,. \tag{3.4}$$

And after normalization, we end up with a state that we call the mean-field thermal vacuum, defined as

$$|0(\alpha,\beta)\rangle = \prod_p \left(x_p + y_p c_p^\dagger \tilde{c}_p^\dagger\right)|-;-\rangle\,, \tag{3.5}$$

where $x_p = 1/\sqrt{1+e^{\alpha-\beta\epsilon_p}}$, $y_p = e^{(\alpha-\beta\epsilon_p)/2}/\sqrt{1-e^{\alpha-\beta\epsilon_p}}$, and $x_p^2 + y_p^2 = 1$. Note that the coefficients x_p and y_p are related to the Fermi-Dirac distribution function.

Thermal Bogoliubov transformation

The identity state and the mean-field thermal vacuum have the familiar form of a BCS state,

$$|BCS\rangle = \prod_p \left(u_p + v_p c_{p\uparrow}^\dagger c_{p\downarrow}^\dagger\right)|-\rangle\,, \tag{3.6}$$

where the cooper pairs in $|\mathbb{I}\rangle$ and $|0(\alpha,\beta)\rangle$ are formed between physical and auxiliary orbitals as compared to spin singlet pairs in BCS. Following the BCS theory, we can define a thermal analogue of the quasiparticles and Bogoliubov transformation, i.e. we can construct α- and β-dependent operators $\{a_p(\alpha,\beta), a_p^\dagger(\alpha,\beta), \tilde{a}_p(\alpha,\beta), \tilde{a}_p^\dagger(\alpha,\beta)\}$ that annihilate/create quasiparticle excitations on the mean-field thermal vacuum. This thermal Bogoliubov transformation is given by

$$\begin{pmatrix} a_p(\alpha,\beta) \\ \tilde{a}_p^\dagger(\alpha,\beta) \end{pmatrix} = \begin{pmatrix} x_p & -y_p \\ y_p & x_p \end{pmatrix} \begin{pmatrix} c_p \\ \tilde{c}_p^\dagger \end{pmatrix}, \tag{3.7}$$

such that, for x_p and y_p defined in Eq. 3.5, the thermal quasiparticle annihilation operators annihilate the mean-field thermal vacuum, i.e.,

$$a_p\,|0(\alpha,\beta)\rangle = 0 = \tilde{a}_p\,|0(\alpha,\beta)\rangle\,, \tag{3.8a}$$

$$\langle 0(\alpha,\beta)|\,a_p^\dagger = 0 = \langle 0(\alpha,\beta)|\,\tilde{a}_p^\dagger. \tag{3.8b}$$

Here and after, we drop the explicit α- and β-dependence in the thermal quasiparticle operators. The Bogoliubov transformation in Eq. 3.7 also allows us to form a physical intuition about the thermal operators: in the low T (or high β) limit, the annihilation of an occupied orbital in the physical space $\mathcal{H}$ is equivalent to creating a particle in the corresponding orbital in the *tilde*-space $\tilde{\mathcal{H}}$ and vice-versa, whereas in the high T limit, these operators are completely mixed.

The general electronic Hamiltonian, presented in Eq. 2.2, can be expressed in terms of the thermal operators and takes the form

$$\begin{aligned} H = h_0 &+ \sum_{ab}\left[h_{ab}^{(11)}\left(a_a^\dagger\tilde{a}_b^\dagger + \text{h.c.}\right) + h_{ab}^{(20)}a_a^\dagger a_b + h_{ab}^{(02)}\tilde{a}_a^\dagger\tilde{a}_b\right] \\ &+ \sum_{abcd}\left[h_{abcd}^{(221)}\left(a_a^\dagger a_b^\dagger\tilde{a}_d^\dagger\tilde{a}_c^\dagger + \text{h.c.}\right) + h_{abcd}^{(222)}a_a^\dagger\tilde{a}_b^\dagger\tilde{a}_d a_c + h_{abcd}^{(31)}\left(a_a^\dagger a_b^\dagger\tilde{a}_c^\dagger a_d + \text{h.c.}\right)\right. \\ &\left. + h_{abcd}^{(13)}\left(a_a^\dagger\tilde{a}_b^\dagger\tilde{a}_c^\dagger\tilde{a}_d + \text{h.c.}\right) + h_{abcd}^{(40)}a_a^\dagger a_b^\dagger a_d a_c + h_{abcd}^{(04)}\tilde{a}_a^\dagger\tilde{a}_b^\dagger\tilde{a}_d\tilde{a}_c\right], \end{aligned} \tag{3.9}$$

where we use h_0, $h^{(11)}$, etc. to denote the effective matrix elements of the general quasiparticle Hamiltonian ($h^{(11)}$ is associated with terms that contain one non-*tilde* and a *tilde* quasiparticle operator each, $h^{(20)}$ with two non-*tilde* quasiparticle operators, and so on), all of which are defined as

$$h_0 = \sum_a y_a^2 h_{aa} + \frac{1}{2}\sum_{ab} y_a^2 y_b^2 v_{abab} \tag{3.10a}$$

$$h_{ab}^{(11)} = x_a y_b f_{ab}, \quad h_{ab}^{(20)} = x_a x_b f_{ab}, \quad h_{ab}^{(02)} = -y_a y_b f_{ab}, \tag{3.10b}$$

$$\begin{aligned} h_{abcd}^{(221)} &= \frac{1}{4} x_a x_b y_c y_d v_{abcd}, \quad h_{abcd}^{(222)} = x_a x_c y_b y_d v_{adbc}, \\ h_{abcd}^{(31)} &= -\frac{1}{2} x_a x_b y_c x_d v_{abcd}, \quad h_{abcd}^{(13)} = -\frac{1}{2} x_a y_b y_c y_d v_{adbc}, \\ h_{abcd}^{(40)} &= \frac{1}{4} x_a x_b x_c x_d v_{abcd}, \quad h_{abcd}^{(04)} = \frac{1}{4} y_a y_b y_c y_d v_{abcd}, \end{aligned} \tag{3.10c}$$

where $f_{ab} = \delta_{ab} h_{ab} + \sum_c y_c^2 v_{acbc}$. Note that in obtaining these expressions, we have assumed real matrix elements in the Hamiltonian. The foregoing expression for the Hamiltonian is normal-ordered with respect to the thermal vacuum. The ordering we follow here is $a^\dagger \to \tilde{a}^\dagger \to \tilde{a} \to a$.

Mean-field internal energy

The thermal average of H at the mean-field level can be computed simply by extracting the scalar component from its normal ordered expression,

$$\begin{aligned} E_{mf} &= \sum_p y_p^2 h_{pp} + \sum_{p,q} \frac{1}{2} y_p^2 y_q^2 v_{pqpq} \\ &= \sum_p \frac{h_{pp}}{1 + \mathrm{e}^{\beta(\epsilon_p - \mu)}} + \frac{1}{2}\sum_{p,q} \frac{v_{pqpq}}{(1 + \mathrm{e}^{\beta(\epsilon_p - \mu)})(1 + \mathrm{e}^{\beta(\epsilon_q - \mu)})}, \end{aligned} \tag{3.11a}$$

which recovers the standard thermal Hartree-Fock [31, 32] expression for the energy. One can find the appropriate one-electron basis or molecular orbitals by variationally

minimizing the grand potential. For reasons that will become clear later, we use an un-optimized, β-independent mean-field Hamiltonian to construct $|0(\alpha,\beta)\rangle$.

3.2 Framework for correlated wave function theories

Correlated methods frequently use a mean-field reference as the starting point, and we wish to do so here as well, but we face an additional choice which we wish to explore. Recall that the thermal state $|\Psi(\alpha,\beta)\rangle$ is obtained not from an eigenvalue problem but from an imaginary-time Schrödinger equation. For the reference state, we can choose the mean-field thermal state corresponding to a fixed temperature β_0, or we can use a β-dependent mean-field thermal state. By analogy with similar frameworks for coordinates in fluid dynamics and general relativity, we call the former approach a *fixed-reference* formulation and the latter a *covariant* formulation. Mathematically, the exact thermal state in the fixed-reference approach is represented as

$$|\Psi(\beta)\rangle = \Gamma(\beta,\beta_0)\,|0(\beta_0)\rangle\,, \tag{3.12}$$

where $\hat{\Gamma}$ is a wave operator which builds correlation on the reference. On the other hand, in the covariant formalism, the thermal state is parameterized as

$$|\Psi(\beta)\rangle = \Gamma(\beta,\beta)\,|0(\beta)\rangle\,. \tag{3.13}$$

The fixed-reference wave operator $\Gamma(\beta,\beta_0)$ is constructed using quasiparticle creation operators corresponding to $|0(\beta_0)\rangle$, i.e. $\{a_p^\dagger(\beta_0),\tilde{a}_p^\dagger(\beta_0)\}$, while the covariant operator $\Gamma(\beta,\beta)$ is a function of $\{a_p^\dagger(\beta),\tilde{a}_p^\dagger(\beta)\}$. The same idea is also applicable to α-dependence. For brevity, we will only consider the imaginary-time evolution here.

On the one hand, the covariant approach would seem to be more sensible, as less is demanded of the wave operator Γ; on the other hand, the fixed-reference approach

has the advantage that the quasiparticle creation and annihilation operators given by the thermal Bogoliubov transformation of Eq. 3.7 are not themselves temperature-dependent, which considerably simplifies the formulation of correlated methods. In principle, any inverse temperature β_0 can be used in the fixed-reference case. However, in practice, the most convenient choice is $\beta_0 = 0$ for which the mean-field thermal state is exact and the wave operator $\Gamma(0,0)$ is simply the identity operator.

In addition to deciding between the fixed-reference and covariant cases, we have a second decision to make: the choice of splitting the β-dependence on the *bra* and *ket*, or the choice of the parameter σ discussed in Section 2.3.6. For simplicity of notation, we will use a subscript to denote the choice of σ, and define our correlated wave function ansätze as

$$|\Psi_\sigma(\beta)\rangle_{\text{fix. ref.}} = \Gamma_\sigma(\beta,\beta_0)\,|0_\sigma(\beta_0)\rangle\,, \tag{3.14a}$$

$$|\Psi_\sigma(\beta)\rangle_{\text{cov.}} = \Gamma_\sigma(\beta,\beta)\,|0_\sigma(\beta)\rangle\,, \tag{3.14b}$$

3.2.1 Fixed-reference formalism

For the fixed-reference thermal wave function ansatz (Eq. 3.12), assuming that we evolve in β starting from $\beta = 0$, we get

$$|\Psi_\sigma(\beta)\rangle = \Gamma_\sigma(\beta,0)\,|\mathbb{I}\rangle\,. \tag{3.15}$$

Substituting this ansatz in to the imaginary time evolution equation gives

$$\left(\frac{\partial}{\partial\beta}\Gamma(\beta,0)\right)|\mathbb{I}\rangle = -\sigma H\Gamma(\beta,0)\,|\mathbb{I}\rangle\,, \tag{3.16}$$

such that $\Gamma_\sigma(0,0) = \hat{1}$, i.e. the identity operator.

3.2.2 Covariant formalism

In contrast with the fixed-reference approach, the thermal state for the covariant case is defined as

$$|\Psi_\sigma(\beta)\rangle = \Gamma_\sigma(\beta,\beta)\,|0_\sigma(\beta)\rangle\,, \tag{3.17}$$

which, after substituting in to the imaginary time evolution equation, gives

$$\frac{\partial}{\partial\beta}\,|0_\sigma(\beta)\rangle = -\sigma H_0\,|0_\sigma(\beta)\rangle\,, \tag{3.18a}$$

$$\left(\frac{\partial}{\partial\beta}\Gamma_\sigma(\beta,\beta)\right)|0_\sigma(\beta)\rangle = -\sigma\left(H\Gamma_\sigma(\beta,\beta) - H_0\right)|0_\sigma(\beta)\rangle\,. \tag{3.18b}$$

Once again, at $\beta = 0$, the mean-field thermal stae is exact and $\Gamma_\sigma(0,0) = \hat{1}$. By appropriately defining the wave operator Γ_σ, we can derive the equations for configuration interaction and coupled cluster theories.

3.3 Configuration interaction theory

In this section, we will discuss both the fixed-reference and the covariant formulations of thermal CI theory in detail. Since we are working with imaginary time evolution, thermal CI theories are very similar to time-dependent CI [85,86] at zero temperature. While CI is not size-extensive, a property which is highly desirable [87] in the study of many-electron systems, we use it as an example to introduce thermofield-based quantum chemistry methods because of its simplicity.

3.3.1 Fixed-reference Thermal CI

In this first approach, we consider the asymmetric parameter $\sigma = 1$, such that the thermal expectation value of a physical observable $\mathcal{O}$ is defined as

$$\langle\mathcal{O}\rangle(\alpha,\beta) = \frac{1}{\mathcal{Z}}\,\langle\mathbb{I}|\mathcal{O}|\Psi_{\sigma=1}(\alpha,\beta)\rangle\,, \tag{3.19}$$

where the definition and evolution equations for $|\Psi_{\sigma=1}(\alpha,\beta)\rangle$ are given by

$$|\Psi_{\sigma=1}(\alpha,\beta)\rangle = e^{\alpha N-\beta H}\,|\mathbb{I}\rangle\,, \tag{3.20a}$$

$$\frac{\partial}{\partial\beta}\,|\Psi_{\sigma=1}(\alpha,\beta)\rangle = -H\,|\Psi_{\sigma=1}(\alpha,\beta)\rangle\,, \tag{3.20b}$$

$$\frac{\partial}{\partial\alpha}\,|\Psi_{\sigma=1}(\alpha,\beta)\rangle = N\,|\Psi_{\sigma=1}(\alpha,\beta)\rangle\,. \tag{3.20c}$$

In the CI theory, The thermal state $|\Psi_{\sigma=1}(\alpha,\beta)\rangle$ is approximated as a linear expansion in the configuration space, starting from the reference $|\mathbb{J}\rangle = e^{\alpha_0 N}\,|\mathbb{I}\rangle$, i.e.

$$|\Psi_{\sigma=1}(\alpha,\beta)\rangle_{CI} = e^{s_0}(1+S)|\mathbb{J}\rangle, \tag{3.21}$$

where the CI-operator S is defined as

$$S = \sum_{pq} s_{pq} b_p^\dagger \tilde{b}_q^\dagger + \frac{1}{(2!)^2}\sum_{pqrs} s_{pqrs}\, b_p^\dagger b_q^\dagger \tilde{b}_s^\dagger \tilde{b}_r^\dagger + \ldots \tag{3.22}$$

All the α- and β-dependence in Eq. 3.22 is carried by the expansion coefficients s_{pq}, s_{pqrs}, etc. The first term is equivalent to single-excitations in ground-state CI, the second to double-excitations and so on. Here, we will consider CI with singles and doubles. Notice that the wave operator in Eq. 3.21 is written in intermediate normalization with an exponential normalization constant, i.e. $\langle\mathbb{J}|\Psi_{\sigma=1}(\alpha,\beta)\rangle_{CI} = e^{s_0}$, which is the partition function. The partition function grows/decays exponentially. Therefore, an exponential parametrization of the norm provides numerical stability. The (α- and β-independent) quasiparticle operators b, $\tilde{b}^\dagger$ are the same a-operators defined in Eq. 3.7 with the Bogoliubov parameters

$$x_p = \frac{1}{\sqrt{1+e^{\alpha_0}}}, \qquad y_p = \sqrt{\frac{e^{\alpha_0}}{1+e^{\alpha_0}}}, \tag{3.23}$$

where α_0 ensures that the correct total filling at $\beta = 0$, or infinite temperature, for a given basis set. It is interesting to note that the CI operator in Eq. 3.22 is composed

of terms that contain equal number of *tilde* and *non-tilde* quasiparticle creation operators. This is because, by virtue of the thermal Bogoliubov transformation in Eq. 3.7, the difference in the total number of *tilde* and *non-tilde* quasiparticles is a symmetry of the Hamiltonian, i.e.

$$[\mathcal{N}, H] = 0, \quad \mathcal{N} = \sum_p (b_p^\dagger b_p - \tilde{b}_p^\dagger \tilde{b}_p) \tag{3.24}$$

and only these terms in the CI wave function will have any non-trivial evolution and contribution to the expectation values of physical operators.

Substituting this ansatz into Eq. 3.20, and projecting the equation against quasiparticle excitation manifolds, we obtain the following set of β-evolution equations for thermal CISD,

$$\frac{\partial s_0}{\partial \beta} = -\frac{1}{\mathcal{Z}_{\mathbb{J}}} \langle \mathbb{J}|H(1+S)|\mathbb{J}\rangle \,, \tag{3.25a}$$

$$\frac{\partial s_{pq}}{\partial \beta} = -s_{pq}\frac{\partial s_0}{\partial \beta} - \frac{1}{\mathcal{Z}_{\mathbb{J}}} \langle \mathbb{J}|\tilde{b}_q b_p H(1+T)|\mathbb{J}\rangle \,, \tag{3.25b}$$

$$\frac{\partial s_{pqrs}}{\partial \beta} = -s_{pqrs}\frac{\partial s_0}{\partial \beta} - \frac{1}{\mathcal{Z}_{\mathbb{J}}} \langle \mathbb{J}|\tilde{b}_r \tilde{b}_s b_q b_p H(1+T)|\mathbb{J}\rangle \,, \tag{3.25c}$$

and similarly for α-evolution, we have

$$\frac{\partial s_0}{\partial \alpha} = \frac{1}{\mathcal{Z}_{\mathbb{J}}} \langle \mathbb{J}|N(1+S)|\mathbb{J}\rangle \,, \tag{3.26a}$$

$$\frac{\partial s_{pq}}{\partial \alpha} = -s_{pq}\frac{\partial s_0}{\partial \alpha} + \frac{1}{\mathcal{Z}_{\mathbb{J}}} \langle \mathbb{J}|\tilde{b}_q b_p N(1+T)|\mathbb{J}\rangle \,, \tag{3.26b}$$

$$\frac{\partial s_{pqrs}}{\partial \alpha} = -s_{pqrs}\frac{\partial s_0}{\partial \alpha} + \frac{1}{\mathcal{Z}_{\mathbb{J}}} \langle \mathbb{J}|\tilde{b}_r \tilde{b}_s b_q b_p N(1+\hat{T})|\mathbb{J}\rangle \,. \tag{3.26c}$$

The infinite-temperature partition function $\mathcal{Z}_{\mathbb{J}}$ is given by

$$\mathcal{Z}_{\mathbb{J}} = \langle \mathbb{J}|\mathbb{J}\rangle = \langle \mathbb{I}|e^{\alpha_0 N}|\mathbb{I}\rangle \,. \tag{3.27}$$

Having already absorbed α_0 in to the definition of the identity state, we can integrate these evolution equations starting from $(\alpha, \beta) = (0, 0)$, with the initial conditions

$$s_0 = 0; s_{pq} = 0; s_{pqrs} = 0, \ldots, \tag{3.28}$$

and obtain the CI coefficients at any given thermodynamic coordinate (α, β).

3.3.2 Covariant CI

In the covariant formulation, we wish to work with an α- and $\beta-$dependent reference and the expectation values are best described with the $\sigma = 1/2$ formulation of TFD and take the form of a symmetric expectation value

$$\langle A\rangle(\alpha,\beta) = \frac{1}{\mathcal{Z}} \langle \Psi(\alpha,\beta)|A|\Psi(\alpha,\beta)\rangle\,, \quad |\Psi(\alpha,\beta)\rangle = e^{(\alpha N-\beta H)/2}\,|\mathbb{I}\rangle\,, \tag{3.29}$$

where the thermal state $|\Psi(\alpha,\beta)\rangle$ is the same as the state described in Eq. 3.1 and is governed by the imaginary time evolution equation described in Eq. 3.2. The covariant thermal CI state is approximated as

$$|\Psi(\alpha,\beta)\rangle = e^{s_0}(1+S)\,|0(\alpha,\beta)\rangle\,, \tag{3.30}$$

where the CI operator S is given by

$$S = \sum_{pq} s_{pq} a_p^\dagger \tilde{a}_q^\dagger + \frac{1}{(2!)^2}\sum_{pqrs} s_{pqrs} a_p^\dagger a_q^\dagger \tilde{a}_s^\dagger \tilde{a}_r^\dagger + \ldots \tag{3.31}$$

Unlike the fixed-reference CI operator in Eq. 3.22, both the coefficients and the field operators in the covariant ansatz are α- and β-dependent. Accordingly, the operators a_p, $\tilde{a}_p^\dagger$, etc. have non-trivial α and β derivatives. For example, using the thermal Bogoliubov transformation of Eq. 3.7, we see that

$$\frac{\partial a_p^\dagger}{\partial\beta} = \frac{\epsilon_p}{2} x_p y_p \tilde{a}_p, \tag{3.32a}$$

$$\frac{\partial \tilde{a}_p^\dagger}{\partial\beta} = -\frac{\epsilon_p}{2} x_p y_p a_p. \tag{3.32b}$$

Taking these details into considerations and substituting the wave function ansatz, Eq. 3.30, into Eq. 3.2, we obtain the following working equations for the β-evolution

of the CI amplitudes s_0, s_{pq}, etc.,

$$\frac{\partial s_0}{\partial \beta} = -\frac{1}{\mathcal{Z}_0} \langle 0(\alpha,\beta)| \left(\frac{1}{2}\bar{H} + \frac{\partial_{\text{op}} S}{\partial \beta} \right) |0(\alpha,\beta)\rangle \,, \tag{3.33a}$$

$$\frac{\partial s_0}{\partial \beta} = -s_{pq}\frac{\partial s_0}{\partial \beta} - \frac{1}{\mathcal{Z}_0} \langle 0(\alpha,\beta)|\tilde{a}_q a_p \left(\frac{1}{2}\bar{H} + \frac{\partial_{\text{op}} S}{\partial \beta} \right) |0(\alpha,\beta)\rangle \,, \tag{3.33b}$$

and so on. Similarly, for α-evolution, we get

$$\frac{\partial s_0}{\partial \alpha} = \frac{1}{\mathcal{Z}_0} \langle 0(\alpha,\beta)| \left(\frac{1}{2}\bar{N} - \frac{\partial_{\text{op}} S}{\partial \alpha} \right) |0(\alpha,\beta)\rangle \,, \tag{3.34a}$$

$$\frac{\partial s_{pq}}{\partial \alpha} = -s_{pq}\frac{\partial s_0}{\partial \alpha} + \frac{1}{\mathcal{Z}_0} \langle 0(\alpha,\beta)|\tilde{a}_q a_p \left(\frac{1}{2}\bar{N} - \frac{\partial_{\text{op}} S}{\partial \alpha} \right) |0(\alpha,\beta)\rangle \,, \tag{3.34b}$$

and so forth. Here, $\mathcal{Z}_0$ denotes the mean-field partition function, defined in Eq. 2.37, and the effective CI Hamiltonian $\bar{H}$ and number operator $\bar{N}$ are defined as

$$\bar{H} = H(1+S) - (1+S)H_0, \tag{3.35a}$$

$$\bar{N} = NS - SN, \tag{3.35b}$$

and the operator derivative $\partial_{\text{op}} S/\partial x$ (with $x = \alpha, \beta$) denotes the derivative of only the operator parts of S, i.e.,

$$\frac{\partial_{\text{op}} S}{\partial x} = \sum_{pq} s_{pq} \frac{\partial}{\partial x}\left(a_p^\dagger \tilde{a}_q^\dagger\right) + \frac{1}{(2!)^2}\sum_{pqrs} s_{pqrs}\frac{\partial}{\partial x}\left(a_p^\dagger a_q^\dagger \tilde{a}_s^\dagger \tilde{a}_r^\dagger\right) + \ldots \tag{3.36}$$

As with the fixed-reference case, we can integrate Eqs. 3.33 and 3.34 starting from $(\alpha,\beta) = (0,0)$ with the initial conditions

$$s_0 = 0; s_{pq} = 0; s_{pqrs} = 0; \ldots,$$

to the desired temperature and chemical potential. Once again, we consider a covariant thermal CI truncated at single and double quasiparticle excitations (CISD) for all applications. Our primitive implementation of both the fixed-reference and the

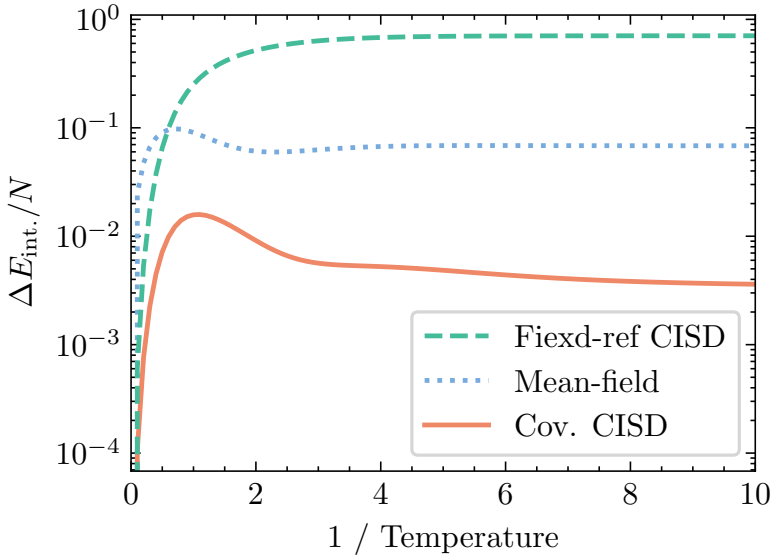

Figure 3.1 : Internal energy error per site for the six-site Hubbard model at $U/t = 2$ and half-filling on average. The results compare thermal mean-field, covariant therma CISD and the fixed-reference counterpart.

covariant formulations of thermal CI is publicly accessible through a GitHub repository [88] where we make use of *drudge* [89] (computer algebra system) to generate equations and codes.

We will see detailed analysis and comments on the performance of thermal CI theory along with thermal CC later in this chapter. However, we would like to highlight the stark difference in the quality of results between fixed-reference and covariant CI theories. In Fig. 3.1, we compare the error in internal energies computed using fixed-reference and covariant thermal CISD for the six-site Hubbard model at $U/t = 2$ and with two electrons on average. Covariant CI absolutely outperforms the same level of fixed-reference CI, except near $\beta = 0$. In fact, fixed-reference theory is even inferior to thermal mean-field results. This is because as we evolve away from $\beta_0 = 0$, which is used to construct the reference state in the fixed-reference

theory, the mean-field contribution to any other property remains constant, and all the temperature dependence and correlation effects need to be taken care of by the CI operator. Analogous to the reference-dependent behavior of zero temperature ground-state CI, such a method would perform poorly compared to one with a β-dependent mean-field reference. Given the substandard quality of results, for the remainder of this thesis, we will focus our attention solely on the covariant wave function theories.

3.4 Coupled cluster theory

We noted in Eq. 2.26 that the CC expectation value of any operator $\mathcal{O}$ can be evaluated as an asymmetric expectation value,

$$\langle \mathcal{O} \rangle_{\mathrm{CC}} = \frac{\langle \Psi' | \mathcal{O} | \Psi \rangle}{\langle \Psi' | \Psi \rangle}, \tag{3.37}$$

where both $\langle \Psi' |$ and $| \Psi \rangle$ states are approximations to the same wave function; while the *ket* is approximated with a truncated CC wave function ansatz, the *bra* is approximated as a truncated CI expansion. For thermal coupled cluster, we employ a similar parametrization, i.e., a CC *ket* and a CI *bra* which evolve according to Eq. 3.2 and their adjoints respectively.

Recall that the mean-field thermal state (Eq. 3.5) has the form of a BCS state, i.e., p^{th}-orbitals in the physical and auxiliary Hilbert spaces, $\mathcal{H}$) and $\tilde{\mathcal{H}}$, are coupled in just the same way as two opposite momentum single-particle levels in a BCS-wave function. Given this correspondence of $|0(\alpha, \beta)\rangle$ with a BCS, we parametrize the *ket* state as an exponential of quasiparticle creation operators acting on the mean-field

thermal reference,

$$|\Psi\rangle = e^{S} |0(\alpha,\beta)\rangle\,, \tag{3.38a}$$

$$S = s_0 + \sum_{p,q} s_{pq} a_p^\dagger \tilde{a}_q^\dagger + \frac{1}{(2!)^2} \sum_{p,q,r,s} s_{pqrs} a_p^\dagger a_q^\dagger \tilde{a}_s^\dagger \tilde{a}_r^\dagger + \ldots \tag{3.38b}$$

This also follows from the ground-state quasiparticle coupled cluster theory. [90] On the other hand, the *bra* state, as in the traditional CC formalism, is approximated using a CI expansion, i.e.

$$\langle\Psi'| = \langle 0(\alpha,\beta)| \, (1+Z) e^{z_0} e^{-S}, \tag{3.39}$$

and as explained in Eq. 2.29, it can be expressed as an effective CI wave function

$$\langle\Psi'| = \langle 0(\alpha,\beta)| \, (1+W) e^{w_0}, \tag{3.40a}$$

$$W = \sum_{p,q} w_{pq} \tilde{a}_q a_p + \frac{1}{4} \sum_{p,q,r,s} w_{pqrs} \tilde{a}_r \tilde{a}_s a_q a_p + \ldots \tag{3.40b}$$

The evolution equations and associated technical details for this covariant thermal CI ansatz have been discussed in Section 3.3, and the same can be employed to obtain the evolution equations for w_0, w_{pq}, w_{pqrs}, etc.

For the evolution of $|\Psi\rangle$, substituting the CC ansatz from Eq. 3.38a into Eq. 3.2 gives

$$e^{-S} \left(\frac{\partial}{\partial\alpha} e^{S} \right) |0(\alpha,\beta)\rangle = \frac{1}{2} \left(e^{-S} N e^{S} - N \right) |0(\alpha,\beta)\rangle\,, \tag{3.41a}$$

$$e^{-S} \left(\frac{\partial}{\partial\beta} e^{S} \right) |0(\alpha,\beta)\rangle = -\frac{1}{2} \left(e^{-S} H e^{S} - H_0 \right) |0(\alpha,\beta)\rangle\,. \tag{3.41b}$$

Analogous to the CI theory, the evolution equations for the amplitudes can be obtained by left projecting Eq. 3.41 against various excited quasiparticle states.

Wilcox identity

In order to simplify Eq. 3.41 and obtain evolution equations for CC amplitudes, we need to overcome the hurdle that the derivative of the cluster operator does not

commute with the operator itself, i.e.

$$\left[\frac{\partial S}{\partial x}, S\right] \neq 0, \tag{3.42}$$

for $x \in \{\alpha, \beta\}$. This introduces extra complications in computing the α- or β-derivative of the the exponential operator e^S. To address this derivative, we make use of the Wilcox identity, [91] which states that the derivative of the exponential of an operator M with respect to a scalar parameter λ can be evaluated as

$$\frac{\partial}{\partial \lambda} e^M = \int_0^1 dy\, e^{(1-y)M} \frac{\partial M}{\partial \lambda} e^{yM}. \tag{3.43}$$

Using the Wilcox identity, the expressions on the left-hand side of Eq. 3.41 become

$$e^{-S}\left(\frac{\partial}{\partial x} e^S\right) = \int_0^1 dy\, e^{-yS} (\partial_x S) e^{yS}, \tag{3.44a}$$

$$= (\partial_x S) + \frac{1}{2!}[(\partial_x S), S] + \frac{1}{3!}\left[[(\partial_x S), S], S\right] + \ldots, \tag{3.44b}$$

where we have used the shorthand ∂_x for $\partial/\partial x$, and employed the Baker-Campbell-Hausdorff expansion in going from Eq. 3.44a to 3.44b. Finally, breaking the derivative $\partial_x S$ into the amplitude ($\partial_{\text{amp}} S$) and operator ($\partial_{\text{op}} S$) derivatives,

$$\frac{\partial S}{\partial x} = \frac{\partial_{\text{amp}} S}{\partial x} + \frac{\partial_{\text{op}} S}{\partial x}, \tag{3.45a}$$

$$\frac{\partial_{\text{amp}} S}{\partial x} = \sum_{pq} \frac{\partial s_{pq}}{\partial x} a_p^\dagger \tilde{a}_q^\dagger + \frac{1}{(2!)^2} \sum_{pqrs} \frac{\partial s_{pqrs}}{\partial x} a_p^\dagger a_q^\dagger \tilde{a}_s^\dagger \tilde{a}_r^\dagger + \ldots \tag{3.45b}$$

$$\frac{\partial_{\text{op}} S}{\partial x} = \sum_{pq} s_{pq} \frac{\partial}{\partial x}\left(a_p^\dagger \tilde{a}_q^\dagger\right) + \frac{1}{(2!)^2} \sum_{pqrs} s_{pqrs} \frac{\partial}{\partial x}\left(a_p^\dagger a_q^\dagger \tilde{a}_s^\dagger \tilde{a}_r^\dagger\right) + \ldots \tag{3.45c}$$

and realizing that the former commutes with S, we can compactly write the left-hand side of Eq. 3.41 as

$$e^{-S}\left(\partial_x e^S\right) = \frac{\partial_{\text{amp}} S}{\partial x} + D_x, \tag{3.46}$$

where D_x is derived from the operator derivative of S, and is defined as

$$D_x = \int_0^1 dy\, e^{-yS} \frac{\partial_{\text{op}} S}{\partial x} e^{yS}, \tag{3.47}$$

where the integration over y in the second equation can be carried out analytically, as explained in Eq. 3.44b

Evolution equations for thermal CC

With the help of the Wilcox identity and the simplifications highlighted above, Eq. 3.41 can be further simplified into

$$\frac{\partial_{\text{amp}} S}{\partial \alpha} |0(\alpha,\beta)\rangle = \left[\frac{1}{2}\left(e^{-S} N e^{S} - N\right) - S_\alpha\right] |0(\alpha,\beta)\rangle \,, \tag{3.48a}$$

$$\frac{\partial_{\text{amp}} S}{\partial \beta} |0(\alpha,\beta)\rangle = -\left[\frac{1}{2}\left(e^{-S} H e^{S} - H_0\right) + S_\beta\right] |0(\alpha,\beta)\rangle \,, \tag{3.48b}$$

which can then be left-projected with various thermal quasiparticle states to yield a set of differential equations governing the evolution of the S-amplitudes in the α-β space. Complete expressions for the CCSD evolution equations are included in Appendix A.

3.5 Implementation details

3.5.1 Integration

The Dormand-Prince algorithm, [92,93] a fourth-order Runge-Kutta method with an adaptive step size, has been employed for integrating the resulting set of differential equations, both for CI and CC. The integration step size is adaptively modified so as to keep the relative error in evolution within 10^{-6}. Furthermore, a tolerance value of 10^{-5} in the number of electrons is used to find the target chemical potential.

While computing properties at a fixed electron filling, we first evolve in β to the desired temperature while treating α as a constant. After this integration, the number of electrons in the thermal state moves away from the desired value. To

find the correct target α that restores the right average electron number, we use a bisection scheme and integrate along the α-direction while keeping β fixed.

3.5.2 Choice of thermal mean-field

As mentioned earlier, for the covariant formulations of correlated wave function theories, we use a mean-field Hamiltonian of the form $H_0 = \sum_p \epsilon_p c_p^\dagger c_p$ to construct the mean-field thermal reference state $|0(\alpha, \beta)\rangle$. There are many different ways to pick this mean-field Hamiltonian. In thermal HF theory, [31, 32] one uses an H_0 that optimizes the grand potential, and therefore, H_0 is a function of α and β. While such a choice may yield an excellent mean-field thermal reference state, it will result in highly convoluted expressions for the mean-field evolution as well as the operator derivatives and is beyond the scope of current work.

In our implementation, we use ground-state HF, which may or may not preserve the symmetries, to construct the energy eigenvalues used in H_0. Using an α- and β-independent H_0 is analogous to the imaginary-time interaction picture formalism and simplifies our implementation because

1. an α- and β-independent H_0 leads to clean analytical forms for the mean-field evolution operator as well as the α- and β-derivatives of the thermal quasiparticle operators, and

2. a diagonal form of H_0 yields a straightforward thermal Bogoliubov transformation in Eq. 3.7.

3.6 Results

Armed with the working equations, we are now in a position to assess the quality of various thermal wave function approximations. We will focus our attention on the application of covariant thermal wave function theories, namely mean-field, CI with single (CIS) and double (CISD) excitations, and CCSD, to various electronic systems, *viz.* the one-dimensional Hubbard model, the pairing or reduced BCS model, as well as chemical systems (atomic Beryllium and molecular H_2). In order to make correspondence with the canonical ground-state limit, we present results for all of these systems with a fixed number of particles on average. We compare our results with the exact grand canonical ensemble averages.

3.6.1 One-dimensional Hubbard model

First, we compare thermal mean-field, CIS, CISD and, CCSD against exact results for the temperature dependence of internal energy in the 1D Hubbard model (c.f. Section 2.1.2 for more details) with periodic boundary conditions in the grand canonical ensemble. We will consider different values of correlation strength (or U/t) for the Hubbard model.

Let us start with a simple two-site Hubbard model at $U/t = 1$ with two electrons on average. In Fig. 3.2, we plot error in internal energy per electron, with respect to the exact results, calculated using the thermal mean-field, covariant CI, and CC methods. All the methods start with zero errors at $\beta = 0$ (due to the exactness of the underlying mean-field) but start deviating from the exact results at finite temperatures. Both mean-field and CIS results show large errors among all the results; it appears that thermal CIS only marginally improves over mean-field. On the other hand, thermal CISD and CCSD improve significantly over mean-field as well as CIS.

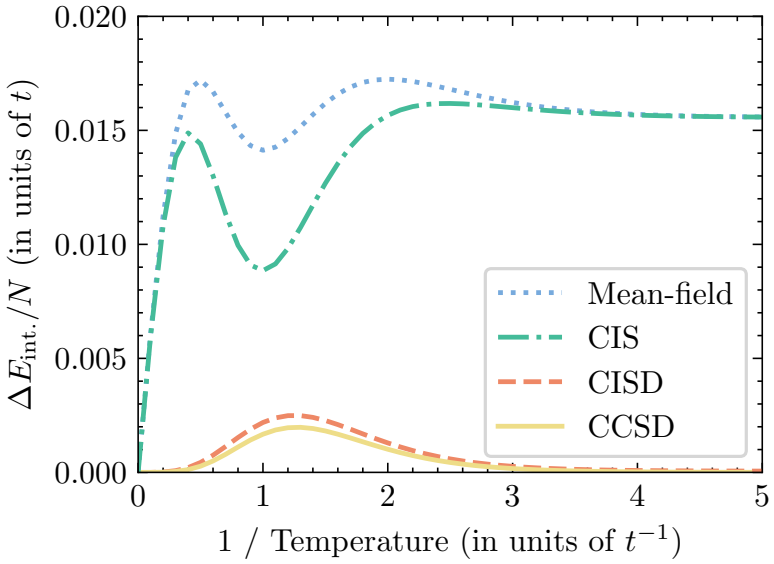

Figure 3.2 : Error per particle in internal energy for the two-site Hubbard model with $U/t = 1$ and half-filling on average. The results compare thermal HF, covariant CIS, CISD, and CCSD theories.

In the zero-temperature limit, thermal CISD and CCSD converge to the exact ground-state energy, the same as standard ground-state CISD and CCSD. This demonstrates that in the limit of zero-temperature, i.e., as $\beta \to \infty$, thermal mean-field reduces to the canonical, zero-temperature ground-state restricted HF (RHF), which was the choice of H_0, to begin with. Similarly, thermal CI and CC approach the corresponding ground-state restricted CI and CC. This also explains why thermal CISD and CCSD become exact in the zero-temperature limit: both are exact for two-particle systems. On the other hand, thermal CISD/CCSD are generally not exact at intermediate values of β, as is reflected in the finite errors in Fig. 3.2. This is because singles and doubles are insufficient to parameterize any general state in the grand-canonical ensemble.

Figure 3.3 presents total internal energy and error in internal energy for the six-

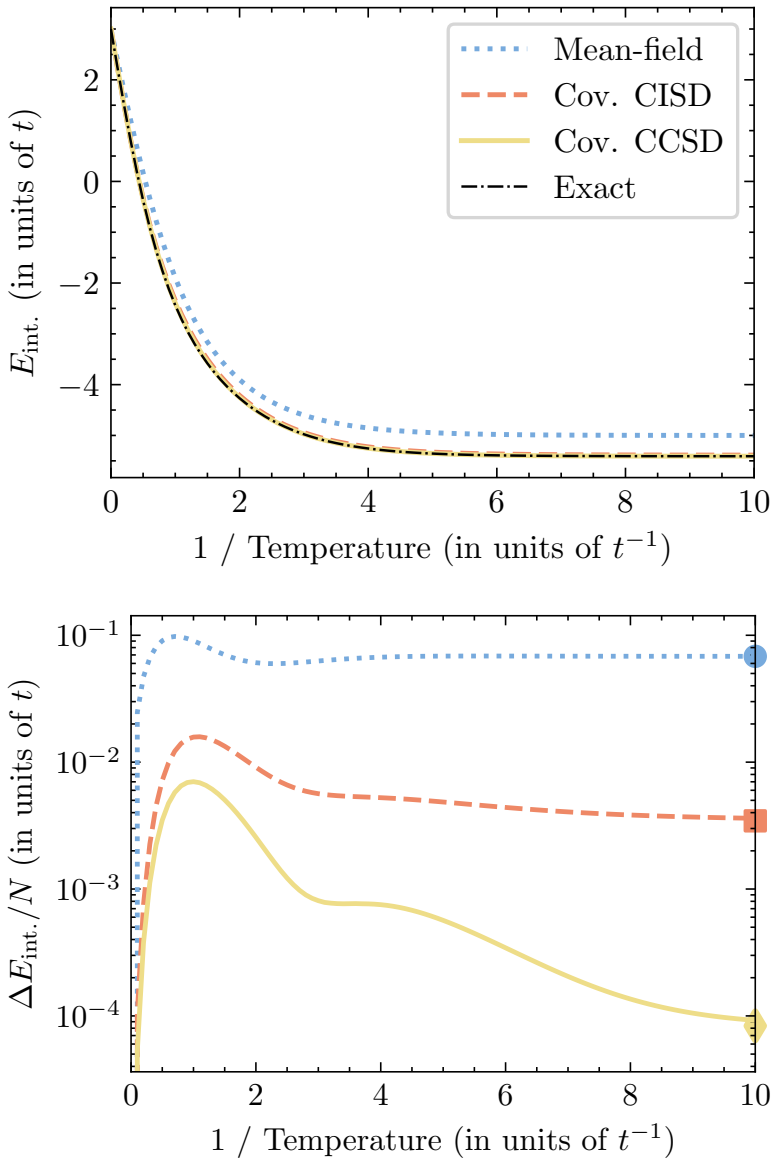

Figure 3.3 : Total internal energy (top panel) and associated errors per electron (bottom panel) for the six-site Hubbard model with $U/t = 2$ and half-filling on average. The results compare thermal HF, covariant CISD, and CCSD. The solid circle, square, and diamond on the right y-axis of the are the ground-state RHF, RCISD and RCCSD energy errors per particle.

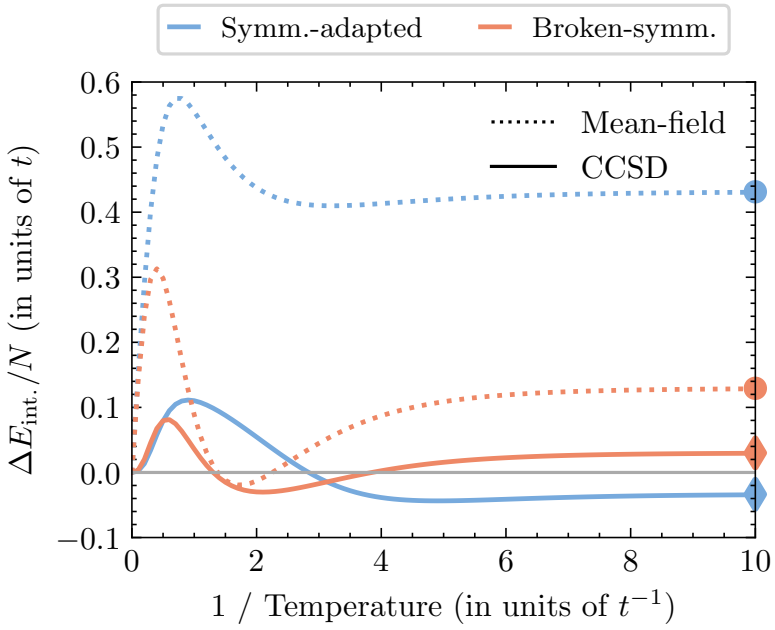

Figure 3.4 : Error in internal energy per electron for thermal mean-field and covariant CCSD, each constructed using a symmetry-adapted and broken-symmetry H_0, for the six-site Hubbard model with $U/t = 5$ at half-filling on average. The blue circle and diamond on the right y-axis indicate ground-state RHF and RCCSD energy error per particle, while the red ones plot the same for UHF and UCCSD.

site Hubbard model at $U/t = 2$ and half filling on average. Again, we consider only the covariant formalism. The story is similar to the simpler two-site model: there are large errors in the mean-field and CIS results, which are substantially reduced by thermal CISD and CCSD. For large β, all the results approach those corresponding to the respective ground-state theories.

In all the applications so far, H_0 is constructed using RHF energy eigenvalues, which is why in the zero-temperature limit, thermal HF approaches ground-state RHF and thermal CCSD approaches ground-state RCCSD. In the strongly correlated regime, where zero-temperature RCCSD fails to converge, the evolution of thermal CCSD would eventually diverge. Such an issue can be avoided by using unrestricted

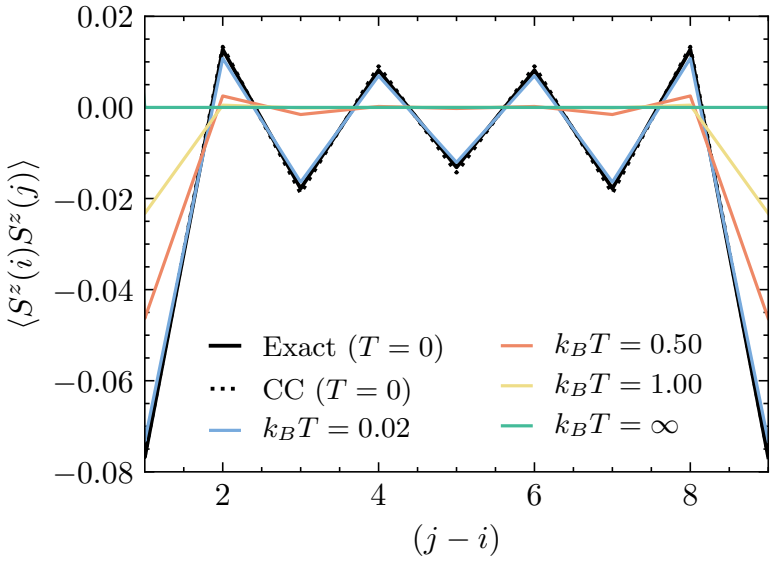

Figure 3.5 : Trends in z-component spin-spin correlation function for the ten-site Hubbard model with $U/t = 2$ at various temperatures k_BT, and a fixed chemical potential $\mu = 0.9$ (which ensures half-filling in the $k_BT \to 0$ limit). The results were computed using thermal CCSD. Exact and RCCSD results for the ground-state correlation functions are also included for reference.

HF (or UHF) energy eigenvalues to construct H_0 and therefore $|0(\alpha,\beta)\rangle$. Fig. 3.4 shows the performance of RHF and UHF-based thermal CCSD for the six-site Hubbard model at $U/t = 5$ and half-filling on average. As usual, we compare errors in internal energies with respect to exact results. For the selected value of U/t, both RCCSD and UCCSD are well defined for the ground state. The thermal theories also approach their respective ground-state analogs in the infinite β limit.

In addition to the internal energy, we can also compute other physical properties such as correlation functions as a function of temperature and chemical potential. In Figure 3.5, we present thermal CCSD results for the z-component spin-spin correlation function, defined as

$$\chi(i,j) = \langle S^z(i)S^z(j)\rangle\,, \tag{3.49}$$

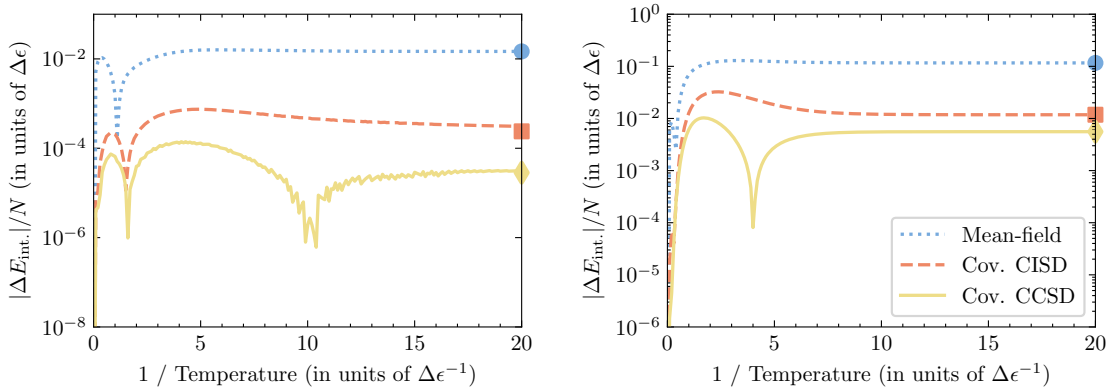

(a) 6-levels, $G = 0.2$

(b) 6-levels, $G = 0.5$

Figure 3.6 : Absolute error in internal energy per electron for the six-level Pairing model and (a) $G = 0.2$, and (b) $G = 0.5$, at half-filling on average. The results compare thermal mean-field, covariant CISD, and CCSD. The markers on the right y-axis indicate the corresponding ground-state errors.

for the ten-site Hubbard model at $U/t = 2$. Note that $S^z(i)$ denotes the z-directional spin operator at the i^{th} lattice site, and is defined as

$$S^z(i) = \frac{1}{2}\sum_{\mu\nu} c^\dagger_{i\mu}\tau^z_{\mu\nu}c_{i\nu} = \frac{1}{2}\left(c^\dagger_{i\uparrow}c_{i\uparrow} - c^\dagger_{i\downarrow}c_{i\downarrow}\right), \tag{3.50}$$

where τ^z is the z Pauli matrix. The expectation values are computed using linear-response density matrices, and just as for the internal energy, orbital relaxation effects (i.e., optimization of the reference state $|0(\alpha,\beta)\rangle$) have not been considered. As one would expect, at extremely high temperatures, there is no correlation between adjacent spins. As T is reduced, the correlation appears and becomes maximal in the zero-temperature limit. To make correspondence with the ground-state, we also plot the exact and CCSD estimate of the ground-state correlation function. We can clearly see that thermal CCSD properties approach the appropriate ground-state CCSD properties in the limit $\beta \to \infty$.

Pairing model

Next, we consider the reduced BCS or the pairing model (c.f. Section 2.1.2 for details). The pairing model is characterized by the energy levels ϵ_p and the pariing interaction G. Here we choose the energy levels with a uniform spacing of 1 unit, i.e., $\Delta\epsilon = \epsilon_{p+1} - \epsilon_p = 1$. Figure 3.6a describes the absolute error in internal energy per electron for the six-level pairing model with $G = 0.2$ (weakly correlated) as a function of temperature at half-filling on average. Figure 3.6b plots similar results for $G = 0.5$ (near-critical regime). Again, we use RHF eigenvalues and integrals to construct H_0 and H, and we see that the covariant thermal CCSD improves significantly over both the HF and CISD. The kinks in the error curves correspond to the points where the CI/CC and exact energy curves intersect. This is a result of the non-variational character of the internal energy. Meanwhile, the wiggly nature of the CC error curve in Fig. 3.6a is because we use a precision of 10^{-5} in fixing the number electrons and relative tolerance value of 10^{-6} in the evolution.

3.6.2 Molecular systems

In Figs. 3.7 and 3.8, we plot the error in internal energy, as a function of temperature, for atomic Beryllium and molecular Hydrogen. The chemical potential is adjusted so as to maintain charge neutrality in the systems. These results show trends similar to those observed for Hubbard and Pairing. The H_2 molecule is considered at a bond length of 0.74Å, and we employ STO-3G basis sets for both Be and H_2.

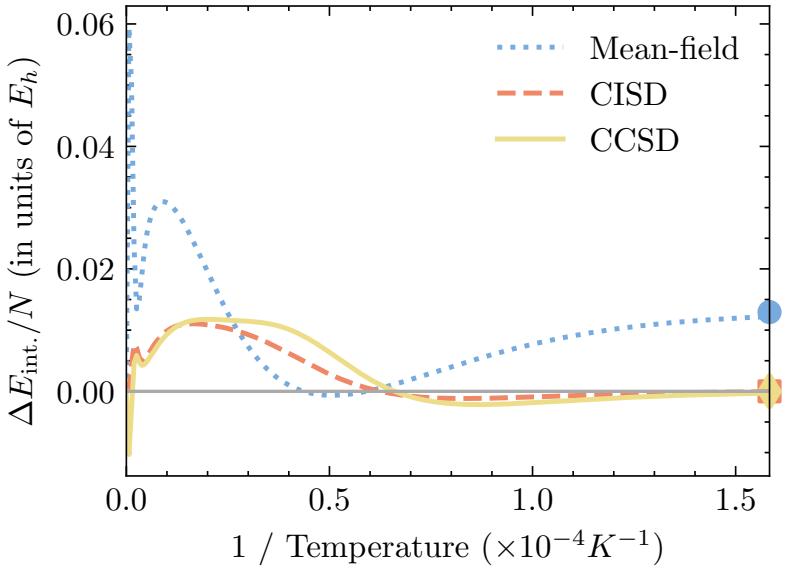

Figure 3.7 : Error in internal energy per electron for Be atom, in STO-3G basis, as function of inverse temperature. The plot compares thermal mean-field, covariant CISD and CCSD. The colored markers on the right y-axis denote the error per particle in the corresponding ground-state theories.

3.7 Summary

We have utilized the framework of thermofield dynamics (in the grand canonical ensemble) to derive finite-temperature generalizations of well-known ground-state wave function theories, *viz.* mean-field, CI, and CC. These theories were benchmarked on different models and *ab-initio* many-electron systems. The relative performance of thermal wave function methods is analogous to their ground-state counterparts, i.e., thermal CI improves upon mean-field while CC outperforms both of the former in weak-to-moderately correlated systems. The asymptotic computational scaling of thermal methods is similar to the ground-state theories: both thermal CI and CC scale as $\mathcal{O}(N^6)$, where N is the number of spin-orbitals in the system. The number of grid points used to integrate the first-order initial value problem, which governs

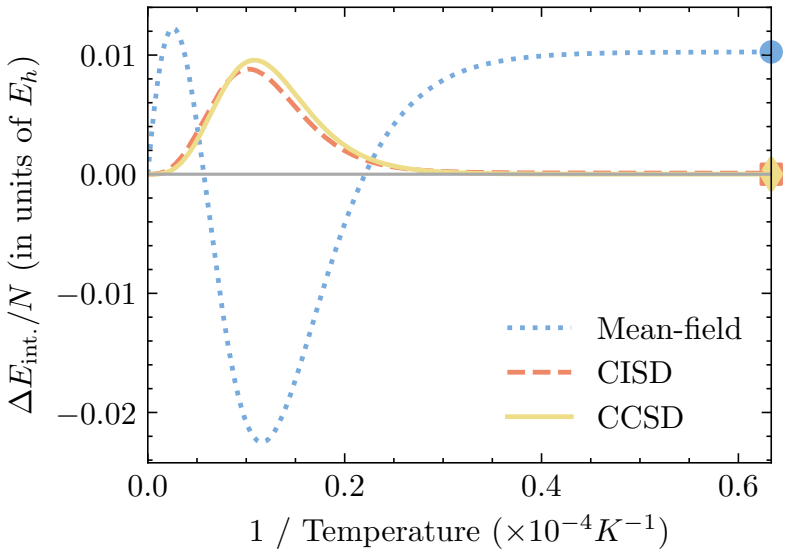

Figure 3.8 : Internal energy error per particle for the Hydrogen molecule, in the STO-3G basis and at a bond length of 0.74Å, as function of inverse temperature. The results compare thermal HF, covariant CISD and CCSD. The markers on the right y-axis indicate errors in the corresponding ground-state theories.

the CI/CC amplitudes, adds a modest pre-factor to the scaling. So does the fact that we work within the basis of thermal quasiparticles. As would be expected of any well-defined theory, all the thermal methods converge to their respective ground-state counterparts in the limit $\beta \to \infty$.

Chapter 4

Thermal wave function theories for the canonical ensemble

Thermal properties of many-body systems can be computed either in the canonical ensemble or the grand canonical ensemble. The choice of the ensemble makes no practical difference in the final result in large systems. It does so, however, for a finite system. This is because the relative fluctuation in particle number in the grand canonical ensemble scales as the inverse square root of particle number itself, i.e.

$$\frac{\sqrt{\langle N^2 \rangle_{\text{g.can.}} - \langle N \rangle^2_{\text{g.can.}}}}{\langle N \rangle_{\text{g.can.}}} \sim \frac{1}{\sqrt{\langle N \rangle_{\text{g.can.}}}}. \tag{4.1}$$

Therefore, the fluctuation effects related to the particle number vanishes in the limit $\langle N \rangle_{\text{g.can.}} \to \infty$, where $\langle \ldots \rangle_{\text{g.can.}}$ denotes thermal expectation values in the grand canonical ensemble.

In Chapter 1, we highlighted the wide variety of methods available to study thermal properties of quantum systems, e.g., thermal Hartree-Fock, perturbation theories, Green's function methods, QMC, etc. Most of them work in the grand canonical ensemble. In Chapter 3, we also explored a grand canonical finite-temperature wave function formalism (mean-field, CI and CC) for fermionic systems.

In contrast, canonical ensemble techniques are scarce, and even fewer are suitable for efficient application to correlated electronic systems. One way to enforce a fixed number of particles is by introducing a second Lagrange multiplier μ_2 for the fluctuation operator, in much the same spirit as the chemical potential μ_1 acts as a

Lagrange multiplier to fix the number of particles. That is, one can either define a generalization of the density operator as

$$\rho = \exp\left[-\beta\left(H - \mu_1(N - N_0) - \mu_2(N^2 - N_0^2)\right)\right], \tag{4.2}$$

where the parameters μ_1 and μ_2 enforce the constraints,

$$\langle N\rangle_{\text{g.can.}} = N_0, \quad \text{and}, \quad \langle N^2\rangle_{\text{g.can.}} = N_0^2, \tag{4.3}$$

or introduce corrections to the grand canonical ensemble averages by subtracting contributions from undesirable number sectors in the Hilbert space. [94] While this provides the convenience of using several available grand canonical methods, such simultaneous optimization problems can be numerically tedious as the optimized values of μ_2 are generally very large (ideally infinite). This has also been observed in the context of spin-projection. [95] Alternatively, we can evaluate the ensemble averages in the appropriate number sector to begin with, e.g. in the minimally entangled typical thermal states algorithm, [50, 96] canonical ensemble perturbation theory, [36] projection based techniques, [97–100] and canonical ensemble auxiliary field QMC. [101]

The canonical ensemble is better suited for a wide variety of problems, which involve isolated finite systems with a fixed number of particles. Examples of such systems include molecules in warm gaseous phase (of interest in geochemistry), [30] ultra-cold chemical systems, [28, 29] quantum wires with number conserving Majorana modes, [102–104] and superconductivity in small grain systems. [105] Besides, the canonical ensemble provides a potential computational advantage over grand canonical alternatives since it eliminates the need to find the chemical potential to adjust particle number. Evidently, a robust and convenient framework to study canonical-ensemble finite-temperature properties of finite many-body fermionic systems is desirable.

In this chapter, we will make use of the number-projection operator and construct a canonical ensemble formalism for thermofield-based wave function theories. The resultant canonical ensemble thermal state obeys an imaginary-time evolution equation similar to the one discussed for the grand canonical ensemble in Chapter 3, which can be integrated at various levels of approximation. The mean-field approximation to this thermal state is a number-projected BCS wave function, also known as the antisymmetrized geminal power (AGP) state. [106] A similar number-projected BCS theory for the canonical thermal state was also proposed by the authors of Refs. 97–99. Mean-field description, however, misses out on a lot of important, correlation-driven physics. Therefore, the aim here is to construct a thermal framework for correlated wave function theories. We restrict our discussion to electronic systems, but generalization to other fermionic and bosonic systems is straightforward.

4.1 Canonical ensemble state

In Chapter 2, we saw that the identity state in the canonical ensemble can be constructed by projecting the grand canonical identity state against the desired particle number N_0 (Eq. 2.40b). The canonical ensemble thermal state at any β-value can similarly be constructed as

$$|\Psi(\beta)\rangle_{\text{canonical}} = \mathcal{P}_{N_0} |\Psi(\beta)\rangle_{\text{grand canonical}} , \tag{4.4}$$

where $\mathcal{P}_{N_0}$ projects $|\Psi(\beta)\rangle_{g.can.}$ onto the Fock-space with N_0 electrons. The particle-conserving property of H implies that $[H, \mathcal{P}_{N_0}] = 0$, and we get

$$|\Psi(\beta)\rangle_{\text{canonical}} = e^{-\beta H/2} |\mathbb{I}\rangle_{\text{canonical}} . \tag{4.5}$$

Therefore, the resulting canonical thermal state obeys an imaginary-time evolution equation analogous to its grand-canonical counterpart,

$$\frac{\partial}{\partial\beta}\left|\Psi(\beta)\right\rangle_{\text{canonical}} = -\frac{1}{2}H\left|\Psi(\beta)\right\rangle_{\text{canonical}}. \tag{4.6}$$

For the remainder of this chapter, we will drop the explicit subscripts and assume $|\Psi(\beta)\rangle$ to be the canonical ensemble thermal state unless stated otherwise.

4.2 Mean-field theory

Akin to the grand-canonical theory, exact integration of Eq. 4.6 is not feasible except for very small unrealistic systems. Approximations such as mean-field theory, perturbation, CI, etc., are therefore necessary. In the mean-field approximation, we use an effective one-body Hamiltonian to perform the evolution in Eq. 4.5 or construct the thermal state in Eq. 4.6, i.e. $H \approx H_0$. Following our work with the grand-canonical ensemble, we use $H_0 = \sum_p \epsilon_p c_p^\dagger c_p$, where neither ϵ_p's nor the fermion operators carry any temperature dependence. The mean-field state then becomes

$$\begin{aligned}
\left|\Psi_0(\beta)\right\rangle &= e^{-\beta H_0/2}\left|\mathbb{I}\right\rangle_{\text{canonical}} && \text{(4.7a)}\\
&= \mathcal{P}_{N_0}\left|0(\alpha=0,\beta)\right\rangle, && \text{(4.7b)}\\
&= \mathcal{P}_{N_0}\prod_p\left(1+e^{-\beta\epsilon_p/2}c_p^\dagger\tilde{c}_p^\dagger\right)\left|-;-\right\rangle, && \text{(4.7c)}\\
&= \mathcal{P}_{N_0}\prod_p\left(1+\eta_p P_p^\dagger\right)\left|-;-\right\rangle, && \text{(4.7d)}\\
&= \frac{1}{N_0!}\left(\Gamma_\beta^\dagger\right)^{N_0}\left|-;-\right\rangle = \left|\Psi_{AGP}(\beta)\right\rangle, && \text{(4.7e)}
\end{aligned}$$

where $\eta_p = e^{-\beta\epsilon_p/2}$, and we have identified $P_p^\dagger = c_p^\dagger\tilde{c}_p^\dagger$ as the pair-creation operator. As already noted, the un-projected product state in Eq. 4.7c is a BCS state and its number-projected version is well known as AGP, with the geminal creation operator

$\Gamma^\dagger_\beta$ defined as

$$\Gamma^\dagger_\beta = \sum_p \eta_p P^\dagger_p. \tag{4.8}$$

Identification of thermal mean-field state as an AGP is interesting and timely since a lot of developments have recently been reported on efficient evaluation of AGP density matrices and geminal-based correlated wave function theories. [107–111]

An improved mean-field description can also be obtained by optimizing both ϵ_p's and the one-electron basis to find an H_0 that minimizes the Helmholtz free energy, in much the same way as Mermin's thermal Hartree Fock theory. 31 This is also explored in Refs. 97–99.

4.3 Framework for correlated wave function theories

Several approximate wave function methods are available to study ground-state properties of correlated electronic systems, most of which add correlation on a mean-field reference. As we have seen for the case of the grand canonical ensemble in Chapter 3, thermofield dynamics allows for a direct generalization of these methods to finite-temperature. For correlated theories in the presence of number projection operator, there are two ways to parameterize the canonical ensemble thermal state: *projection after correlation* (PAC), and *correlation after projection* (CAP).

4.3.1 Projection v/s correlation

In PAC, we first construct an approximate grand-canonical thermal state by adding correlation on a number non-conserving mean-field reference (thermal BCS in our case) and then perform the number-projection,

$$|\Psi\rangle \simeq \mathcal{P}_{N_0}\Omega(\beta)\,|0(\beta)\rangle\,; \quad |0(\beta)\rangle = e^{-\beta H_0/2}\,|\mathbb{I}\rangle_{\text{g. can.}}\,. \tag{4.9}$$

The correlation operator Ω is built out of BCS quasiparticles, [90, 112] and the unprojected part of the thermal state, $\Omega(\beta)|0(\beta)\rangle$, looks like a standard single-reference wave function discussed in Chapter 3. This simplifies the process of correlating the reference. In order to efficiently carry out the projection, we use an integral form for the projection operator, [113–115] i.e.

$$\mathcal{P}_{N_0} = \frac{1}{2\pi}\int_0^{2\pi} d\phi e^{i\phi(N_0-N)}. \tag{4.10}$$

Computing matrix elements and overlaps in the presence of $\mathcal{P}$ involves the use of transition density matrices and can be tedious (see e.g., Refs. 116–120). For CAP, we use the thermal AGP in Eq. 4.7 as the reference and add correlation using a number-conserving wave operator,

$$|\Psi\rangle \simeq \Lambda(\beta)\,|\Psi_{AGP}(\beta)\rangle = \Lambda(\beta)\mathcal{P}_{N_0}\,|0(\beta)\rangle\,. \tag{4.11}$$

Contrasting with PAC, the projection problem here is trivial but adding correlation becomes complicated.

Both of these techniques have been explored extensively in symmetry projected ground-state methods. [108–111, 117, 119–123] Here, we present an example for each: a finite-temperature generalization of the number-projected CI, along the lines discussed by Tsuchimochi et al. in Ref. 117, and an imaginary-time perturbation theory with thermal AGP as the reference, as explored in Refs. 108–110.

4.4 Number-projected configuration interaction

For the number-projected thermal CI theory, we approximate the canonical ensemble thermal state by projecting the covariant grand-canonical CI wave function in Eq. 3.30. While the fixed-reference state may also be used, we have already ruled out

its usefulness in the previous chapter. Therefore, the number-projected thermal CI state is written as

$$|\Psi(\beta)\rangle = \mathcal{P}_{N_0} e^{t_0} \left(1 + T\right) |0(\beta)\rangle \,, \tag{4.12}$$

where, as usual, $|0(\beta)\rangle$ is the thermal BCS state at inverse temperature β, t_0 keeps track of the norm of the state (related to the grand potential) and T creates quasiparticle excitations on the BCS,

$$T = \sum_{pq} t_{pq} a_p^\dagger \tilde{a}_q^\dagger + \frac{1}{4} \sum_{pqrs} t_{pqrs} a_p^\dagger a_q^\dagger \tilde{a}_s^\dagger \tilde{a}_r^\dagger + \ldots . \tag{4.13}$$

The CI amplitudes can be determined in two different ways. We can compute them in the grand-canonical ensemble, as discussed in Chapter 3 or Ref. 68, and then perform a one-shot projection. This approach is generally known as *projection after variation* (PAV). Alternatively, the amplitudes can be computed in the presence of the projection operator by solving the imaginary-time evolution equation. The second approach is known as *variation after projection* (VAP). VAP allows for more variational freedom and thus performs better than PAV. We will focus our attention on VAP hereafter.

Substituting this CI ansatz into Eq. 4.6 and evaluating overlaps of the resulting equation against the ground and excited BCS states, we get

$$\begin{aligned} \int_0^{2\pi} d\phi \, \langle 0(\beta)| \nu e^{i\phi(N_0 - N)} \left((1+T) \frac{dt_0}{d\beta} + \frac{dT}{d\beta} \right) |0(\beta)\rangle \\ = \int_0^{2\pi} d\phi \, \langle 0(\beta)| \nu e^{i\phi(N_0 - N)} \bar{H} |0(\beta)\rangle, \end{aligned} \tag{4.14}$$

where $\bar{H}$ is the effective Hamiltonian, defined as

$$\bar{H} = -\frac{1}{2} \Big(H(1+T) - (1+T) H_0 \Big), \tag{4.15}$$

and ν takes values from $\{1, \tilde{a}_q a_p, \tilde{a}_r \tilde{a}_s a_q a_p, \ldots\}$ to construct ground and excited BCS states for the bra. Both the amplitudes as well as the quasiparticle operators are

functions of temperature, therefore the β-derivative can be broken down into the derivative of the amplitudes and that of the operator parts,

$$\frac{dT}{d\beta} = \frac{d_{amp}T}{d\beta} + \frac{d_{op}T}{d\beta}. \tag{4.16}$$

We can rewrite Eq. 4.14 as a system of first-order ODEs that govern the evolution of the CI-amplitudes,

$$\sum_{\mu} A_{\nu\mu} \cdot \frac{\partial t_\mu}{\partial \beta} = B_\nu, \tag{4.17}$$

where the overlap matrix A is defined as

$$A_{\nu\mu} = \int_0^{2\pi} d\phi \, \langle \nu(\beta)| e^{-i\phi(N-N_0)} \mathcal{L}_\mu |0(\beta)\rangle, \tag{4.18a}$$

$$\text{with} \quad \mathcal{L}_\mu = \begin{cases} 1+T, & \mu = 1 \\ \mu, & \mu \in \{a_p^\dagger \tilde{a}_q^\dagger,\ a_p^\dagger a_q^\dagger \tilde{a}_s^\dagger \tilde{a}_r^\dagger\} \end{cases}, \tag{4.18b}$$

and the driver vector on the right hand side B_ν is given by

$$B_\nu = \int_0^{2\pi} d\phi \, \langle \nu(\beta)| e^{-i\phi(N-N_0)} \mathcal{R} |0(\beta)\rangle, \tag{4.19a}$$

$$\mathcal{R} = \bar{H} - \frac{d_{op}T}{\partial \beta}. \tag{4.19b}$$

Here, we have used ν, μ as a composite notation for the ground and excited quasiparticle states. Equation 4.17 can be integrated starting from $\beta = 0$, where $T = 0$ is the exact initial condition. Hereafter, we will work with number-projected CI with double excitations only (CID). The number-projected quasiparticle CID theory spans the same section of the Hilbert space as number-projected quasiparticle CISD. In fact, CISD is an over-parametrizes of the number-projected state since the partial traces of the double-excitation operator lead to single-excitation and constant terms (see Appendix B for a mathematical proof).

4.5 Imaginary-time perturbation theory

For correlation after projection method, a numerical integration to perform the projection is not required as it uses a strictly number conserving state, the thermal AGP, as the reference. As an example for this approach, we consider the imaginary-time perturbation theory (PT), where we partition the Hamiltonian as $H = H_0 + \lambda V$, H_0 being the same mean-field Hamiltonian used in constructing $|0(\beta)\rangle$, while V acts as a perturbation. The canonical ensemble thermal state can be expanded as a power series in the perturbation parameter λ,

$$|\Psi(\beta)\rangle = |\Psi_0\rangle + \lambda\,|\Psi_1\rangle + \lambda^2\,|\Psi_2\rangle + \ldots, \tag{4.20a}$$

$$= e^{-\beta H_0/2}\left(|\phi_0\rangle + \lambda|\phi_1\rangle + \lambda^2|\phi_3\rangle + \ldots\right). \tag{4.20b}$$

Substituting this form for $|\Psi(\beta)\rangle$ in Eq. 4.6 and collecting terms at various orders in λ gives $\partial\,|\phi_0\rangle\,/\partial\tau = 0$, or equivalently $|\Psi_0\rangle = |\Psi_{AGP}(\beta)\rangle$ for terms at $\mathcal{O}(\lambda^0)$, and

$$\frac{\partial}{\partial\tau}\,|\phi_n\rangle = -\frac{1}{2}e^{\tau H_0/2}Ve^{-\tau H_0/2}\,|\phi_{n-1}\rangle \tag{4.21}$$

for $\mathcal{O}(\lambda^n)$, $\forall n \geq 1$. Integrating Eq. 4.21 yields perturbative corrections identical to those in a time-dependent interaction picture theory. The diagonal structure of H_0 allows us to integrate the equations analytically. Here, we will present results for second-order perturbation theory (PT2). Detailed Notes on both the projected CI and the AGP-based perturbation theory are available in the Appendix C.

4.6 Implementation Details

We use ground-state Hartree-Fock eigenvalues to build H_0, which in turn are used to define the mean-field reference state (thermal BCS for the projected CI, and thermal AGP for the perturbation theory). All the HF calculations were performed using

PySCF. [80, 81] As we have emphasized in Section 4.2, a mean-field Hamiltonian $H_0(\beta)$ that optimizes the Helmholtz free energy at every β may also be used. While this may lead to a better thermal reference state, it makes the underlying equations more complicated, and therefore, we work with a fixed H_0, which is analogous to the interaction picture grand-canonical ensemble theories discussed previously.

Nevertheless, to gauge the relevance of optimization, in Fig. D.1 of Appendix D, we compare the performance of thermal AGP with optimized and un-optimized η's for various benchmark systems, which we study below. Notice that for larger systems, the optimization of η's does not introduce any significant improvement, which justifies the use of un-optimized H_0.

Both the projected CI (Eq. 4.17) and perturbation theory (Eq. 4.21) equations are integrated starting from $\beta = 0$, where mean-field is exact. The computational cost of implementation is $\mathcal{O}(N^6)$ times the number of grid points used in the integration for each of the projected CI and AGP-PT2. While the second-order PT corrections can be obtained by a straightforward integration of the underlying quantities along the imaginary-time axis, the projected CI amplitudes satisfy a set of linear ordinary differential equations (ODE). The exact solution of these ODE's requires an inversion of the overlap matrix A, which is computationally expensive. Moreover, A may also have zero or near-zero eigenmodes. To avoid problems related to inverting A, at each β-grid point, we solve for the derivative vector iteratively using MinresQLP, [124, 125] a robust algorithm for singular linear systems, and then use the Dormand-Prince method to perform the integration. This adds an additional cost to the projected CI theory. In all the data presented below, we use a step size of $\Delta\beta = 0.01$ or smaller to integrate the ODE in projected CI, which is sufficiently small to guarantee convergence for the Runge-Kutta method (see Appendix D for data on step-size convergence).

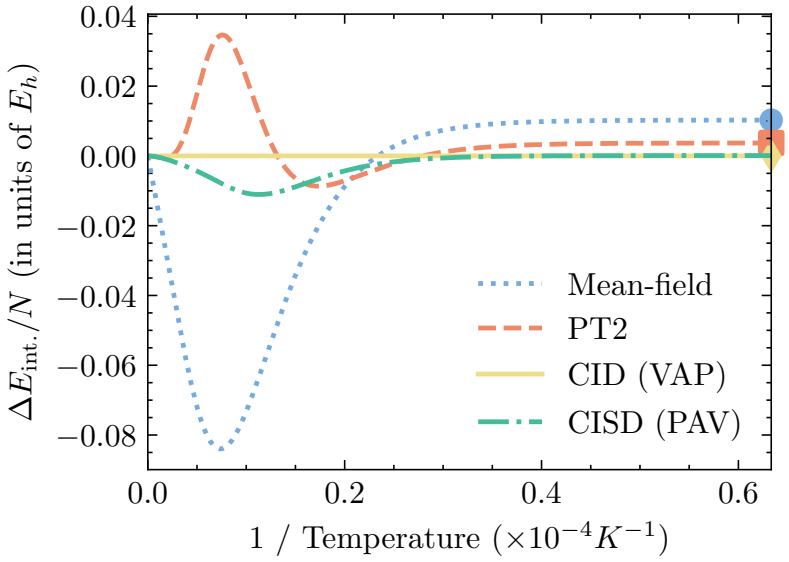

Figure 4.1 : Error-per-electron in the canonical-ensemble internal energy for the Hydrogen molecule in STO-3G basis with a bond length of 0.74Å. The results compare thermal AGP, i.e., the projected BCS wave function, AGP-based perturbation theory, PAV-style projected CISD, and VAP-style projected CID.

4.7 Results

We apply the projected CID and the second-order perturbation theory (PT2) to small molecular and model systems to quantify the performance of these finite-temperature canonical ensemble methods against exact benchmark results. Figure 4.1 plots errors in the canonical-ensemble internal energy (with respect to the exact results) for the Hydrogen molecule in the minimal STO-3G basis and at a bond length of 0.74Å. The results compare the performance of projected thermal BCS or AGP (which is indicated in the plot as mean-field), PAV and VAP projected thermal CISD and CID, respectively, and AGP-based PT2. The markers in the right y-axis indicate the energy error per particle for the corresponding ground-state methods. We use the ground-state spin-restricted Hartree-Fock (RHF) to build H_0. Even for the trivial

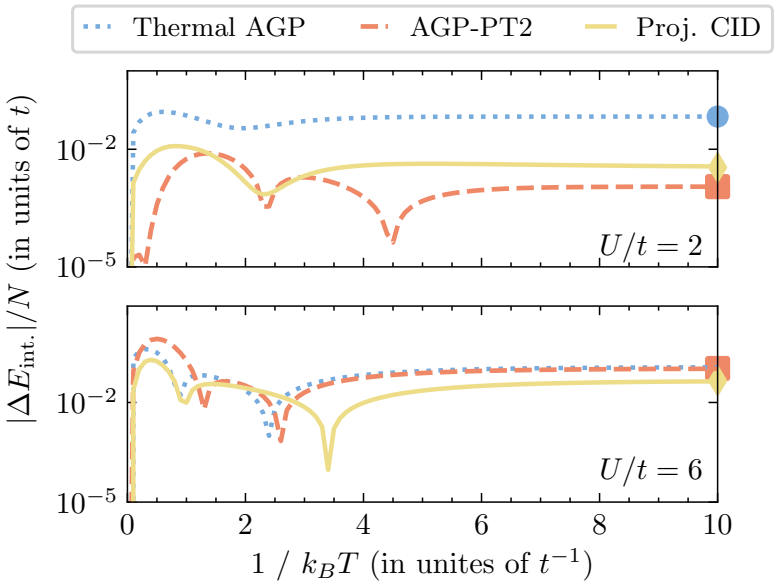

Figure 4.2 : Error-per-electron in the canonical-ensemble internal energy for the half-filled six-site Hubbard models at $U/t = 2$ and 6. The results compare thermal AGP, i.e., the projected BCS wave function, AGP-based perturbation theory, and VAP-style projected CID. The colored markers on the right y-axis indicate the energy error per particle for the corresponding ground-state methods

case of the Hydrogen molecule in a minimal basis, which comprises two electrons in four spin-orbitals, we find that the mean-field approach misses a lot of correlation, a part of which is recovered by CID and PT2. The VAP-CID, like its ground-state analog and unlike the grand-canonical CISD discussed in Chapter 3, is exact for this two-electron system and expectedly outperforms the PAV approach. The second-order perturbation theory, though not exact for the two-electron case, also improves upon the mean-field results. All the CI and PT results approach their appropriate ground-state counterparts in the zero-temperature limit, i.e., the number-projected CID converges to ground-state CISD and the AGP-based perturbation theory to ground-state perturbation theory as $\beta \to \infty$.

Figure 4.2 plots the absolute error in internal energies for six-site Hubbard models

with $U/t = 2, 6$ and half-filling. We use RHF and UHF to construct the H_0 in the $U/t = 2$ and $U/t = 6$ cases respectively. Having noted that VAP completely outperforms PAV, here we consider only the former. The story is more or less the same as for the Hydrogen molecule: mean-field, though decent, misses out a lot of correlation, which is recovered by number-projected CID and AGP-based PT2. We notice that the AGP-PT2 performs better than projected-CI for $U/t = 2$ but does not introduce any significant improvement over the mean-field for $U/t = 6$. This is analogous to the ground-state performance of these theories, as indicated by the markers in the right y-axis of the error plots.

To highlight the merits of the number-projected CI over mean-field theory, as well as the distinction between canonical and grand-canonical ensemble properties, we plot the total internal energy (top panel) and the specific heat (bottom panel) for the six-site Hubbard model with $U/t = 6$ at half-filling in Fig. 4.3. We compare the mean-field theory, grand-canonical CISD, and VAP style number-projected CID against exact numerical results. Recall that the grand-canonical mean-field state is a thermal BCS which, upon number-projection, gives the canonical ensemble thermal state. As for the $U/t = 6$ case in Fig. 4.2, we use UHF to build H_0. The results show a striking difference in the behavior of the specific heat in the two ensembles. The two different peaks in the exact specific heat curves (shown in solid blue and red lines), which correspond to the spin and charge excitation energy (or temperature) scales, are more pronounced and distinct in the canonical ensemble. While the mean-field theory completely fails to account for the spin-excitation peak, the projected CID performs better qualitatively and quantitatively.

We repeat this exercise for the hole-doped six-site Hubbard model with $U/t = 2$ and four electrons to further demonstrate the difference between the two ensembles.

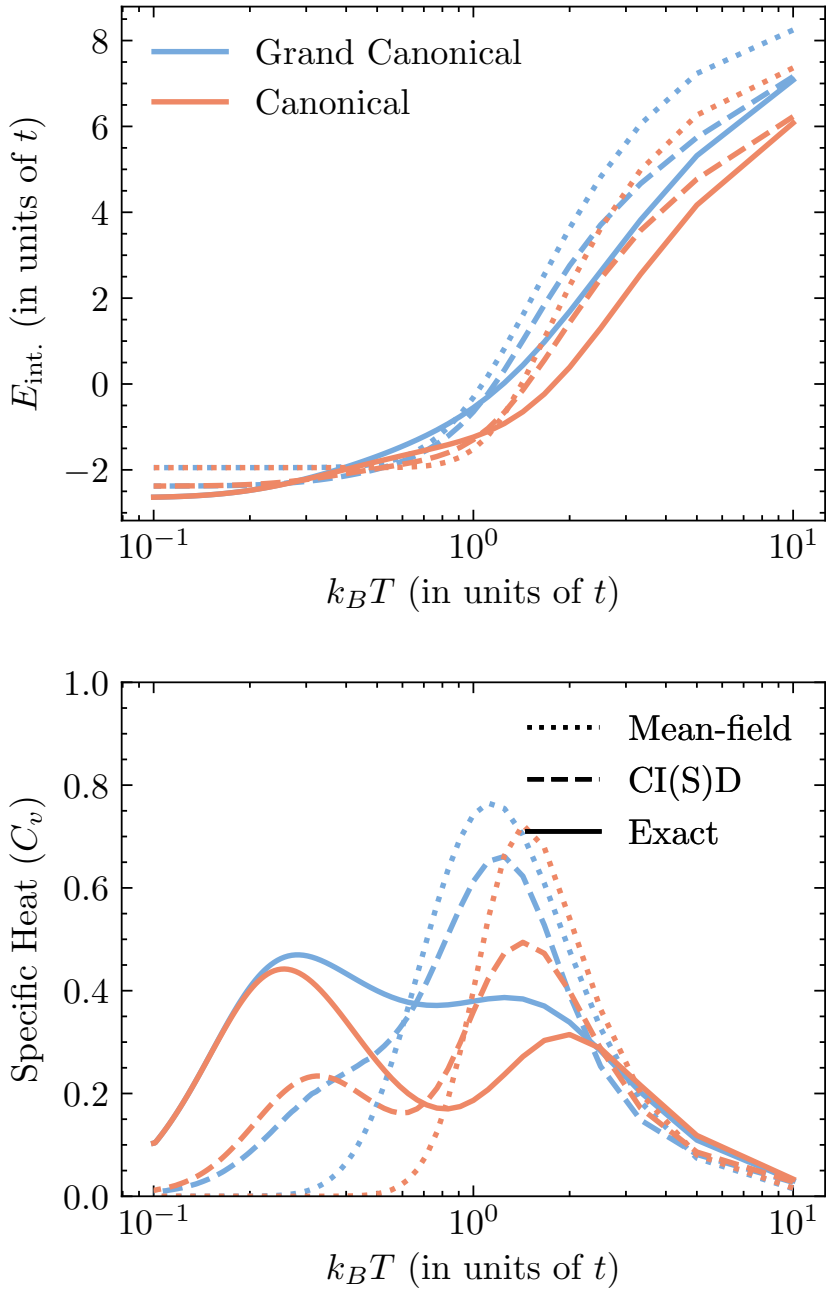

Figure 4.3 : Temperature dependence of total internal energies and specific heats for the half-filled six-site Hubbard model with $U/t = 6$. The mean-field, CI and exact results highlight the difference between the grand-canonical (blue) and the canonical (red) ensemble properties.

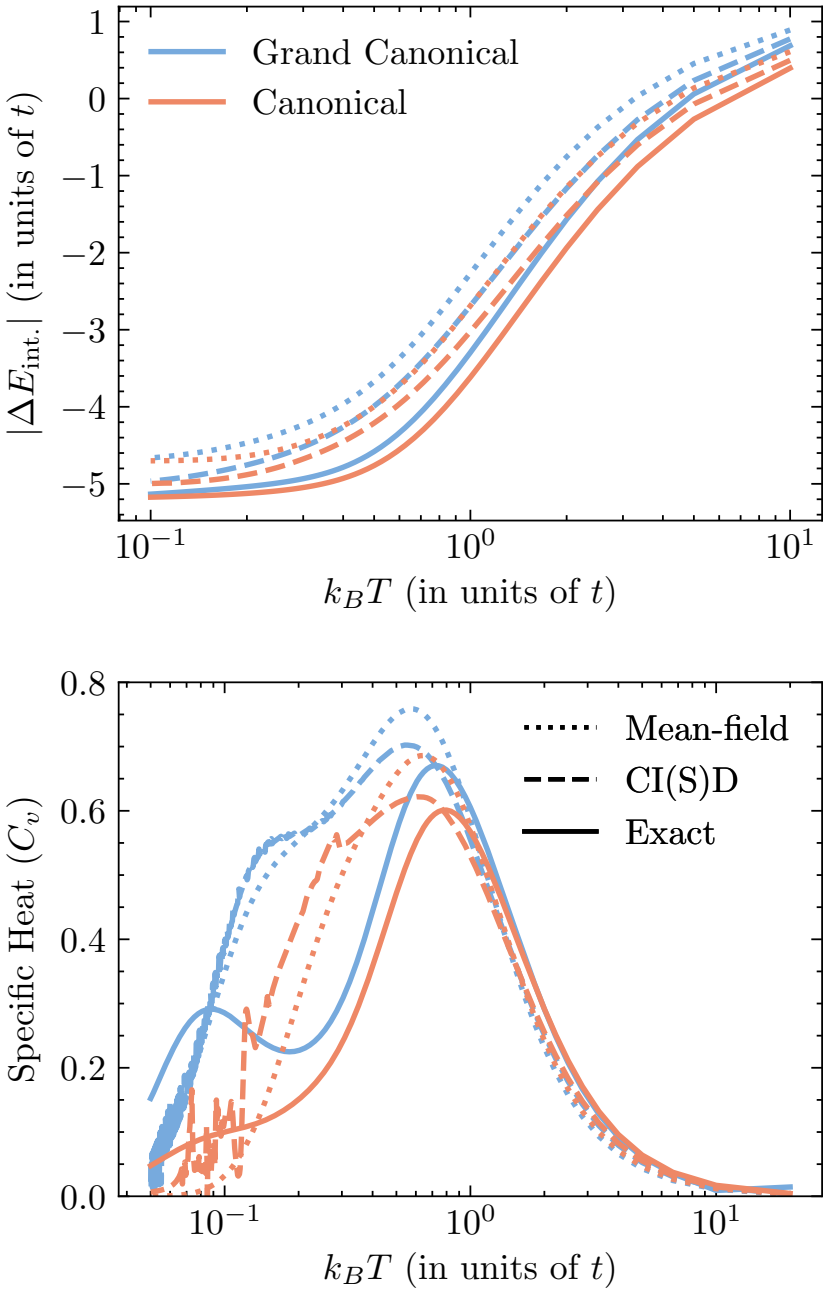

Figure 4.4 : Temperature dependence of total internal energies and specific heats for the hole-doped six-site Hubbard model with $U/t = 4$ and four electrons. The mean-field, CI and exact results highlight the difference between the grand-canonical (blue) and the canonical (red) ensemble properties.

This time, we use the RHF eigenvalues to construct H_0. The results are plotted in Fig. 4.4. Notice that, unlike the half-filled case, the hole-doped Hubbard model shows an appreciable difference between the canonical and grand-canonical ensemble results. This is because the half-filled Hubbard model has the lowest energy states in Fock space. Excitation to sectors with different particle numbers are high in energy and are effectively frozen out in the low-temperature limit so that the grand canonical ensemble becomes effectively canonical. This is not the case for the doped Hubbard model. At the same time, we also note that the low-temperature specific heat results in Fig. 4.4, for both the grand-canonical and the canonical CI, are noisy. We attribute this noise to two different sources:

1. The evolution of the CI amplitudes is carried out with respect to the inverse temperature β, and we compute the specific heat as

$$C_v = -\frac{\beta^2}{N_0}\frac{\partial E}{\partial \beta}. \tag{4.22}$$

   Any error in the integration due to the finite step size would be amplified by a factor of β^2. This explains the noise present in both the grand-canonical and the canonical CI.

2. Recall that for the projected CI, we solve a generalized linear equation (see Eq. 4.14). As we approach low temperatures (or large β), the number of near-zero modes in the overlap matrix A becomes large, which leads to inconsistencies in the solution, further adding to the noise.

4.8 Summary

Using thermofield dynamics in conjunction with number-projection, we have formulated a canonical ensemble framework for finite-temperature wave function theories.

While we have focussed on correlated many-body fermionic systems, the work is readily generalizable to bosons. We use this framework to construct canonical ensemble mean-field, number-projected CI and perturbation theories. As benchmark applications, we apply these theories to study thermal properties of the Hydrogen molecule (at $r_{H-H} = 0.74$Å) in a minimal basis and six-site Hubbard models at various correlation strength and filling fractions. In the low-temperature regime, where the canonical ensemble is most applicable, these methods perform as well as their ground-state counterparts for the benchmark problems studied. At zero temperature, one is generally required to go to much higher orders in CI or PT to obtain highly accurate results, and better alternatives, such as the coupled cluster theory and multi-reference methods, are generally preferred. While a number-projected formulation of the coupled cluster theory for the ground-state has been worked out in Ref. 120, the underlying equations are complicated for a direct generalization to finite temperatures. This work is a first step towards achieving finite-temperature analogs of such sophisticated techniques. It also establishes a foundation to build number-conserving finite-temperature Monte Carlo methods. [101]

Chapter 5

Framework for SU(2) systems

The $su(2)$ algebra forms the basis for understanding a wide range of phenomena in the condensed matter and chemical systems. For instance, spin systems, such as the transverse field Ising [126] model and variants of the Heisenberg model, provide one of the most effective ways to study magnetic properties in materials. Hamiltonians for some fermionic systems can also be represented using the $su(2)$-generators, e.g. the Lipkin-Meshkov-Glick [127–129] and the reduced-BCS models. [74–76] However, even for spin systems, efficient solutions of the many-body Schrödinger equation is prohibited by the exponential computational barrier. The status of approximate ground-state and finite-temperature theories is also similar to that of fermions. Truncated CC theory in the broken-symmetry basis (e.g., in the on-site basis for spin Hamiltonian, and where symmetries may not be preserved) is reasonably accurate for SU(2) systems. Furthermore, owing to the fact that its performance is not affected by the dimensionality of the lattice, CC has a potential advantage over alternatives such as DMRG. This has led to an extensive application of CC theory in the exploration of ground-state phases in SU(2) systems. [90, 109, 122, 130–136]

Motivated by the success of CC theory for ground-state phases in spin systems, we would like to have a thermal CC framework, similar to the one explored for fermions in Chapter 3, to study finite-temperature phases. However, most thermal wave function theories, including thermal CC discussed in the preceding chapters, are tailored to work with bosons or fermions. The difference in the structure of $su(2)$ and

fermion/boson algebras requires further work to extend the existing thermal methods to spin systems. In this chapter, we will explore a thermofield-based wave function formalism for SU(2) systems and use it to construct a thermal CC theory.

5.1 Thermofield dynamics for $su(2)$ algebra

The discussion on thermofield dynamics in Section 2.3 is very general and independent of algebra that defines the system. The thermal state (Eq. 2.36) is given by

$$|\Psi(\beta)\rangle = e^{-\beta H/2}\,|\mathbb{I}\rangle\,, \tag{5.1}$$

where $|\mathbb{I}\rangle$ is the identity state. In Chapters 3 and 4 we presented the details about the identity state for fermions in the grand-canonical and canonical ensembles respectively, i.e.,

$$|\mathbb{I}\rangle_{\text{grand canonical}} = \prod_p \Big(1 + c_p^\dagger \tilde{c}_p^\dagger\Big)|-;-\rangle, \tag{5.2a}$$

$$|\mathbb{I}\rangle_{\text{canonical}} = \frac{1}{N!}\Big(\sum_p c_p^\dagger \tilde{c}_p^\dagger\Big)^N |-;-\rangle, \tag{5.2b}$$

where $c_p^\dagger$ ($\tilde{c}_p^\dagger$) creates a particle in the p^{th} spin-orbital in the physical (auxiliary) space, and the product / sum runs over all spin-orbital indices, while the state $|-;-\rangle$ denotes the vacuum for both the physical and conjugate spaces. For SU(2) spins, we adopt a similar definition for the identity state that was proposed in Refs. 137–139,

$$|\mathbb{I}\rangle_{su(2)} = \prod_p \Big(1 + J_p^+ \tilde{J}_p^+\Big)\,|\Downarrow\rangle\,, \tag{5.3a}$$

$$|\Downarrow\rangle = |\downarrow\downarrow\downarrow\cdots;\downarrow\downarrow\downarrow\cdots\rangle\,, \tag{5.3b}$$

where J_p^+ ($\tilde{J}_p^+$) is the conventional spin-1/2 ladder operator for the p^{th} physical (auxiliary) spin and the state $|\Downarrow\rangle$ describes all the physical and auxiliary spins, which

are written respectively to the left and right of the semicolon in Eq. 5.3b, pointing downwards. By definition, the thermal state obeys the same imaginary-time evolution equation as Eq. 2.45,

$$\frac{\partial}{\partial\beta}\left|\Psi(\beta)\right\rangle = -\frac{1}{2}H\left|\Psi(\beta)\right\rangle, \tag{5.4}$$

which can be integrated from $\beta = 0$, where $|\mathbb{I}\rangle$ is the exact thermal state, to the desired value of β. Evolution equation for chemical potential is not required as the total number of spins is conserved in this framework. In the following sections, we will discuss mean-field and coupled cluster theories to integrate this imaginary-time evolution equation.

5.2 Mean-field theory

The simplest sensible approximation to construct the thermal state is the mean-field approach, where an effective one-body Hamiltonian of the form $H_0 = \sum_p \epsilon_p J_p^z$ is used to evolve the thermal state and results in

$$\left|0(\beta)\right\rangle = e^{-\beta H_0/2}\left|\mathbb{I}\right\rangle = \prod_p \left(e^{\beta\epsilon_p/4} + e^{-\beta\epsilon_p/4} J_p^+ \tilde{J}_p^+\right)\left|\Downarrow\right\rangle, \tag{5.5}$$

which can be normalized and written as a spin-BCS state,

$$\left|0(\beta)\right\rangle = \prod_p \left(u_p + v_p J_p^+ \tilde{J}_p^+\right)\left|\Downarrow\right\rangle, \tag{5.6}$$

where $u_p = 1/\sqrt{1+e^{-\beta\epsilon_p}}$ and $v_p = \sqrt{1-u_p^2}$. The BCS parameters, u_p and v_p can also be found by minimizing the mean-field free energy of the system. However, following the convention used in the previous chapters, we will not perform reference optimization for the results presented here.

5.3 Framework for correlated theories

To construct correlated thermal wave function theories, we follow an approach similar to Sections 3.2 and 4.3. Starting with the mean-field thermal state as a reference, we use a wave operator $\Omega(\beta)$ to incorporate correlation effects in constructing an approximate thermal state, i.e.,

$$|\Psi(\beta)\rangle \simeq \Omega(\beta)\ |0(\beta)\rangle\,. \tag{5.7}$$

In most ground-state correlated wave function theories, it is convenient to express the wave operator Ω as excitations on the mean-field reference. For spin systems, this is achieved by transforming the problem to a new $su(2)$ basis in which the mean-field is a vector product of quasi-spins pointing down at each site. Then, Ω can simply be built out of the new (transformed) J^+ ladder-operators. Similarly, for thermal wave function theories, we introduce a canonical transformation that rotates the physical and auxiliary spin operator basis in such a way that in the new basis, the thermal mean-field state $|0(\beta)\rangle$ has the same form as $|\Downarrow\rangle$ in Eq. 5.3b, i.e., with all the physical and auxiliary quasi-spins pointing downwards. At each lattice site, the fifteen generators,

$$J^\mu,\, \tilde{J}^\nu,\, J^\mu \otimes \tilde{J}^\nu \quad \forall \quad \mu,\nu \in \{\pm, z\}$$

collectively span an $su(4)$ algebra. The thermal canonical transformation that we seek is a basis rotation in this $su(4)$ algebra. It was first proposed by Suzuki et

al., [137] and is defined as

$$S_p^{\pm}(\beta) = u_p J_p^{\pm} + 2v_p J_p^z \tilde{J}_p^{\mp}, \tag{5.8a}$$

$$\tilde{S}_p^{\pm}(\beta) = u_p \tilde{J}_p^{\pm} + 2v_p \tilde{J}_p^z J_p^{\mp}, \tag{5.8b}$$

$$S_p^z(\beta) = u_p^2 J_p^z - v_p^2 \tilde{J}_p^z - u_p v_p \left(J_p^+ \tilde{J}_p^+ + J_p^- \tilde{J}_p^- \right), \tag{5.8c}$$

$$\tilde{S}_p^z(\beta) = u_p^2 \tilde{J}_p^z - v_p^2 J_p^z - u_p v_p \left(J_p^+ \tilde{J}_p^+ + J_p^- \tilde{J}_p^- \right), \tag{5.8d}$$

where the coefficients u_p and v_p are same as the ones discussed above. The new S^- and $\tilde{S}^-$ operators annihilate the mean-field reference, i.e.

$$S_p^-(\beta) \left|0(\beta)\right\rangle = 0 = \tilde{S}_p^-(\beta) \left|0(\beta)\right\rangle. \tag{5.9}$$

The inverse transformation of Eq. 5.8 can be obtained by swapping J with S, and taking $v_p \to -v_p$. For the sake of brevity, in the remainder of this manuscript, we will use the label S for thermal and J for zero-temperature $su(2)$ operators, and drop the explicit β-dependence.

The basis rotation in Eq. 5.8 can also be envisioned as a non-linear canonical transformation of the physical and auxiliary $su(2)$ algebras. In our implementation, however, we prefer to work with the $su(4)$ representation. We use the symbolic algebraic manipulator *drudge* [89] to encode the $su(4)$ commutation relations and perform the necessary operator algebra to obtain the expressions for the equations discussed below.

5.4 Coupled cluster theory

The development of thermal CC theory in $su(2)$ systems follows directly from the discussion from Section 3.4. We parameterize the thermal state as

$$\left|\Psi(\beta)\right\rangle = e^{T(\beta)} \left|0(\beta)\right\rangle, \tag{5.10}$$

where $T(\beta)$ creates excitations on the thermal mean-field reference $|0(\beta)\rangle$. For all practical applications, the cluster operator T is truncated to a finite order in excitation rank, usually at the level of single and double excitations (CCSD). Due to the non-linear nature of the thermal transformation in Eq. 5.8, the Hamiltonian becomes quartic in $su(2)$ generators, although it remains quadratic in the $su(4)$-generators. Therefore, we choose a cluster operator that is quadratic in terms of the $su(4)$ generators to capture the exact finite-temperature behavior in the simplest two-site systems. Although symmetries of the system under consideration can be used to simplify its structure, the most general form of the cluster operator $T(\beta)$, with single and double excitations, is defined as

$$T(\beta) = t_0 + T_1 + T_2, \tag{5.11a}$$

$$T_1 = \sum_p t_p S_p^+ + \sum_p \tilde{t}_p \tilde{S}_p^+ + \sum_p \alpha_p Y_p^{++}, \tag{5.11b}$$

$$T_2 = \frac{1}{2}\sum_{pq}\left(t_{pq} S_p^+ S_q^+ + \tilde{t}_{pq}\tilde{S}_p^+\tilde{S}_q^+ + \alpha_{pq} Y_p^{++} Y_q^{++}\right) + \sum_{pq} m_{pq} S_p^+ \tilde{S}_q^+, \tag{5.11c}$$

where we define $Y_p^{\mu\nu} = S_p^\mu \otimes \tilde{S}_p^\nu$. The scalar parameter t_0 keeps track of the norm of the thermal CC state (i.e. the partition function). For brevity, we will write $T = \sum_\mu t_\mu \tau_\mu$, where t_μ and τ_μ are compact notations for amplitudes and operators respectively. Substituting the CC ansatz (Eq. 5.10) into the imaginary-time evolution equation, we get

$$\left(e^{-T}\frac{\partial}{\partial\beta}e^{T}\right)|0(\beta)\rangle = -\frac{1}{2}\left(\bar{H} - H_0\right)|0(\beta)\rangle\,, \tag{5.12}$$

where the similarity transformed Hamiltonian, $\bar{H} = e^{-T}He^{T}$, can be expanded using the Baker-Campbell-Hausdorff (BCH) expansion. While the BCH expansion truncates at the fourth-order for a general fermionic Hamiltonian, due to the non-trivial

nature of the transformation in Eq. 5.8, it truncates at the eighth order for SU(2) Hamiltonians.

Once again, since the cluster operator T is constructed from the ladder operators in a β-dependent basis, we have

$$\left[\frac{\partial \tau_\mu}{\partial \beta}, T\right] \neq 0, \tag{5.13}$$

for $\tau_\mu \in \{S^\pm, \tilde{S}^\pm, S^z, \tilde{S}^z, \ldots\}$. Therefore, the similarity transformation of the β-derivative in the left hand side of Eq. 5.12 should be performed using the Wilcox identity and gives

$$e^{-T}\frac{\partial}{\partial \beta}e^{T} = \sum_\mu \frac{\partial t_\mu}{\partial \beta}\tau_\mu + D, \tag{5.14}$$

where D represents the contributions from the derivative of the operator part of T, and is given by

$$D = \sum_\mu t_\mu \bar{\tau}_\mu, \tag{5.15a}$$

$$\bar{\tau}_\mu = \frac{\partial \tau_\mu}{\partial \beta} + \frac{1}{2!}\left[\frac{\partial \tau_\mu}{\partial \beta}, T\right] + \frac{1}{3!}\left[\left[\frac{\partial \tau_\mu}{\partial \beta}, T\right], T\right] + \ldots \tag{5.15b}$$

After these manipulations, we arrive at the imaginary-time evolution equation for the amplitudes,

$$\sum_\mu \frac{\partial t_\mu}{\partial \beta}\tau_\mu \left|0(\beta)\right\rangle = \Big[-\frac{1}{2}\left(\bar{H} - H_0\right) - D\Big] \left|0(\beta)\right\rangle, \tag{5.16}$$

which can be projected against various subspaces to yield the evolution equations for the CC parameters $\{t_\mu\}$,

$$\sum_\mu \left\langle \tau_\nu^\dagger \tau_\mu \right\rangle \frac{\partial t_\mu}{\partial \beta} = \left\langle \tau_\nu^\dagger \Big[-\frac{1}{2}\left(\bar{H} - H_0\right) - D\Big] \right\rangle, \tag{5.17}$$

where the expectation value is calculated over the normalized mean-field thermal state. In practice, the excitation operators are orthogonal, so that $\langle \tau_\mu^\dagger \tau_\nu \rangle = \delta_{\mu\nu} \langle \tau_\nu^\dagger \tau_\nu \rangle$.

The system of first-order differential equations in Eq. 5.17 can be integrated starting from $\beta = 0$, where the exact initial value for the cluster amplitudes is known ($t_\mu(\beta = 0) = 0$), to the desired inverse temperature. For all the results discussed here, we use the Dormand-Prince integrator, [92, 93] a fourth-order Runge-Kutta algorithm with adaptive grid size (available in SciPy [140]), with a tolerance value of 10^{-5} to perform the integration.

5.4.1 Configuration interaction for thermal *bra*

We have already seen in Chapter 3 that properties in thermal CC are calculated as asymmetric expectation values,

$$\langle \mathcal{O} \rangle = \langle 0(\beta)|(1+Z)e^{-T}\mathcal{O}e^{T}|0(\beta)\rangle\,, \tag{5.18}$$

where we have a CC approximation for the *ket*, while the *bra*, approximated using configuration interaction (CI), is defined as

$$\langle \Psi_{CI}| = \langle 0(\beta)|\,(1+Z)e^{z_0}e^{-T}. \tag{5.19}$$

The scalar z_0 tracks the norm of the thermal *bra* and the CI-operator Z is defined as

$$Z = Z_1 + Z_2, \tag{5.20a}$$

$$Z_1 = \sum_p z_p S_p^- + \sum_p \tilde{z}_p \tilde{S}_p^- + \sum_p \gamma_p Y_p^{--}, \tag{5.20b}$$

$$Z_2 = \frac{1}{2}\sum_{pq}\left(z_{pq}S_p^- S_q^- + \tilde{z}_{pq}\tilde{S}_p^-\tilde{S}_q^- + \gamma_{pq}Y_p^{--}Y_q^{--}\right) + \sum_{pq} l_{pq}S_p^-\tilde{S}_q^-. \tag{5.20c}$$

To make the evolution equations more convenient, we can re-parameterize $\langle \Psi_{CI}|$ as

$$\langle \Psi_{CI}| = \langle 0(\beta)|\,(1+W)e^{w_0}, \tag{5.21}$$

where W has the same structure as Z, and is related to Z via a disentangled similarity transformation,

$$\langle 0(\beta)| \left(1 + Z\right) e^{z_0} e^{-T} = \langle 0(\beta)| \left(1 + W\right) e^{w_0 - t_0}. \tag{5.22}$$

The coefficients in W (and therefore Z) can be obtained using an imaginary-time evolution equation for the bra, in the same way as for CC theory discussed above.

5.4.2 Properties

When studying quantum magnetism, we are generally more interested in physical properties other than internal energy. In Chapter 3 and in Eq. 5.18, we have seen that properties in CC can be evaluated as an asymmetric expectation value. It is interesting to explore another approach to compute observables in CC. Once again, this is inspired by ground-state CC and uses Lagrange multipliers.

First, we redefine the Hamiltonian as $H \to H + \lambda\mathcal{O}$, where $\mathcal{O}$ is the observable of interest. Using this new Hamiltonian, we perform the imaginary-time evolution for the thermal state. The expectation value of $\mathcal{O}$ can then be computed as the λ-derivative of the free energy,

$$\langle \mathcal{O} \rangle = \lim_{\lambda \to 0} \frac{\partial F}{\partial \lambda}. \tag{5.23}$$

For thermal CC, the partition function and the free energy F are defined as

$$\frac{\mathcal{Z}}{\mathcal{Z}_0} = \langle \Psi_{CI} | \Psi_{CC} \rangle, \quad \text{and} \quad F = -\frac{1}{\beta} \log \mathcal{Z}. \tag{5.24}$$

We call the first approach (Eq. 5.18) as CC expectation value and the latter (Eq. 5.23) as λ-derivative approach.

While constructing the thermal state in the λ-derivative approach, we should use

a mean-field reference that also depends on λ, i.e., define the partition function as

$$\frac{\mathcal{Z}}{\mathcal{Z}_0} = e^{w_0+t_0} \langle 0(\beta,\lambda)|(1+W)e^T|0(\beta,\lambda)\rangle \,. \tag{5.25}$$

Comparing with *ab-initio* CC theory, a λ-dependent reference is similar, though not identical, to orbital-optimized linear response CC theory. [78] Properties calculated using CC expectation values and λ-derivative approach (with an optimized mean-field) are generally different. Only as the CC approximation becomes accurate, properties from CC expectation and λ-derivative formalism will become equivalent. We present results for both these techniques in the following section.

5.5 Results

We study the Lipkin-Meshkov-Glick (or simply, the Lipkin) model and the transverse field Ising model (TFIM) to assess the performance of our thermal CC theory. As indicated in Eq. 5.10, we consider a cluster operator that is quadratic in $su(4)$-generators. For the Lipkin model, we present results for error in internal energy while we consider both the energetics and properties for TFIM.

5.5.1 Lipkin-Meshkov-Glick model

The Lipkin-Meshkov-Glick [127–129] model describes a closed shell nucleus with schematic monopole interactions. The system consists of N spins on a lattice in the presence of an external magnetic field in the z-direction. Any two spin-up (down) states can flip to spin-down (up) states and lower the energy of the system. The Hamiltonian can be expressed as

$$H = xJ_z - \frac{1-x}{N}\left(J_+J_+ + J_-J_-\right), \tag{5.26}$$

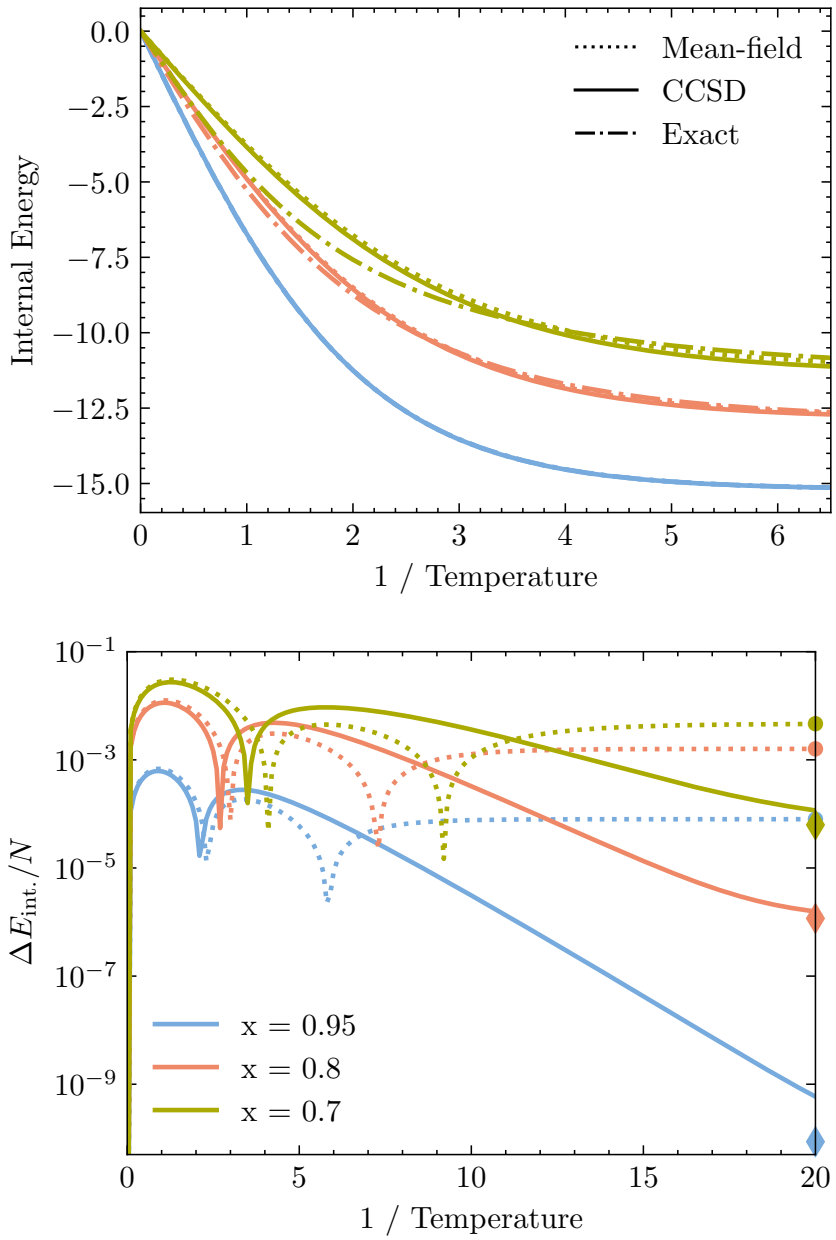

Figure 5.1 : Total internal energy per site and associated absolute errors as a function of the inverse temperature for 32-site Lipkin models in the weakly interacting regime. A mean-field Hamiltonian H_0 that preserves the symmetry of the ground state is used to construct the thermal mean-field. The plots compare mean-field theory and thermal CCSD against exact results. The colored circle and diamond markers on the right y-axis indicate the corresponding energy error per site for ground-state RHF and RCCSD, respectively.

where $J_\mu = \sum_{p=1}^{N} J_{\mu p}$ for $\mu \in \{\pm, z\}$ are the global SU(2) operators. The parameter x tunes the interaction strength. The system is non-interacting for $x = 1$ while correlation strength grows as x is reduced, and becomes extremely correlated at $x = 0$. Here, we only consider the parameter regime $0 \leq x \leq 1$.

The Lipkin model is exactly solvable within the Richardson-Gaudin ansatz. [141, 142] Exact diagonalization (or full configuration interaction) is also straightforward as the size of the Hilbert space grows linearly with the number of spins. Despite its seemingly simple structure, the Lipkin model exhibits non-trivial physics, particularly near the transition from weak to strong correlation regimes. For this reason, the Lipkin model serves as an ideal test-bed for new computational methods and theories in many-body physics and chemistry, c.f. Refs. 122, 134.

The transition from weak to strong correlations in the exact theory generally implies an associated spontaneous symmetry breaking at the mean-field level. For example, as we increase U/t in the Hubbard model, a symmetry-broken unrestricted Hartree-Fock (UHF) solution appears, which has lower energy than the symmetry-adapted restricted HF. In our thermal CC implementation, we choose a symmetry-broken mean-field Hamiltonian H_0 whenever possible. In the Lipkin model, the relevant symmetry is the parity symmetry, $P = e^{i\pi J_z}$, which breaks for $x < x_c = (2N - 2)/(3N - 3)$. Appendix E contains more details on symmetry breaking and mean-field theory for the Lipkin model.

Figure 5.1 shows the total internal energy per site and associated absolute errors, computed at the level of mean-field and CCSD approximations (Eq. 5.18), as a function of the inverse temperature and for various values of the interaction parameter x in a weakly interacting 32-site Lipkin model. The top panel shows the total internal energy per site, while the bottom panel shows the corresponding absolute error per

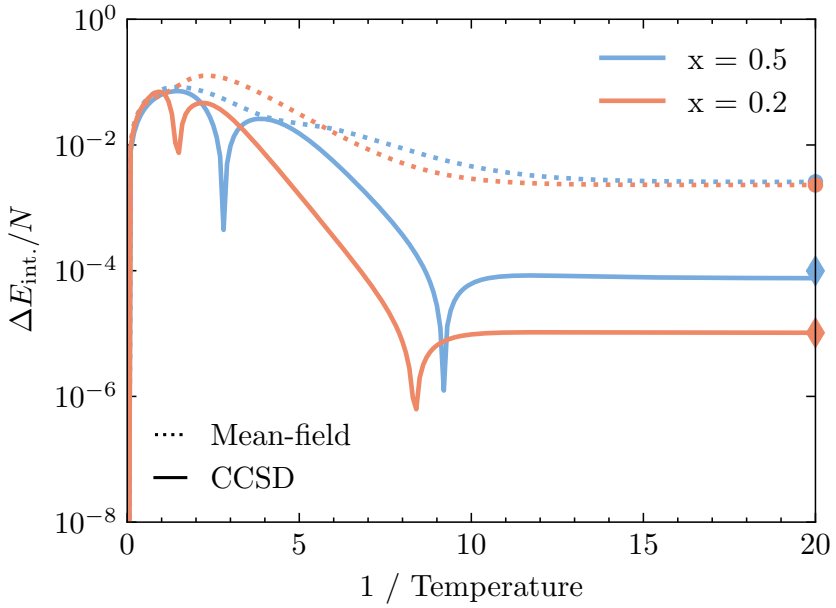

Figure 5.2 : Absolute values of internal energy error per site as a function of the inverse temperature for 32-site Lipkin models in the strongly interacting regime. A mean-field Hamiltonian H_0 that breaks the parity symmetry of the ground state is used to construct the thermal mean-field. The plots compare mean-field theory and thermal CCSD against exact results. The colored circles and diamonds on the right y-axis indicate the corresponding energy error per site for ground-state UHF and UCCSD, respectively.

site. The internal energies were computed using the CC-expectation value approach (Eq. 5.18). The mean-field reference for the approximate theories in Fig. 5.1 is constructed using a symmetry preserving Hamiltonian, i.e., $H_0 = xJ_z$. Figure 5.2 shows a similar energy error plot for strongly interacting 32-site Lipkin model, where the mean-field reference is constructed using a symmetry-breaking Hamiltonian, i.e.,

$$H_0 = \left(h_z - v_z \frac{N}{2}\right) \frac{(1-\kappa^2)J_z - \kappa(J_+ + J_-)}{1+\kappa^2} \tag{5.27}$$

where κ parameterizes symmetry breaking in Lipkin, while h_z and v_z are κ-dependent parameters that are defined in Appendix E.

The general observation in both the figures is that thermal CC improves significantly over mean-field, particularly for low temperatures. Most of the loss in accuracy occurs at intermediate temperatures and near $x = x_c$, where a single-reference description of the system is inadequate. Both the symmetry-adapted as well as symmetry-broken thermal mean-field and CCSD results approach the respective ground-state theories in the limit of zero temperature. The ground-state mean-field (CCSD) energy errors are indicated by the colored O and X markers on the y-axis in the figure. We note that for $x = 0.5$, while it may appear otherwise, thermal CC does converge the correct ground-state limit as we evolve the system to a very large value of inverse temperature, $\beta \simeq 1000$. We would like to remind the reader that at finite temperatures, the free energy obeys the variational theorem while the internal energy does not, i.e., an estimate of the free energy is an upper bound to the exact free energy. However, much like the ground-state CC, due to the asymmetric nature of expectation values, we do not expect thermal CC to satisfy this variational theorem. The spikes in the energy error curves of Figs. 5.1 and 5.2 correspond to the crossing of the mean-field/CC and exact internal energy curves and arise due to the non-variational character of the property.

Implementation details

The global SU(2) symmetry in the Lipkin model significantly reduces the structure of the cluster operator. We can drop the summation over the dummy indices and use

$$T(\beta) = t_0 + t_1 S^+ + \tilde{t}_1 \tilde{S}^+ + \alpha_1 Y^{++} + m S^+ \tilde{S}^+ + t_2 S^+ S^+ + \tilde{t}_2 \tilde{S}^+ \tilde{S}^+ + \alpha_2 Y^{++} Y^{++}. \tag{5.28}$$

Here, the $su(4)$-operators represent the global operators, i.e. for any generator X,

$$X \equiv \sum_p X_p. \tag{5.29}$$

The operators Y^{++} and $S^+\tilde{S}^+$ have overlapping contributions to the thermal state since,

$$Y^{++} = \sum_p S_p^+ \tilde{S}_p^+, \quad \text{and} \quad S^+\tilde{S}^+ = \sum_{pq} S_p^+ \tilde{S}_q^+. \tag{5.30}$$

To avoid making the imaginary-time evolution complicated, we choose either Y^{++} or $S^+\tilde{S}^+$ (but not both) in our cluster operator. We find that these choices lead to very similar result. Therefore, for all the work presented here, we use Y^{++} in the cluster operator. The number of parameters in the cluster operator is independent of the system size and depends only on the order of approximation. Hence, the computational scaling of thermal CC in Lipkin depends only on the number of grid points over which we perform the integration.

5.5.2 Transverse field Ising model

The 1D TFIM is considered as the canonical model to study quantum criticality and phase transitions. The reason behind its popularity is that the model exhibits a quantum phase transition between ordered and disordered phases while also being tractable both analytically and numerically. Consequently, it serves as an ideal model

to benchmark new computational theories like our thermal CC. The Hamiltonian is given by

$$H = -\sum_i \sigma_i^z \sigma_{i+1}^z + g \sum_i \sigma_i^x, \tag{5.31}$$

where g (chosen to be positive) quantifies the strength of the transverse magnetic field, and σ^x, σ^z are the Pauli matrices. In our work, we only consider 1D chains with periodic boundary conditions. In the absence of the transverse field, we have a ferromagnetic Ising model that breaks the $\mathbb{Z}_2$ symmetry in the thermodynamic limit (TDL). On the other hand, for large g, the model has a disordered paramagnetic ground-state. The one-dimensional chains exhibit a quantum phase transition from a ferromagnetically ordered phase to a disordered phase at $g = 1$. It is well known that the mean-field theory overestimates the magnetic order and predicts a transition at $g = 2$ instead. For our thermal CC theory, once again, we artificially break the $\mathbb{Z}_2$ symmetry to obtain an energetically lower mean-field solution when possible. Appendix F contains further details about the mean-field theory and the choice of H_0 for thermal mean-field.

Figure 5.3 plots absolute error in internal energy per site for thermal mean-field and CCSD as a function of inverse temperature for a 10-site TFIM at various values of the transverse field. Here, we have used Eq. 5.18 to compute the thermal CCSD internal energy. Similar to Lipkin, thermal CC significantly improves over mean-field. We should note that for $g = 0$ and $g >> 1$, both the mean-field theory and thermal CCSD are exact for the ground-state. However, even when ground-state CC or mean-field theory are exact, the finite-temperature theories may not be so. As we can observe from the $g = 0$ results in Fig. 5.3, both thermal mean-field and CC give non-zero errors for the internal energy, which decrease exponentially as we evolve towards zero temperature.

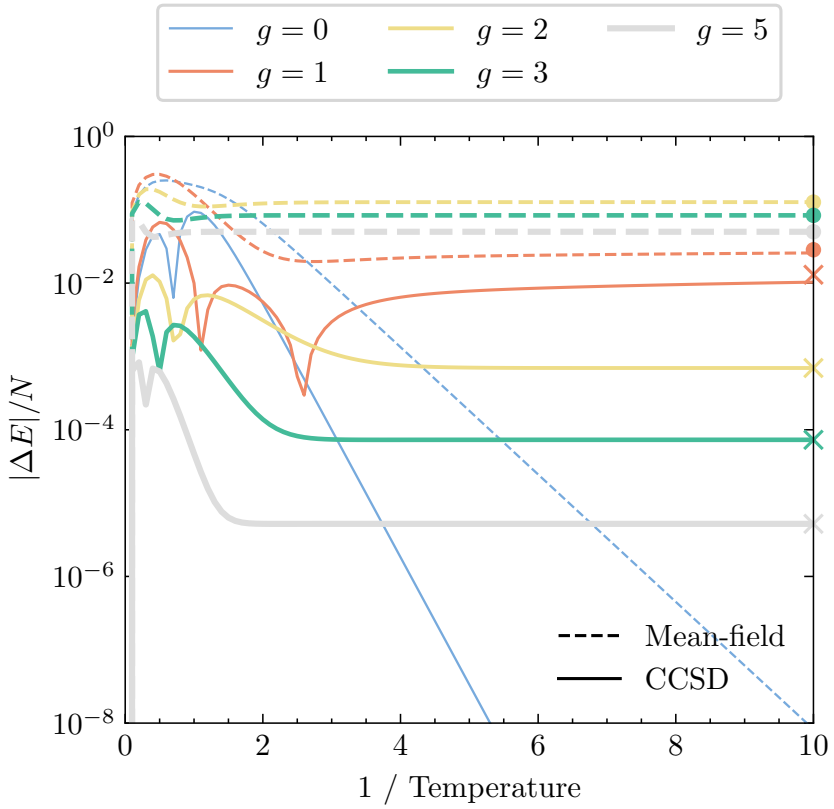

Figure 5.3 : Absolute error in internal energy per site for 10-site transverse field Ising models at various values of the transverse field g. The colored 'o' and 'x' markers on the y-axis indicate the corresponding errors for the ground-state mean-field and CCSD energies, respectively.

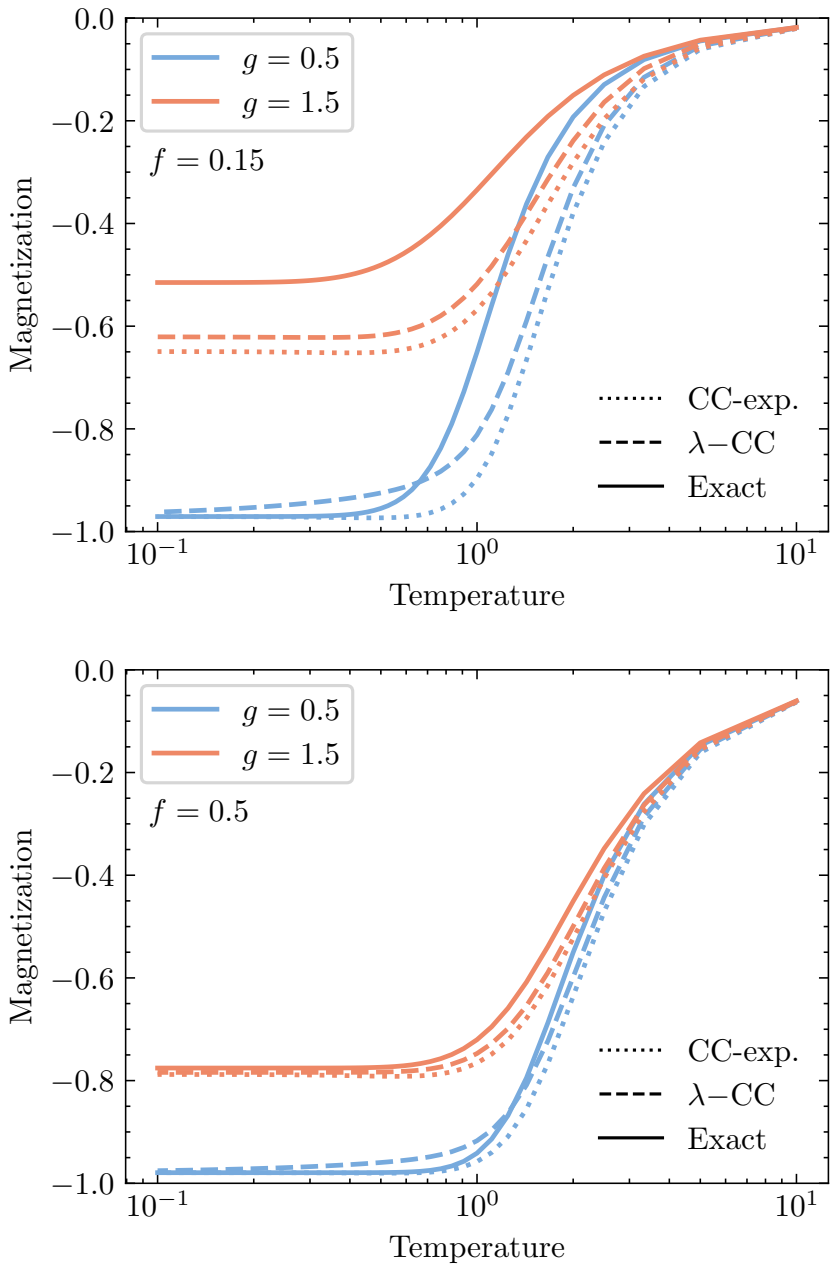

Figure 5.4 : Magnetization curves for 10-site transverse field Ising models for transverse fields $g = 0.5, 1.5$, indicated by red and blue colors respectively, and magnetizing fields $f = 0.15$ (top panel) and $f = 0.5$ (bottom panel). The plots compare magnetization calculated using CC expectation value (Eq. 5.18) and λ-derivative CC (Eq. 5.23) against exact magnetization, which was calculated as the f-derivative of the exact free energy. Different colors indicate results for different g-values, while the line-styles distinguish between various approximations.

For TFIM, we also compute properties, namely magnetization density and spin-spin correlation functions. We first consider the magnetization density, which we calculate using both the CC expectation value and λ-derivative of free energy (as already noted in Sec. 5.4.1). To make a sensible comparison, we first introduce an external field f in the z-direction, i.e., redefine the Hamiltonian as

$$H = -I \sum_i \sigma_i^z \sigma_{i+1}^z + g \sum_i \sigma_i^x + f \sum_i \sigma_i^z. \tag{5.32}$$

We have also introduced the Ising coupling constant I for book keeping. The magnetization density can then be calculated as,

$$M_z = \lim_{f \to 0^+} \frac{1}{N} \frac{\partial F}{\partial f}. \tag{5.33}$$

While this definition holds well in the TDL, there are some caveats when working with finite N. Consider the ferromagnetic regime near $g = 0$ and $f > 0$ so that the ground state consists of all spins pointing downwards. Starting from this ground state, we can have two different excitations: single spin-flip, for which the excitation energy is $\sim 2I$, and all spin-flips i.e., the ferromagnetic state with all spins pointing up. For the latter, the excitation energy is $\sim 2fN$. For the ferromagnetic phase, low-energy excitations should be single spin-flips. Therefore, the limit for f in Eq. 5.33 should be carefully defined, and we should have $2fN > 2I$, or $f > I/N$. Therefore, using $I = 1$, magnetization at $g = 0$ should be redefined as

$$M_z = \lim_{f \to (1/N)^+} \frac{1}{N} \frac{\partial F}{\partial f}. \tag{5.34}$$

As we go away from $g = 0$, the correct limiting value of the external field for the ferromagnetic phase will change. To avoid such discrepancies while comparing our benchmark calculations and exact results, we only consider magnetizing fields that are sufficiently large. Figure 5.4 shows the temperature dependence of magnetization as

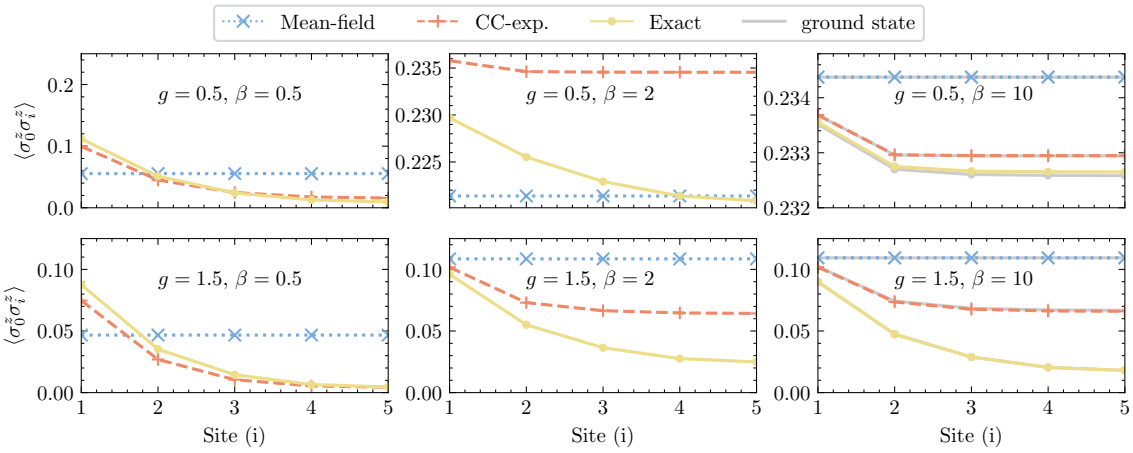

Figure 5.5 : Spin-spin correlation plots for 10-site transverse field Ising models for $g = 0.5$ (top row) and $g = 1.5$ (bottom row) and $f = 0$. We compare the mean-field and CC expectation value (Eq. 5.18) estimates against exact results, which were calculated as ensemble averages, at various values of β. Results for the corresponding ground-state theories are also plotted in grey in the third column ($\beta = 10$), and demonstrate convergence of thermal theories as $\beta \to \infty$. For the 10-site model, with periodic boundary conditions, the correlation function $\langle \sigma_0^z \sigma_i^z \rangle$ is symmetric about $i = 5$. Therefore we plot data only for $i = 1$ to 5.

we compare the results for CC expectation value (Eq. 5.18) and λ-derivative (Eq. 5.23) approaches against the exact results which were obtained by taking the λ-derivative of the exact free energy. Both the CC expectation value and λ-derivative perform reasonably well in the weakly correlated regime ($g = 0.5$) for all the values of the external field. Near the phase transition region ($g = 1.5$), the overall quality of the CC wave function drops. However, the λ-derivative results are marginally better than CC expectation values.

In Fig. 5.5, we also compare mean-field and CC expectation value results for the spin-spin correlation function $\langle \sigma_0^z \sigma_i^z \rangle$ against exact ensemble averages for this 10-site model. This time, we use $f = 0$ and only consider the CC expectation values. Once again, mean-field performs poorly and gives a flat, featureless correlation function.

On the other hand, thermal CCSD adds significant corrections, quantitative and qualitative, for both $g = 0.5$ and $g = 1.5$, particularly at low and high temperatures. Near the thermal phase transition region, i.e. at $\beta = 2.$ where thermal CCSD is the least accurate and the correlation function, despite exhibiting the right qualitative structure, is not quantitatively accurate (see the second column of Fig. 5.5). For large β, i.e., as we approach zero temperature, the correlation curves converge to the corresponding ground-state properties, as we can deduce from the grey ground-state curves in the third panels of each row in Fig. 5.5. We also observe one of the side-effects of the asymmetric expectation values in CC theory. For $g = 0.5$, going from $\beta = 2$ to $\beta = 10$, we find that the strength of thermal CCSD correlation function decreases while the exact correlation increases. While the decrease in correlation is negligible in this case ($\sim 10^{-3}$), the erratic behavior may become severe when CC is not a good approximation to the thermal state. Higher-order approximations to the bra state can be used to address these issues. Finally, we note that $g = 1.5$ results do not exhibit similar problems.

Implementation details

We can exploit the symmetries of the system to simplify the structure of the cluster operator for TFIM, just as we did for the Lipkin model. For the periodic chains under consideration, all the sites are equivalent. Therefore, we can express the cluster operator as

$$\begin{aligned} T(\beta) = t_0 + s\sum_p S_p^+ + \tilde{s}\sum_p \tilde{S}_p^+ + \alpha_0 \sum_p Y_p^{++} \\ + \frac{1}{2}\sum_{pq}\left(d_{pq}S_p^+ S_q^+ + \tilde{d}_{pq}\tilde{S}_p^+\tilde{S}_q^+ + m_{pq}Y_p^{++}Y_q^{++}\right) + \sum_{pq} x_{pq}S_p^+\tilde{S}_q^+, \end{aligned} \tag{5.35}$$

where we enforce that the tensors d, $\tilde{d}$, m and x are symmetric and have zero diagonals. With these simplifications, we can perform the imaginary-time evolution with a computational scaling of $\mathcal{O}(N^4 N_{grid})$. This scaling can be further brought down by realizing that the tensors d_{pq}, $\tilde{d}_{pq}$, m_{pq} and x_{pq} depend only on $|p-q|$.

5.6 Summary

Merging the $su(2)$ framework for thermofield dynamics with our fermionic thermal wave function theory, we have derived a similar framework for spin-1/2 systems. We use this framework to devise a CC theory and find that CC truncated to singles and doubles perform reasonably well for the Lipkin model and TFIM, the benchmark models considered here. At the same time, thermal CC experiences the same problems as its ground-state counterpart: it is insufficient for strongly correlated systems, and the expectation values are asymmetric. Similarly, at intermediate temperatures, single-reference nature of the CC ansatz fails to capture the underlying multi-configurational physics in strongly correlated systems. However, a key advantage of coupled cluster is that it is systematically improvable. Including higher-order excitations (triples, quadruples, etc.) in both the cluster operator and the configuration interaction approximation to the bra state can help alleviate some of the associated issues. In fact, for spin-lattices, where CCSD scales as $\mathcal{O}(N^3)$ or $\mathcal{O}(N^4)$, higher-order excitations can be added without making the theory computationally intractable.

Chapter 6

Conclusions and future work

The thermofield theory purifies the ensemble density matrix by introducing ancillary degrees of freedom, i.e., the auxiliary or the tilde-conjugate space. The resultant thermal state obeys imaginary time (and chemical potential, if applicable) evolution equations. In this thesis, we exploit these features of thermofield dynamics to build thermal generalizations of proven ground-state wave function theories, *viz.*, mean-field, configuration interaction, and coupled cluster for fermions (in both the canonical and the grand canonical ensemble) as well as for SU(2) systems. The ability to build both canonical and grand canonical methods as well as a framework for SU(2) systems also signifies the robustness of thermofield theory for finite-temperature wave function methods.

The increased size of the Hilbert space does not lead to an increase in the computational cost of thermal wave function theories because the Hamiltonian and operators corresponding to any other property of interest live in the physical Hilbert space. Therefore, the auxiliary states merely perform the role of a tracer.

We have used the so-developed thermal wave function methods to study different electronic systems (one-dimensional Hubbard model, reduced-BCS model, and molecules) and spin systems (Lipkin-Meshkov-Glick and transverse field Ising models). Among the theories considered, thermal CC stands out the most. In general, it improves significantly over mean-field and CI. Moreover, the exponential ansatz assures that the computed properties are size-extensive and size-consistent provided

the underlying reference state has these features. In short, the finite-temperature theories inherit all the merits from their corresponding ground-state counterpart. The former also converges to the latter in the limit $\beta \to \infty$.

At the same time, the thermal counterparts also retain the problems associated with the ground-state theories. For instance, it is known that symmetry-adapted CC theory breaks down in the presence of strong correlation. Thermal CC also shows significant errors for strongly correlated systems at intermediate values of β and eventually diverges as we evolve to lower temperatures. Similarly, although thermal CC, with an underlying mean-field Hamiltonian that breaks the symmetry, is well behaved energetically, it predicts incorrect expectation values of other observables, noticeably in the low-temperature limit.

Furthermore, even in the absence of strong correlations and spontaneous symmetry breaking, thermal CC loses accuracy at intermediate temperatures. It is primarily because the mean-field theory is a poor starting point near thermally driven phase transitions. Moreover, at $\beta = 0$, thermal mean-field is exact, and at $\beta = \infty$, the mean-field reference is an optimized Hartree-Fock Slater determinant. However, at intermediate values of β, we do not perform any reference optimization.

Addressing the shortcomings of traditional, ground-state CC theory is an active area of research. Several ideas have emerged as potential candidates to tackle the strong correlation problem, e.g., multi-reference CI/CC, non-orthogonal CI, AGP-based methods, etc. The thermal generalization of these new theories is a clear step beyond the work presented in this thesis. Nevertheless, with our thermal wave function framework, the development of both the ground-state and finite-temperature methods can go hand-in-hand.

6.1 Directions for future work

This doctoral thesis is merely a foot in the door of an entire zoo of thermal wave function theories. At the same time, there are lessons to be learned from the covariant (or interaction picture) imaginary-time evolution and applied to real-time evolution in ground-state theories. Here, we will highlight some of the ongoing and near-future projects that directly emerge from our thermal framework:

1. **Non-orthogonal thermal CI:** While many novel ground-state methods waiting to be generalized to finite temperatures, unconventional mean-field approaches such as symmetry-projected UHF (PHF) are perhaps the lowest hanging fruit. PHF states can often be represented as a linear combination of non-orthogonal Slater determinants (NOCI) and are known to perform well even in the presence of strong correlation (where traditional CC suffers). A NOCI-like thermal wave function ansatz that converges to PHF in the zero-temperature limit is highly desirable.

2. **Imaginary-time variational principle:** In thermal CC, properties are evaluated as asymmetric expectation values, with the *ket* parameterized as a CC wave function and the *bra* as a CI. For the results presented here, we compute both the *bra* and the *ket* by integrating the imaginary-time evolution equation within these ansatzes. An alternate way to derive the evolution equations for the CC and CI amplitudes is to make the free energy functional stationary. The free energy can be defined as

$$\Omega = -\frac{1}{\beta}\int_0^\beta d\tau E(\tau), \tag{6.1}$$

where $E(\tau) = \langle\Psi_L(\tau)|H|\Psi_R(\tau)\rangle \,/\, \langle\Psi_L(\tau)|\Psi_R(\tau)\rangle$ is the internal energy at inverse temperature τ. It is directly related to the time-dependent variational

principle [78] since the free energy functional can be re-written as

$$\Omega = -\frac{1}{\beta}\int_0^\beta d\tau \frac{\langle\Psi_L|H|\Psi_R\rangle}{\langle\Psi_L|\Psi_R\rangle}, \tag{6.2}$$

$$= -\frac{1}{\beta}\int_0^\beta d\tau \frac{\langle\Psi_L|\left(\frac{\partial}{\partial\tau}+\frac{H}{2}\right)|\Psi_R\rangle}{\langle\Psi_L|\Psi_R\rangle}, \tag{6.3}$$

$$= -\frac{1}{\beta}\int_0^\beta d\tau \frac{\langle\frac{\partial\Psi_L}{\partial\tau}|\Psi_R\rangle+\frac{1}{2}\langle\Psi_L|H|\Psi_R\rangle}{\langle\Psi_L|\Psi_R\rangle}. \tag{6.4}$$

In this new approach, the CC equations remain unaltered, while the CI equations do not. We expect the variational approach will improve thermal CC, particularly at intermediate temperatures where the errors are relatively high.

3. **Reference optimization:** One of the reasons behind the relatively high errors associated with thermal CC at intermediate temperatures is that the thermal mean-field reference is not optimized. In our current framework, reference optimization increases the complexity of the imaginary-time evolution equation as well as the β-derivative of the operators. However, if these hurdles can be overcome, an orbital-optimized thermal CC theory would be significantly more valuable.

4. **Applications to quantum dynamics:** Conventional time-dependent CC theory at zero temperature uses an ansatz similar to our fixed-reference formulation, i.e.,

$$|\Psi(t)\rangle = e^{T(t)}|\Phi\rangle, \tag{6.5}$$

where the mean-field $|\Phi\rangle$ does not carry any explicit time dependence. In Chapter 3, we saw that such an approach gradually diverges away from the exact result as the wave function evolves in time. This divergence is also present in the time-dependent CC. We expect a covariant or interaction picture CC ansatz to perform significantly better, just like the finite-temperature theory.

In addition to the classical computational theories, thermofield-inspired quantum algorithms have attracted considerable research interest and present another avenue to explore beyond this work.

Appendix A

Evolution equations for grand canonical thermal configuration interaction and coupled cluster

When the cluster operator S is truncated to singles and double excitation operators only, i.e.,

$$S = s_0 + \sum_{pq} s_{pq} a_p^\dagger \tilde{a}_q^\dagger + \frac{1}{4} \sum_{pqrs} s_{pqrs} a_p^\dagger a_q^\dagger \tilde{a}_s^\dagger \tilde{a}_r^\dagger$$

the evolution equations (c.f. Eq. 3.38a) for the CC amplitudes take the following form for the α-evolution,

$$\frac{\partial s_0}{\partial \alpha} = \frac{1}{2} \mathcal{R}_N^0 - S_\alpha^0 \tag{A.1}$$

$$\frac{\partial s_{pq}}{\partial \alpha} = \frac{1}{2} \mathcal{R}_N^{pq} - S_\alpha^{pq}, \tag{A.2}$$

$$\frac{\partial s_{pqrs}}{\partial \alpha} = \frac{1}{2} \mathcal{R}_N^{pqrs} - S_\alpha^{pqrs}, \tag{A.3}$$

where $\mathcal{R}_N$ denotes the various CC residuals for the α-evolution,

$$\begin{aligned} \mathcal{R}_N^0 &= \langle \Psi_0 | \left(e^{-S} N e^S - N \right) | \Psi_0 \rangle, \\ &= \sum_a x_a y_a s_{aa} \end{aligned} \tag{A.4a}$$

$$\begin{aligned} \mathcal{R}_N^{pq} &= \langle \Psi_0 | \tilde{a}_q a_p \left(e^{-S} N e^S - N \right) | \Psi_0 \rangle, \\ &= (x_p^2 - y_q^2) s_{pq} + \sum_a x_a y_a \left(s_{apaq} - s_{pa} s_{aq} \right) \end{aligned} \tag{A.4b}$$

$$\begin{aligned} \mathcal{R}_N^{pqrs} &= \langle \Psi_0 | \tilde{a}_r \tilde{a}_s a_q a_p \left(e^{-S} N e^S - N \right) | \Psi_0 \rangle, \\ &= (x_p^2 + x_q^2 - y_r^2 - y_s^2) s_{pqrs} + \frac{1}{2} \mathcal{P}(pq) \mathcal{P}(rs) \sum_a x_a y_a \left(s_{as} s_{pqar} - s_{pa} s_{aqrs} \right) \end{aligned} \tag{A.4c}$$

and the operator-derivative terms are given by

$$S^0_\alpha = -\frac{1}{2}\sum_a x_a y_a s_{aa} \tag{A.5a}$$

$$S^{pq}_\alpha = \frac{1}{2}\sum_a x_a y_a \left(s_{pa}s_{aq} + s_{paaq}\right) \tag{A.5b}$$

$$S^{pqrs}_\alpha = \frac{1}{4}\mathcal{P}(pq)\mathcal{P}(rs)\sum_a x_a y_a \left(s_{ar}s_{pqas} - s_{pa}s_{aqrs}\right), \tag{A.5c}$$

where x and y are the thermal Bogoliubov parameters and the dummy indices a, b, ... are summed over all the spin-orbitals. Equations for the β-evolution can be obtained in a similar way,

$$\frac{\partial s_0}{\partial \beta} = \frac{1}{2}\mathcal{R}^0_H - S^0_\beta \tag{A.6}$$

$$\frac{\partial s_{pq}}{\partial \beta} = \frac{1}{2}\mathcal{R}^{pq}_H - S^{pq}_\beta, \tag{A.7}$$

$$\frac{\partial s_{pqrs}}{\partial \beta} = \frac{1}{2}\mathcal{R}^{pqrs}_H - S^{pqrs}_\beta, \tag{A.8}$$

where $\mathcal{R}_H$ denotes the various CC residuals for the β-evolution. Using the thermal Bogoliubov transformation described in Eq. 3.7, a general two-body Hamiltonian,

$$H = \sum_p h_{pq} c^\dagger_p c_p + \frac{1}{4}\sum_{pqrs} u_{pqrs} c^\dagger_p c^\dagger_q c_s c_r,$$

can be expressed in terms of thermal creation/annihilation operators, and takes the form

$$\begin{aligned} H = h_0 &+ \sum_{ab}\left[h^{(11)}_{ab}\left(a^\dagger_a \tilde{a}^\dagger_b + \text{h.c.}\right) + h^{(20)}_{ab} a^\dagger_a a_b + h^{(02)}_{ab}\tilde{a}^\dagger_a \tilde{a}_b\right] \\ &+ \sum_{abcd}\left[h^{(221)}_{abcd}\left(a^\dagger_a a^\dagger_b \tilde{a}^\dagger_d \tilde{a}^\dagger_c + \text{h.c.}\right) + h^{(222)}_{abcd} a^\dagger_a \tilde{a}^\dagger_b \tilde{a}_d a_c + h^{(31)}_{abcd}\left(a^\dagger_a a^\dagger_b \tilde{a}^\dagger_c a_d + \text{h.c.}\right)\right. \\ &\left. + h^{(13)}_{abcd}\left(a^\dagger_a \tilde{a}^\dagger_b \tilde{a}^\dagger_c \tilde{a}_d + \text{h.c.}\right) + h^{(40)}_{abcd} a^\dagger_a a^\dagger_b a_d a_c + h^{(04)}_{abcd}\tilde{a}^\dagger_a \tilde{a}^\dagger_b \tilde{a}_d \tilde{a}_c\right] \end{aligned} \tag{A.9}$$

where we use h_0, $h^{(11)}$, etc. to denote the effective matrix elements of the general quasiparticle Hamiltonian ($h^{(11)}$ is associated with operators that contain a non-*tilde*

and a *tilde* quasiparticle each, $h^{(20)}$ with two non-*tilde* quasiparticle operators, and so on), which are given by

$$h_0 = \sum_a y_a^2 h_{aa} + \frac{1}{2}\sum_{ab} y_a^2 y_b^2 u_{abab} \tag{A.10}$$

$$h_{ab}^{(11)} = x_a y_b f_{ab}, \quad h_{ab}^{(20)} = x_a x_b f_{ab}, \quad h_{ab}^{(02)} = -y_a y_b f_{ab}, \quad \text{with} \quad f_{ab} = \delta_{ab} h_{ab} + \sum_c y_c^2 u_{acbc} \tag{A.11}$$

$$\begin{aligned} h_{abcd}^{(221)} &= \frac{1}{4} x_a x_b y_c y_d u_{abcd}, \quad h_{abcd}^{(222)} = x_a x_c y_b y_d u_{adbc}, \quad h_{abcd}^{(31)} = -\frac{1}{2} x_a x_b y_c x_d u_{abcd}, \\ h_{abcd}^{(13)} &= -\frac{1}{2} x_a y_b y_c y_d u_{adbc}, \quad h_{abcd}^{(40)} = \frac{1}{4} x_a x_b x_c x_d u_{abcd}, \quad h_{abcd}^{(04)} = \frac{1}{4} y_a y_b y_c y_d u_{abcd}. \end{aligned} \tag{A.12}$$

In obtaining the above expressions, we have assumed real matrix elements in the Hamiltonian. The residuals can then be expressed compactly in terms of the effective Hamiltonian matrix elements,

$$\begin{aligned} \mathcal{R}_H^0 &= \langle 0| \left(e^{-S} H e^S - H_0 \right) |0\rangle , \\ &= h_0 - \sum_a y_a^2 \epsilon_a + \sum_{ab} h_{ab}^{(11)} s_{ab} + \sum_{abcd} \left(2 s_{ac} s_{bd} + s_{abcd} \right) h_{abcd}^{(221)} \end{aligned} \tag{A.13a}$$

$$\begin{aligned} \mathcal{R}_H^{pq} &= \langle 0| \tilde{a}_q a_p \left(e^{-S} H e^S - H_0 \right) |0\rangle, \\ &= h_{pq}^{(11)} - \delta_{pq} \epsilon_p x_p y_p + \sum_a \left(h_{aq}^{(02)} s_{pa} + h_{ap}^{(20)} s_{aq} \right) \\ &\quad - \sum_{ab} \left(h_{ab}^{(11)} \left(s_{aq} s_{pb} + s_{pabq} \right) - h_{pqab}^{(222)} s_{ab} \right) \\ &\quad + \sum_{abc} \left(h_{abcq}^{(13)} \left(2 s_{ab} s_{pc} + s_{apbc} \right) - h_{abcp}^{(31)} \left(2 s_{ac} s_{bq} + s_{abcq} \right) \right) \\ &\quad - 2 \sum_{abcd} h_{abcd}^{(221)} \left(2 s_{ac} (s_{bq} s_{pd} + s_{pbdq}) - s_{aq} s_{bpcd} - s_{pc} s_{abdq} \right) \end{aligned} \tag{A.13b}$$

$$
\begin{aligned}
\mathcal{R}_H^{pqrs} &= \langle 0|\tilde{a}_r\tilde{a}_s a_q a_p \left(e^{-S}He^S - H_0\right)|0\rangle, \\
&= \mathcal{P}(pq)\mathcal{P}(rs)\left[h^{(221)}_{pqrs} + \sum_a \left(\frac{1}{2}\left(h^{(02)}_{ar}s_{pqas} + h^{(20)}_{ap}s_{aqrs}\right) + h^{(13)}_{prsa}s_{qa} + h^{(31)}_{pqsa}s_{ar}\right)\right. \\
&+ \frac{1}{2}\sum_{ab}\left(h^{(04)}_{abrs}(2s_{pa}s_{qb} + s_{pqab}) + h^{(40)}_{abpq}(2s_{ar}s_{bs} + s_{abrs}) - h^{(11)}_{ab}(s_{ar}s_{pqbs} + s_{pb}s_{aqrs})\right. \\
&- 2h^{(222)}_{prab}(s_{qabs} + s_{as}s_{qb})\Big) + \sum_{abc}\left(h^{(13)}_{abcr}\left(s_{ab}s_{pqcs} + \frac{1}{2}s_{as}(2s_{pb}s_{qc} + s_{pqbc}) - 2s_{pb}s_{aqcs}\right)\right. \\
&+ h^{(31)}_{abcq}\left(s_{ac}s_{bprs} + \frac{1}{2}s_{pc}(2s_{ar}s_{bs} + s_{abrs}) - 2s_{ar}s_{bpcs}\right)\Big) \\
&- \sum_{abcd} h^{(221)}_{abcd}\left(2s_{ac}(s_{br}s_{pqds} + s_{pd}s_{bqrs}) - \frac{1}{2}s_{ar}s_{bs}(2s_{pc}s_{qd} + s_{pqcd}) + 4s_{ar}s_{pc}s_{bqds}\right. \\
&\left.\left. - \frac{1}{4}s_{abrs}(2s_{pc}s_{qd} + s_{pqcd}) + (s_{abcr}s_{pqds} + s_{apcd}s_{bqrs}) + 2s_{bqdr}s_{apcs}\right)\right]. \qquad \text{(A.13c)}
\end{aligned}
$$

where we have used the Baker-Campbell-Hausdorff expansion to simplify the similarity transformation, i.e.

$$e^{-S}He^S = H + [H,S] + \frac{1}{2!}[[H,S],S] + \ldots. \qquad \text{(A.14)}$$

For a two-body Hamiltonian, with S truncated to at most double quasiparticle excitations, this expansion truncates at fourth order. Diagrammatic expressions for these equations can also be formulated along similar lines as Bogoliubov coupled cluster methods. [112] The operator-derivative terms in the β-evolution are given by

$$S^0_\beta = \frac{1}{2}\sum_a \epsilon_a x_a y_a s_{aa} \qquad \text{(A.15a)}$$

$$S^{pq}_\beta = -\frac{1}{2}\sum_a \epsilon_a x_a y_a \left(s_{pa}s_{aq} + s_{paaq}\right) \qquad \text{(A.15b)}$$

$$S^{pqrs}_\beta = \frac{1}{4}\mathcal{P}(pq)\mathcal{P}(rs)\sum_a \epsilon_a x_a y_a \left(s_{as}s_{pqar} - s_{qa}s_{aprs}\right). \qquad \text{(A.15c)}$$

Appendix B

Equivalence of number-projected quasiparticle CISD and CID ansätze

The grand-canonical thermal CI results presented in this thesis use an ansatz truncated at single and double quasiparticle excitations. On the other hand, for the canonical ensemble number-projected CI theory, we use only double quasiparticle excitations. Here, we provide proof that quasiparticle CISD and CID span the same portion of the Hilbert space. Consider a general CID state,

$$\Omega_{CID} \left|0(\alpha,\beta)\right\rangle = e^{t_0} \left(1 + \sum_{pqrs} t_{pqrs} a_p^\dagger \tilde{a}_r^\dagger a_q^\dagger \tilde{a}_s^\dagger\right) \left|0(\alpha,\beta)\right\rangle . \tag{B.1}$$

Using the thermal Bogoliubov transformation in Eq. 3.7, the pair=creation operator $a_p^\dagger \tilde{a}_r^\dagger$ can be rewritten in terms of the zero-temperature Fermi operators,

$$a_p^\dagger \tilde{a}_r^\dagger = x_p x_r c_p^\dagger \tilde{c}_r^\dagger - y_p y_r \tilde{c}_p c_r + x_p y_r \left(c_p^\dagger c_r + \tilde{c}_r^\dagger \tilde{c}_p - 1\right), \tag{B.2}$$

which, for $p = r$, simplifies into

$$a_p^\dagger \tilde{a}_p^\dagger = x_p^2 c_p^\dagger \tilde{c}_p^\dagger - y_p^2 \tilde{c}_p c_p + x_p y_p \left(c_p^\dagger c_p + \tilde{c}_p^\dagger \tilde{c}_p - 1\right). \tag{B.3}$$

Re-parametrizing the CI amplitudes as

$$t_{pqrs} = s_{pqrs} + \frac{\delta_{pr}}{x_p y_p} \lambda_{qs}, \tag{B.4}$$

we can rearrange the terms in Eq. B.1 to obtain

$$\Omega_{CID}\left|0(\alpha,\beta)\right\rangle = e^{t_0}\left(1+\sum_{pqrs} s_{pqrs}a_p^\dagger\tilde{a}_r^\dagger a_q^\dagger\tilde{a}_s^\dagger + \sum_{pqs}\frac{\lambda_{qs}}{x_p y_p}\left(x_p^2 c_p^\dagger\tilde{c}_p^\dagger - y_p^2\tilde{c}_p c_p\right)a_q^\dagger\tilde{a}_s^\dagger\right.$$
$$\left. + \sum_{pqs}\frac{\lambda_{qs}}{x_p y_p}x_p y_p\left(n_p+\tilde{n}_p-1\right)a_q^\dagger\tilde{a}_s^\dagger\right)\left|0(\alpha,\beta)\right\rangle, \tag{B.5a}$$
$$= e^{t_0}\left(1+\sum_{pqrs} s_{pqrs}a_p^\dagger\tilde{a}_r^\dagger a_q^\dagger\tilde{a}_s^\dagger + \sum_{pqs}\frac{\lambda_{qs}}{x_p y_p}\left(x_p^2 c_p^\dagger\tilde{c}_p^\dagger - y_p^2\tilde{c}_p c_p\right)a_q^\dagger\tilde{a}_s^\dagger\right.$$
$$\left. + \sum_{qs}\lambda_{qs}\left(N+\tilde{N}-N_{\text{levels}}\right)a_q^\dagger\tilde{a}_s^\dagger\right)\left|0(\alpha,\beta)\right\rangle. \tag{B.5b}$$

In the canonical ensemble, or in the presence of a number-projection operator, the total number operator for the physical and auxiliary particles is a symmetry of the thermal wave function. Therefore, $\mathcal{P}_{N_0}\Omega_{CID}$ reduces to

$$\mathcal{P}_{N_0}\Omega_{CID} = \mathcal{P}_{N_0}e^{t_0}\left(1+\sum_{pqrs} s_{pqrs}a_p^\dagger\tilde{a}_r^\dagger a_q^\dagger\tilde{a}_s^\dagger + \sum_{pqs}\frac{\lambda_{qs}}{x_p y_p}\left(x_p^2 c_p^\dagger\tilde{c}_p^\dagger - y_p^2\tilde{c}_p c_p\right)a_q^\dagger\tilde{a}_s^\dagger\right.$$
$$\left. + \left(2N_0 - N_{\text{levels}}\right)\mathcal{P}_{N_0}\sum_{qs}\lambda_{qs}a_q^\dagger\tilde{a}_s^\dagger\right)\left|0(\alpha,\beta)\right\rangle. \tag{B.6}$$

Finally, reexpressing $c_p^\dagger\tilde{c}_p^\dagger$ and $\tilde{c}_p c_p$ in terms of quasiparticle operators, we get,

$$c_p^\dagger\tilde{c}_p^\dagger = \left(x_p a_p^\dagger + y_p\tilde{a}_p\right)\left(x_p\tilde{a}_p^\dagger - y_p a_p\right), \tag{B.7a}$$
$$= x_p^2 a_p^\dagger\tilde{a}_p^\dagger - y_p^2\tilde{a}_p a_p - x_p y_p\left(a_p^\dagger a_p + \tilde{a}_p^\dagger\tilde{a}_p - 1\right), \tag{B.7b}$$
$$\tilde{c}_p c_p = -y_p^2 a_p^\dagger\tilde{a}_p^\dagger + x_p^2\tilde{a}_p a_p - x_p y_p\left(a_p^\dagger a_p + \tilde{a}_p^\dagger\tilde{a}_p - 1\right). \tag{B.7c}$$

As is already apparent from Eq. B.6, substituting these relations into Eq. B.6, followed by normal ordering of the quasiparticle operators, we end up with a number-projected thermal CISD wave function. In general, partial traces of higher rank terms in the number-projected CI operator are proportional to the lower-rank terms.

Appendix C

Equations for number-projected CID and thermal AGP-based PT2

In this appendix, we present detailed equations for the number-projected CID and thermal AGP-based second-order perturbation theory. Both of these theories were discussed in Chapter 4. For the number-projected CID, we will also present data for the convergence of imaginary-time evolution as a function of the step size in β.

C.1 Number-projected CI

C.1.1 Ansatz

In the number-projected CI theory, we start with a thermal BCS as our mean-field reference state,

$$|0(\beta)\rangle = e^{-\beta H_0/2}|\mathbb{I}\rangle, \quad \text{with} \quad H_0 = \sum_p \epsilon_p c_p^\dagger c_p. \tag{C.1}$$

The normalized form $|0(\beta)\rangle$ becomes,

$$|0(\beta)\rangle = \prod_p \left(x_p + y_p c_p^\dagger \tilde{c}_p^\dagger\right)|-;-\rangle, \tag{C.2}$$

where x and y coefficients are defined as,

$$x_p = \frac{1}{\sqrt{1+e^{-\beta\epsilon_p}}}, \tag{C.3a}$$

$$y_p = \frac{e^{-\beta\epsilon_p/2}}{\sqrt{1+e^{-\beta\epsilon_p}}}. \tag{C.3b}$$

The thermal state is then parameterized as a number-projected quasiparticle CI doubles (CID) state,

$$|\Psi\rangle = \mathcal{P} e^{t_0}(1+T)|0(\beta)\rangle, \tag{C.4a}$$

$$T = \frac{1}{4}\sum_{pqrs} t_{pqrs} a_p^\dagger a_q^\dagger \tilde{a}_s^\dagger \tilde{a}_r^\dagger. \tag{C.4b}$$

where T creates double quasiparticle excitations on the reference. Here, $a, \tilde{a}$ are quasiparticle operators that annihilate the mean-field reference, i.e. $a_p|0(\beta)\rangle = 0 = \tilde{a}_p|0(\beta)\rangle$, and are related to the physical creation/annihilation operators via a BCS transformation,

$$\begin{bmatrix} a_p \\ \tilde{a}_p^\dagger \end{bmatrix} = \begin{bmatrix} x_p & -y_p \\ y_p & x_p \end{bmatrix} \begin{bmatrix} c_p \\ \tilde{c}_p^\dagger \end{bmatrix}, \tag{C.5}$$

It is convenient to express the Hamiltonian in terms of the quasiparticle creation/annihilation operators,

$$\begin{aligned} H = h_0 &+ h_{pq}^{(20)} a_p^\dagger a_q + h_{pq}^{(02)} \tilde{a}_p^\dagger \tilde{a}_q + h_{pq}^{(11)}(a_p^\dagger \tilde{a}_q^\dagger + \text{h.c.}) + h_{pqrs}^{(31)}(a_p^\dagger a_q^\dagger \tilde{a}_r^\dagger a_s + \text{h.c.}) \\ &+ h_{pqrs}^{(13)}(a_p^\dagger \tilde{a}_q^\dagger \tilde{a}_r^\dagger \tilde{a}_s + \text{h.c.}) + h_{pqrs}^{(221)}(a_p^\dagger a_q^\dagger \tilde{a}_s^\dagger \tilde{a}_r^\dagger + \text{h.c.}) + h_{pqrs}^{(222)} a_p^\dagger \tilde{a}_q^\dagger \tilde{a}_s a_r. \end{aligned} \tag{C.6}$$

where we have assumed Einstein summation convention. The matrix elements have been worked out in the Appendix of Ref. 69. Lastly, we note that we employ an integral representation for the number-projection operator,

$$\mathcal{P}_{N_0} = \frac{1}{2\pi}\int_0^{2\pi} d\phi\, e^{i\phi(N_0 - N)}, \tag{C.7}$$

where N is the physical number operator and N_0 is the target number of particles.

C.1.2 CID equations

Substituting the number-projected CID ansatz in to the imaginary-time evolution equation, and using the fact that the Hamiltonian commutes with the number-

projection operator $\mathcal{P}_{N_0}$, we get

$$\mathcal{P}_{N_0}\left[\frac{dt_0}{d\beta}(1+T)+\frac{dT}{d\beta}\right]|0(\beta)\rangle = -\frac{1}{2}\mathcal{P}_{N_0}\left[H(1+T)-(1+T)H_0\right]|0(\beta)\rangle \tag{C.8}$$

We have noted in the main text (as well as in our recent work in Refs. 68, 69) that the derivative of the CI operator splits into the derivative of the amplitudes and that of the temperature-dependent quasiparticle creation operators,

$$\frac{dT}{d\beta} = \frac{d_{amp}T}{d\beta} + \frac{d_{op}T}{d\beta}, \tag{C.9}$$

where the operator derivative can be worked out directly from the BCS transformation. Using the above relations and expanding out the integral form of $\mathcal{P}_{N_0}$, the time-evolution equation simplifies as

$$\int_0^{2\pi} d\phi\, g(\phi)\, e^{-i\phi N}\, \mathcal{L}\,|0\rangle = \int_0^{2\pi} d\phi\, g(\phi)\, e^{-i\phi N}\, \mathcal{R}\,|0\rangle, \tag{C.10}$$

where $g(\phi)$ is the weight of integration, $\mathcal{L}$ and $\mathcal{R}$ are effective LHS and RHS kernels respectively, each defined as

$$g(\phi) = e^{i\phi N_0}/2\pi, \tag{C.11a}$$

$$\mathcal{L} = \frac{dt_0}{d\beta}(1+T) + \frac{d_{amp}T}{d\beta}, \tag{C.11b}$$

$$\mathcal{R} = -\frac{1}{2}\left[H(1+T)-(1+T)H_0\right] - \frac{d_{op}T}{d\beta}. \tag{C.11c}$$

The RHS kernel is effectively a four-body operator, and we find it convenient to re-write it in terms of antisymmetrized matrix elements,

$$\mathcal{R} = R_0 + R_{pq}a_p^\dagger\tilde{a}_q^\dagger + R_{[pq][rs]}a_p^\dagger a_q^\dagger\tilde{a}_s^\dagger\tilde{a}_r^\dagger + R_{[pqr][ijk]}a_p^\dagger a_q^\dagger a_r^\dagger\tilde{a}_k^\dagger\tilde{a}_j^\dagger\tilde{a}_i^\dagger + R_{[pqrs][ijkl]}a_p^\dagger a_q^\dagger a_r^\dagger a_s^\dagger\tilde{a}_l^\dagger\tilde{a}_k^\dagger\tilde{a}_j^\dagger\tilde{a}_i^\dagger, \tag{C.12}$$

where we have assumed Einstein summation, and [...] denotes antisymmetrized indices. The matrix elements of $\mathcal{R}$ are defined as,

$$R_0 = -\frac{1}{2}\left(h_0 - \sum_a \epsilon_a y_a^2 + \sum_{abcd} h^{(221)}_{abcd} t_{abcd}\right), \tag{C.13a}$$

$$R_{ab} = \frac{1}{2}\left(\delta_{ab}\epsilon_a x_a y_a - h^{(11)}_{ab} + \sum_c \epsilon_c x_c y_c t_{acbc} - \sum_{cd} h^{(11)}_{cd} t_{acbd} + \sum_{cdi}\left[h^{(13)}_{cdib} t_{acdi} - h^{(31)}_{cdia} t_{cdbi}\right]\right), \tag{C.13b}$$

$$R_{abcd} = \frac{1}{4}\chi_{(ab-ba)(cd-dc)} = \frac{1}{4}\left(\chi_{abcd} - \chi_{abdc} - \chi_{bacd} + \chi_{badc}\right), \tag{C.13c}$$

$$\chi_{abcd} = \frac{1}{2}\left(-\frac{1}{4}\left[h_0 t_{abcd} + 4h^{(221)}_{abcd}\right] + \frac{1}{4}\sum_i\left[\epsilon_i y_i^2 t_{abcd} + 2h^{(02)}_{ci} t_{abdi} + 2h^{(20)}_{ai} t_{bicd}\right] - \frac{1}{2}\sum_{ij}\left[t_{abij} h^{(04)}_{ijcd} + 2h^{(222)}_{acij} t_{bidj} + h^{(40)}_{abij} t_{ijcd}\right]\right), \tag{C.13d}$$

$$R_{pqrabc} = \frac{1}{9}\chi_{(pqr-qpr-rqp)(abc-bac-cba)}, \tag{C.13e}$$

$$\chi_{pqrabc} = \frac{1}{2}\left(\frac{1}{4}\delta_{ap}\epsilon_p x_p y_p t_{qrbc} - \frac{1}{4}h^{(11)}_{pa} t_{qrbc}\right) + \frac{1}{4}\sum_i\left(h^{(13)}_{pbci} t_{qrai} + h^{(31)}_{qrai} t_{ipbc}\right), \tag{C.13f}$$

$$R_{pqrsabcd} = \frac{1}{36}\chi_{(pqrs-prqs-rqps-sqrp+rspq+psqr)(abcd-acbd-cbad-dbca+cdab+adbc)}, \tag{C.13g}$$

$$\chi_{pqrsabcd} = -\frac{1}{8}h^{(221)}_{pqab} t_{rscd}. \tag{C.13h}$$

Ultimately, we get the equations governing the β-evolution of the CI amplitudes by taking the expectation value of Eq. C.10 against ground and doubly-excited quasiparticle subspace on the bra state, i.e.

$$\int d\phi\, g(\phi)\, \langle 0|\nu e^{-i\phi N}\, \mathcal{L}\, |0\rangle = \int d\phi\, g(\phi)\, \langle 0|\nu e^{-i\phi N}\, \mathcal{R}\, |0\rangle, \tag{C.14}$$

where $\nu = \{1,\, \tilde{a}_r \tilde{a}_s a_q a_p\}$. After some rearrangements, the working equation takes the form

$$\int d\phi\, w(\phi)\, \langle \phi|\bar{\nu}\, \mathcal{L}\, |0\rangle = \int d\phi\, w(\phi)\, \langle \phi|\bar{\nu}\, \mathcal{R}\, |0\rangle, \tag{C.15}$$

where

$$\bar{\nu} = e^{i\phi N}\,\nu\,e^{-i\phi N}, \tag{C.16a}$$

$$w(\phi) = \frac{1}{2\pi} e^{i\phi N_0} \langle 0|e^{-i\phi N}|0\rangle, \tag{C.16b}$$

$$\langle\phi| = \frac{\langle 0|e^{-i\phi N}}{\langle 0|e^{-i\phi N}|0\rangle}. \tag{C.16c}$$

The overlap in $w(\phi)$ is straightforward to compute:

$$\langle 0|e^{-i\phi N}|0\rangle = \prod_p \left(x_p^2 + y_p^2 e^{-i\phi}\right). \tag{C.17}$$

The construction of the similarity transformed operator $\bar{\nu}$ can be simplified by introducing rotated quasi-particle operators,

$$b_p = e^{i\phi N} a_p e^{-i\phi N}, \quad \text{and,} \quad \tilde{b}_p = e^{i\phi N} \tilde{a}_p e^{-i\phi N}, \tag{C.18}$$

which gives $\bar{\nu} = \{1, \tilde{b}_r \tilde{b}_s b_q b_p\}$. The overlaps in Eq. C.15 can then be evaluated by using a generalized version of Wick's theorem, with the relevant contractions given by,

$$\langle\phi|a_p^\dagger \tilde{a}_q^\dagger|0\rangle = \delta_{pq} G_p = -\langle\phi|\tilde{a}_p^\dagger a_q^\dagger|0\rangle = \langle\phi|\tilde{b}_p b_q|0\rangle, \tag{C.19a}$$

$$\langle\phi|a_p a_q^\dagger|0\rangle = \delta_{pq} = \langle\phi|\tilde{a}_p \tilde{a}_q^\dagger|0\rangle, \tag{C.19b}$$

$$\langle\phi|b_p a_q^\dagger|0\rangle = \delta_{pq} A_p, \tag{C.19c}$$

$$\langle\phi|\tilde{b}_p \tilde{a}_q^\dagger|0\rangle = \delta_{pq} B_p, \tag{C.19d}$$

where we have

$$A_p = \frac{1}{x_p^2 e^{i\phi} + y_p^2}, \tag{C.20a}$$

$$B_p = \frac{1}{x_p^2 + y_p^2 e^{-i\phi}}, \tag{C.20b}$$

$$G_p = \frac{x_p y_p (e^{-i\phi} - 1)}{x_p^2 + y_p^2 e^{-i\phi}}. \tag{C.20c}$$

After all the manipulation, the overlaps for the LHS and the RHS kernels turn out as follows:

1. First, for $\bar{\nu} = 1$,

$$\langle\phi|\mathcal{R}|0\rangle = R_0 + \sum_a G_a R_{aa} + 2\sum_{ab} G_a G_b R_{abab} + 6\sum_{abc} G_a G_b G_c R^{(30)}_{abc} + 24\sum_{abcd} G_a G_b G_c G_d R^{(40)}_{abcd}, \tag{C.21a}$$

$$\langle\phi|\mathcal{L}|0\rangle = \left(1 + \frac{1}{2}\sum_{ij} G_i G_j t_{ijij}\right)\frac{dt_0}{d\beta} + \frac{1}{2}\sum_{ij} G_i G_j \frac{dt_{ijij}}{d\beta} \tag{C.21b}$$

where $R^{(30)}_{abc} = R_{abcabc}$ and $R^{(40)}_{abcd} = R_{abcdabcd}$.

2. And for $\bar{\nu} = \tilde{b}_c\tilde{b}_d b_b b_a$,

$$\chi_{ab} = A_a B_b \left(R_{ab} + 4\sum_i G_i R_{aibi} + 18\sum_{ij} G_i G_j R^{(31)}_{abij} + 96\sum_{ijk} G_i G_j G_k R^{(41)}_{abijk}\right), \tag{C.22a}$$

$$\langle\phi|\tilde{b}_c\tilde{b}_d b_b b_a\mathcal{R}|0\rangle = (1-P_{ab})(1-P_{cd})\left[\frac{1}{2}\delta_{ac}\delta_{bd}G_a G_b\langle\phi|\mathcal{R}|0\rangle + \delta_{ac}G_a\chi_{bd} + A_a A_b B_c B_d\left(R_{abcd} + 9\sum_i G_i R^{(32)}_{abcdi} + 72\sum_{ij} G_i G_j R^{(42)}_{abcdij}\right)\right], \tag{C.22b}$$

$$\zeta_{ab} = A_a B_b\left[\left(\sum_i G_i t_{aibi}\right)\frac{dt_0}{d\beta} + \sum_i G_i\frac{dt_{aibi}}{d\beta}\right] \tag{C.22c}$$

$$\langle\phi|\tilde{b}_c\tilde{b}_d b_b b_a\mathcal{L}|0\rangle = (1-P_{ab})(1-P_{cd})\left[\frac{1}{2}\delta_{ac}\delta_{bd}S_a S_b\langle\phi|\mathcal{L}|0\rangle + \delta_{ac}S_a\zeta_{bd} + \frac{A_a A_b B_c B_d}{4}\left(t_{abcd}\frac{dt_0}{d\beta} + \frac{dt_{abcd}}{d\beta}\right)\right], \tag{C.22d}$$

where $R^{(31)}_{abij} = R_{aijbij}$, $R^{(41)}_{abijk} = R_{aijkbijk}$, $R^{(32)}_{abcdi} = R_{abicdi}$, $R^{(42)}_{abcdij} = R_{abijcdij}$, and P_{ab} is the conventional exchange operator.

C.2 Canonical ensemble perturbation theory

In contrast to the number-projected CI, the perturbation theory adds corrections to the thermal AGP, which is an eigenstate of the total number operator. Moreover, the corrections are also introduced in a number-conserving manner, and therefore an explicit number projection is not required. We first partition the Hamiltonian into a mean-field and an interaction part,

$$H = H_0 + \lambda V, \tag{C.23a}$$

$$H_0 = \sum_p \epsilon_p c_p^\dagger c_p, \tag{C.23b}$$

$$V = \sum_{pq} v_{pq} c_p^\dagger c_q + \frac{1}{4} \sum_{pqrs} v_{pqrs} c_p^\dagger c_q^\dagger c_s c_r. \tag{C.23c}$$

The canonical-ensemble thermal state, which obeys the imaginary-time evolution equation $d_\tau |\Psi(\tau)\rangle = -H|\Psi(\tau)\rangle/2$, can be expressed as a perturbation series expansion,

$$|\Psi(\tau)\rangle = |\Psi_0\rangle + \lambda|\Psi_1\rangle + \lambda^2|\Psi_2\rangle + \ldots. \tag{C.24}$$

Substituting this form of $|\Psi(\tau)\rangle$ into the imaginary-time evolution equation, we get

$$d_\tau \left(|\Psi_0\rangle + \lambda|\Psi_1\rangle + \lambda^2|\Psi_2\rangle + \ldots\right) = -\frac{1}{2}(H_0 + \lambda V)\left(|\Psi_0\rangle + \lambda|\Psi_1\rangle + \lambda^2|\Psi_2\rangle + \ldots\right). \tag{C.25}$$

Equating the terms at various orders in λ on the left and right hand sides gives

$$\mathcal{O}(\lambda^0): \qquad d_\tau|\Psi_0\rangle = -\frac{1}{2}H_0|\Psi_0\rangle, \tag{C.26a}$$

$$\mathcal{O}(\lambda^1): \qquad d_\tau|\Psi_1\rangle = -\frac{1}{2}\big(H_0|\Psi_1\rangle + V|\Psi_0\rangle\big), \tag{C.26b}$$

$$\mathcal{O}(\lambda^2): \qquad d_\tau|\Psi_2\rangle = -\frac{1}{2}\big(H_0|\Psi_2\rangle + V|\Psi_1\rangle\big), \tag{C.26c}$$

and similarly for higher orders. For the purpose of this work, we confine ourselves to the second order perturbation theory. Without the loss of any generality, we can

assume $|\Psi_n\rangle = e^{-\tau H_0/2}|\phi_n\rangle$. This simplifies Eq. C.26 to,

$$d_\tau|\phi_0\rangle = 0, \tag{C.27a}$$

$$d_\tau|\phi_1\rangle = -\frac{1}{2}\, e^{\tau H_0/2} V e^{-\tau H_0/2}|\phi_0\rangle, \tag{C.27b}$$

$$d_\tau|\phi_2\rangle = -\frac{1}{2}\, e^{\tau H_0/2} V e^{-\tau H_0/2}|\phi_1\rangle. \tag{C.27c}$$

These equations can then be integrated, starting from a known initial condition (generally $\tau = 0$), to the desired inverse temperature β. Recognizing that at $\beta = 0$, extreme AGP is the exact canonical thermal state, we get

$$|\phi_0(\beta)\rangle = |AGP(\beta = 0)\rangle = \left(\sum_p P_p^\dagger\right)^{N_0} |-;-\rangle, \tag{C.28}$$

where N_0 is again the desired number of particles and $P_p^\dagger = c_p^\dagger \tilde{c}_p^\dagger$. Consequently, we recover the thermal AGP as the zeroth order approximation,

$$|\Psi_0(\beta)\rangle = e^{-\beta H_0/2}|\mathrm{AGP}(0)\rangle = |\mathrm{AGP}(\beta)\rangle. \tag{C.29}$$

At the first order, we have

$$|\Psi_1(\beta)\rangle = -\frac{e^{-\beta H_0/2}}{2} \int_0^\tau d\tau\, e^{\tau H_0/2} V e^{-\tau H_0/2}|\mathrm{AGP}(0)\rangle, \tag{C.30a}$$

$$= -\frac{1}{2}\int_0^\beta d\tau\, e^{-(\beta-\tau)H_0/2} V e^{(\beta-\tau)H_0/2}|\Psi_0(\beta)\rangle, \tag{C.30b}$$

$$= -\frac{1}{2}\int_0^\beta d\tau\, e^{-\tau H_0/2} V e^{\tau H_0/2}|\Psi_0(\beta)\rangle, \tag{C.30c}$$

Likewise, the second order contribution to the wave function is

$$|\Psi_2(\beta)\rangle = -\frac{e^{-\beta H_0/2}}{2}\int_0^\beta d\tau\, e^{\tau H_0/2} V e^{-\tau H_0/2}|\phi_1(\tau)\rangle, \tag{C.31a}$$

$$= \frac{e^{-\beta H_0/2}}{4}\int_0^\beta d\tau\, e^{\tau H_0/2} V e^{-\tau H_0/2}\int_0^\tau d\tau'\, e^{\tau' H_0/2} V e^{-\tau' H_0/2}|\phi_0\rangle, \tag{C.31b}$$

$$= \frac{1}{4}\int_0^\beta d\tau\, e^{-(\beta-\tau)H_0/2} V e^{(\beta-\tau)H_0/2}\int_0^\tau d\tau'\, e^{-(\beta-\tau')H_0/2} V e^{(\beta-\tau')H_0/2}|\Psi_0(\beta)\rangle, \tag{C.31c}$$

$$= \frac{1}{4}\int_0^\beta d\tau\, e^{-\tau H_0/2} V e^{\tau H_0/2}\int_0^{\beta-\tau} d\tau'\, e^{-(\beta-\tau')H_0/2} V e^{(\beta-\tau')H_0/2}|\Psi_0(\beta)\rangle, \tag{C.31d}$$

$$= \frac{1}{4}\int_0^\beta d\tau\, e^{-\tau H_0/2} V e^{\tau H_0/2}\int_\tau^\tau d\tau'\, e^{-\tau' H_0/2} V e^{\tau' H_0/2}|\Psi_0(\beta)\rangle. \tag{C.31e}$$

These perturbative corrections are analogous to the Dyson series expansion for interaction picture, imaginary-time perturbation theory. The diagonal form of H_0 allows us to perform the similarity transformation of V easily,

$$e^{-\tau H_0/2} V e^{\tau H_0/2} = v_{pq} e^{-\tau\Delta_{pq}/2} p^\dagger q + \frac{1}{4} v_{pqrs} e^{-\tau\Delta_{pqrs}/2} p^\dagger q^\dagger s r, \tag{C.32}$$

where $\Delta_{pq} = \epsilon_p - \epsilon_q$, and $\Delta_{pqrs} = \epsilon_p + \epsilon_q - \epsilon_r - \epsilon_s$. The resulting equations can then be integrated analytically.

C.3 Step-size convergence

As indicated in the main text, we use a step size of $\Delta\beta = 0.001$ or smaller in the fourth-order Runge-Kutta method while integrating the system of ODE's in the projected CI theory. In Fig. C.1, we plot the error in internal energy for the six-site Hubbard models with $U/t = 2$ at half-filling (left panel), and with $U/t = 10$ with four electrons (right panel). The results numerically demonstrate the convergence of the integration with respect to the step size.

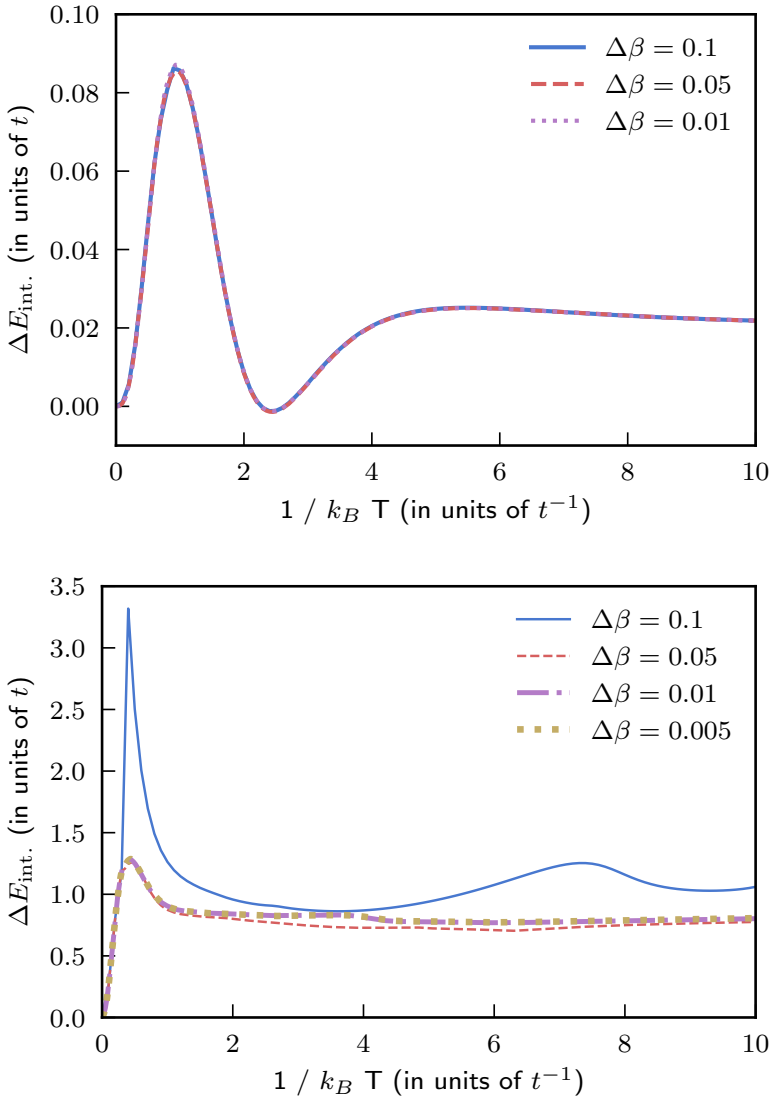

Figure C.1 : Error in the projected CI internal energy for the six-site Hubbard model with $U/t = 2$ and six-electrons (top panel), and $U/t = 10$ and four electrons (bottom panel), with various step-sizes used to integrate the projected-CI ODEs.

Appendix D

Optimization of thermal AGP

In this appendix, we present a comparison between optimized and un-optimized thermal mean-field, the ground-state limit of thermal methods, and convergence of the projected-CI evolution with respect to step size in the integration. For the optimized mean-field, we minimize the free energy with respect to the η's in the thermal AGP. The left panel in Fig. D.1 presents the data for the 6-site Hubbard model with $U/t = 2$ and $N = 4, 6$, as well as $U/t = 10$ and $N = 4$. Except in the case of very high temperatures, or very low β, the optimized and the un-optimized mean-field theories perform more or less similarly. The right panel in Fig. D.1 shows similar data for the Hydrogen molecule at a bond length of $0.74\mathring{A}$ in two different basis sets. In contrast to the Hubbard model results, the difference between the optimized and the un-optimized mean-field theories is more pronounced for Hydrogen. However, as we have noted in the main text, the number-projected CID is exact for a two-electron system whether or not we start with a better reference. This allows us to safely use un-optimized mean-field as a reference to construct correlated theories such as projected CID and AGP-based perturbation theory. We would like to note that these results do not take orbital optimization into account, but instead, minimize the free energy only with respect to the BCS/AGP parameters.

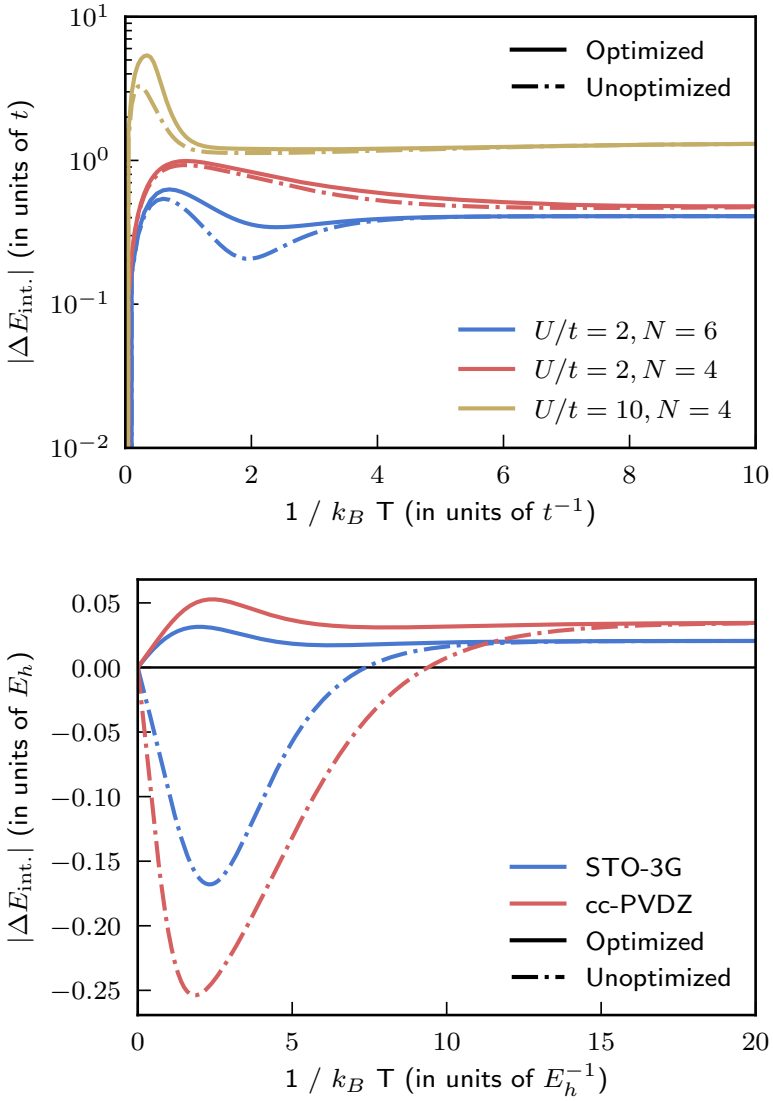

Figure D.1 : Error in the canonical-ensemble internal energy for the 6-site Hubbard model with $U/t = 2$ and 10 at different filling fractions (left panel), and the Hydrogen molecule at bond-length of $0.74\mathring{A}$ in STO-3G and cc-PVDZ bases (right panel). The data compares mean-field thermal AGP results with optimized versus un-optimized η-parameters.

Appendix E

Symmetry breaking in Lipkin model

The Lipkin-Meshkov-Glick Hamiltonian, given by

$$H = xJ_z - \frac{1-x}{n}\big(J_+J_+ + J_-J_-\big), \tag{E.1}$$

commutes with the Casimir operator,

$$J^2 = \frac{J_+J_- + J_-J_+}{2} + J_zJ_z. \tag{E.2}$$

The J^2-eigenvalue is determined by the total number of spins; for n spins, the eigenstates of H reside in the $j = n/2$ sector. The Hamiltonian also commutes with the parity operator, $\hat{P} = e^{i\pi J_z}$, the symmetry of interest. For a given spin-configuration, the parity eigenvalue is 1 (or -1) if the difference in the number of up and down spins is even (or odd). Therefore, simultaneous eigenstates of H and $\hat{P}$ are made out of spin-configurations, all of which have only even or only odd parity. As a result, the symmetry preserving mean-field (or the restricted Hartree-Fock) state that optimizes the energy is simply the configuration with all down-spins, i.e.

$$|\phi_{RHF}\rangle = \bigotimes_i |\downarrow\rangle_i \,. \tag{E.3}$$

The corresponding mean-field Hamiltonian and the mean-field ground-state energy are

$$H_0^{RHF} = xJ_z, \tag{E.4a}$$

$$E_{RHF} = -\frac{nx}{2}. \tag{E.4b}$$

While working in the symmetry adapted basis, we use H_0^{RHF} to define the mean-field thermal state.

We can also consider a rotated product state, which is not an eigenvector of the parity operator, as the ground-state mean-field reference. This unrestricted Hartree-Fock state can be expressed as

$$|\phi_{UHF}\rangle = \frac{1}{(1+\kappa^2)^{n/2}} e^{\kappa J_+} |\phi_{RHF}\rangle \,, \tag{E.5}$$

where κ parametrizes the UHF state. Using a UHF state as an approximation to the ground-state is equivalent to a rotation of the underlying $su(2)$ algebra such that the UHF wave function has all down-spins in the new basis. The $su(2)$ operators in the new basis are related to the original operators via the following transformation,

$$J_+ = \frac{K_+ - \kappa^2 K_- - 2\kappa K_z}{1+\kappa^2}, \tag{E.6a}$$

$$J_- = \frac{K_- - \kappa^2 K_+ - 2\kappa K_z}{1+\kappa^2}, \tag{E.6b}$$

$$J_z = \frac{\kappa(K_+ + K_-) + (1-\kappa^2)K_z}{1+\kappa^2}. \tag{E.6c}$$

The Hamiltonian, expressed in terms of the K-operators, becomes

$$\begin{aligned} H = {} & h_z K_z + h_\pm (K_+ + K_-) + v_\pm (K_+ K_+ + K_- K_-) \\ & + v_z K_z^2 + v_\times K_+ K_- + v_{\pm z}(K_+ K_z + K_z K_-), \end{aligned} \tag{E.7}$$

where the Hamiltonian coefficients are defined as,

$$h_z = \frac{x(1-\kappa^2)}{1+\kappa^2} - \frac{4}{n}\frac{(1-x)\kappa^2}{(1+\kappa^2)^2}, \tag{E.8}$$

$$h_\pm = \frac{x\kappa}{1+\kappa^2} - \frac{2\kappa(1-x)(\kappa^2-1)}{n(1+\kappa^2)^2}, \tag{E.9}$$

$$v_z = -\frac{8\kappa^2(1-x)}{n(1+\kappa^2)^2}, \tag{E.10}$$

$$v_\pm = -\frac{(1-x)(1+\kappa^2)}{n(1+\kappa^2)^2}, \tag{E.11}$$

$$v_\times = \frac{4\kappa^2(1-x)}{n(1+\kappa^2)^2}, \tag{E.12}$$

$$v_{\pm z} = -\frac{4\kappa(1-x)(\kappa^2-1)}{n(1+\kappa^2)^2}. \tag{E.13}$$

The UHF mean-field Hamiltonian and the corresponding mean-field energy are

$$H_0^{UHF} = h_z K_z - \frac{v_z n}{2} K_z, \tag{E.14a}$$

$$E_{UHF} = -\frac{h_z n}{2} + \frac{v_z n^2}{4}. \tag{E.14b}$$

The UHF energy is minimized to find the optimal value of the rotation parameter κ. As noted eariler, $\kappa \neq 0$ only for $x \leq x_c$. While working in the broken-symmetry regime (i.e. $x \leq x_c$), we use H_0^{UHF} to define the mean-field thermal state.

Appendix F

Symmetry breaking in TFIM

The TFIM has a $\mathbb{Z}_2$ symmetry, i.e. if all the spins (in z-basis) are flipped, then the energy remains unchanged. In the Ising limit, i.e. for $g = 0$, the model has a doubly-degenerate ferromagnetic ground-state. In the thermodynamic limit, the $\mathbb{Z}_2$ symmetry breaks spontaneously. For finite systems, we can break this symmetry artificially by introducing the following symmetry broken mean-field state to approximate the ground-state,

$$|\phi_{UHF}\rangle = \bigotimes_p \left(-\sin\frac{\theta}{2}\,|\uparrow\rangle_p + \cos\frac{\theta}{2}\,|\downarrow\rangle_p \right). \tag{F.1}$$

The mean-field Hamiltonian and its corresponding energy depend on the rotation parameter θ, and for the one-dimensional periodic case with N spins, in the presence of an external magnetizing z-field f (see Eq. 5.32 for the Hamiltonian), they are given by

$$H_0 = \sum_i \left((\cos\theta + f)\sigma_i^z + g\sigma_i^x \right), \tag{F.2a}$$

$$E_{UHF} = -N\big(\cos^2\theta + g\sin\theta + f\cos\theta \big). \tag{F.2b}$$

The UHF energy is minimized with respect to the rotation parameter θ, the optimal values of which (at $f = 0$) are

$$\theta = \begin{cases} \arcsin g/2, & g \le 2 \\ \pi/2, & g > 2 \end{cases}. \tag{F.3}$$

We use this H_0 (with optimized θ) that breaks the $\mathbb{Z}_2$-symmetry, except when $\theta = \pi/2$, to construct the mean-field thermal state for the TFIM.

In the same way as for the Lipkin model, we can introduce a rotation in the $su(2)$ algebra so that in the new basis, the UHF state corresponds to all down-spins. The full Hamiltonian in the rotated basis then becomes

$$H = -\sum_i \Big[\cos^2\theta \sigma_i^z \sigma_{i+1}^z + \sin^2\theta \sigma_i^x \sigma_{i+1}^x - \frac{1}{2}\sin 2\theta \Big(\sigma_i^x \sigma_{i+1}^z + \sigma_i^z \sigma_{i+1}^x \Big) + g \Big(\cos\theta \sigma_i^x + \sin\theta \sigma_i^z \Big) \Big]. \tag{F.4}$$

Similarly, the mean-field Hamiltonian, written in the new basis, becomes simply

$$H_0 = -\sum_i \Big(-\cos^2\theta + g\sin\theta \Big) \sigma_i^z. \tag{F.5}$$

While the results do not depend on the choice of the basis, it is generally convenient to construct CC-like wave functions starting with a mean-field state that corresponds to all down-spins. Our description of the mean-field theory for the TFIM closely follows Ref. 132, and we recommend the reader to refer to this article for further details.

Bibliography

[1] P. A. M. Dirac, "Quantum mechanics of many-electron systems," *Proc. R. Soc. Lond. A*, vol. 123, pp. 714–733, Apr. 1929.

[2] D. R. Hartree, "The wave mechanics of an atom with a non-Coulomb central field. Part II. Some results and discussion," *Mathematical Proceedings of the Cambridge Philosophical Society*, vol. 24, pp. 111–132, Jan. 1928.

[3] J. C. Slater, "The self consistent field and the structure of atoms," *Phys. Rev.*, vol. 32, pp. 339–348, Sept. 1928.

[4] V. Fock, "Näherungsmethode zur Lösung des quantenmechanischen Mehrkörperproblems," *Z. Physik*, vol. 61, pp. 126–148, Jan. 1930.

[5] W. Kohn and L. J. Sham, "Self-consistent equations including exchange and correlation effects," *Phys. Rev.*, vol. 140, pp. A1133–A1138, Nov. 1965.

[6] P. Hohenberg and W. Kohn, "Inhomogeneous electron gas," *Phys. Rev.*, vol. 136, pp. B864–B871, Nov. 1964.

[7] C. Møller and M. S. Plesset, "Note on an approximation treatment for many-electron systems," *Phys. Rev.*, vol. 46, pp. 618–622, Oct. 1934.

[8] T. D. Crawford and H. F. Schaefer, "An introduction to coupled cluster theory for computational chemists," in *Reviews in Computational Chemistry* (K. B. Lipkowitz and D. B. Boyd, eds.), pp. 33–136, John Wiley & Sons, Inc., 2000.

[9] R. J. Bartlett and M. Musiał, "Coupled-cluster theory in quantum chemistry," *Rev. Mod. Phys.*, vol. 79, pp. 291–352, Feb. 2007.

[10] D. M. Ceperley, "Path integrals in the theory of condensed helium," *Rev. Mod. Phys.*, vol. 67, pp. 279–355, Apr. 1995.

[11] B. L. Hammond, W. A. Lester, and P. J. Reynolds, *Monte Carlo methods in ab initio quantum chemistry*, vol. Volume 1 of *World Scientific Lecture and Course Notes in Chemistry*. World Scientific, Mar. 1994.

[12] W. M. C. Foulkes, L. Mitas, R. J. Needs, and G. Rajagopal, "Quantum Monte Carlo simulations of solids," *Rev. Mod. Phys.*, vol. 73, pp. 33–83, Jan. 2001.

[13] S. Zhang and H. Krakauer, "Quantum Monte Carlo method using phase-free random walks with Slater determinants," *Phys. Rev. Lett.*, vol. 90, p. 136401, Apr. 2003.

[14] S. Zhang, "Quantum Monte Carlo methods for strongly correlated electron systems," in *Theoretical Methods for Strongly Correlated Electrons* (D. Sénéchal, A.-M. Tremblay, and C. Bourbonnais, eds.), CRM Series in Mathematical Physics, pp. 39–74, Springer New York, 2004.

[15] W. A. Al-Saidi, S. Zhang, and H. Krakauer, "Auxiliary-field quantum Monte Carlo calculations of molecular systems with a Gaussian basis," *The Journal of Chemical Physics*, vol. 124, p. 224101, June 2006.

[16] S. R. White, "Density-matrix algorithms for quantum renormalization groups," *Phys. Rev. B*, vol. 48, pp. 10345–10356, Oct. 1993.

[17] S. Östlund and S. Rommer, "Thermodynamic Limit of Density Matrix Renormalization," *Phys. Rev. Lett.*, vol. 75, pp. 3537–3540, Nov. 1995.

[18] A. Georges, G. Kotliar, W. Krauth, and M. J. Rozenberg, "Dynamical mean-field theory of strongly correlated fermion systems and the limit of infinite dimensions," *Rev. Mod. Phys.*, vol. 68, pp. 13–125, Jan. 1996.

[19] G. Knizia and G. K.-L. Chan, "Density Matrix Embedding: A Simple Alternative to Dynamical Mean-Field Theory," *Phys. Rev. Lett.*, vol. 109, p. 186404, Nov. 2012.

[20] I. W. Bulik, G. E. Scuseria, and J. Dukelsky, "Density matrix embedding from broken symmetry lattice mean fields," *Phys. Rev. B*, vol. 89, p. 035140, Jan. 2014.

[21] L. N. Tran, S. Iskakov, and D. Zgid, "Spin-unrestricted self-energy embedding theory," *J. Phys. Chem. Lett.*, vol. 9, pp. 4444–4450, Aug. 2018.

[22] G. Carleo and M. Troyer, "Solving the quantum many-body problem with artificial neural networks," *Science*, vol. 355, pp. 602–606, Feb. 2017.

[23] G. Carleo, I. Cirac, K. Cranmer, L. Daudet, M. Schuld, N. Tishby, L. Vogt-Maranto, and L. Zdeborová, "Machine learning and the physical sciences," *Rev. Mod. Phys.*, vol. 91, p. 045002, Dec. 2019.

[24] A. Dreuw and M. Head-Gordon, "Single-reference ab initio methods for the calculation of excited states of large molecules," *Chem. Rev.*, vol. 105, pp. 4009–4037, Nov. 2005.

[25] A. I. Krylov, "Equation-of-Motion coupled-cluster methods for open-shell and electronically excited species: The Hitchhiker's guide to Fock space," *Annual Review of Physical Chemistry*, vol. 59, no. 1, pp. 433–462, 2008.

[26] M. Casida and M. Huix-Rotllant, "Progress in time-dependent density-functional theory," *Annual Review of Physical Chemistry*, vol. 63, no. 1, pp. 287–323, 2012.

[27] P. A. Lee, N. Nagaosa, and X.-G. Wen, "Doping a Mott insulator: Physics of high-temperature superconductivity," *Rev. Mod. Phys.*, vol. 78, pp. 17–85, Jan. 2006.

[28] N. Balakrishnan, "Perspective: Ultracold molecules and the dawn of cold controlled chemistry," *J. Chem. Phys.*, vol. 145, p. 150901, Oct. 2016.

[29] J. L. Bohn, A. M. Rey, and J. Ye, "Cold molecules: Progress in quantum engineering of chemistry and quantum matter," *Science*, vol. 357, pp. 1002–1010, Sept. 2017.

[30] T. Guillot, "Interiors of Giant Planets Inside and Outside the Solar System," *Science*, vol. 286, pp. 72–77, Oct. 1999.

[31] N. D. Mermin, "Stability of the thermal Hartree-Fock approximation," *Annals of Physics*, vol. 21, pp. 99–121, Jan. 1963.

[32] J. Sokoloff, "Some consequences of the thermal Hartree-Fock approximation at zero temperature," *Annals of Physics*, vol. 45, pp. 186–190, Nov. 1967.

[33] T. Matsubara, "A new approach to quantum-statistical mechanics," *Prog Theor Phys*, vol. 14, pp. 351–378, Oct. 1955.

[34] R. Santra and J. Schirmer, "Finite-temperature second-order many-body perturbation theory revisited," *Chemical Physics*, vol. 482, pp. 355–361, Jan. 2017.

[35] S. Hirata and P. K. Jha, "Chapter Two - Converging finite-temperature many-body perturbation theory in the grand canonical ensemble that conserves the average number of electrons," in *Annual Reports in Computational Chemistry* (D. A. Dixon, ed.), vol. 15, pp. 17–37, Elsevier, Jan. 2019.

[36] P. K. Jha and S. Hirata, "Finite-temperature many-body perturbation theory in the canonical ensemble," *Phys. Rev. E*, vol. 101, p. 022106, Feb. 2020.

[37] D. Zgid and E. Gull, "Finite temperature quantum embedding theories for correlated systems," *New J. Phys.*, vol. 19, no. 2, p. 023047, 2017.

[38] S. Zhang, "Finite-temperature Monte Carlo calculations for systems with fermions," *Phys. Rev. Lett.*, vol. 83, pp. 2777–2780, Oct. 1999.

[39] B. Militzer and D. M. Ceperley, "Path integral Monte Carlo calculation of the deuterium Hugoniot," *Phys. Rev. Lett.*, vol. 85, pp. 1890–1893, Aug. 2000.

[40] B. M. Rubenstein, S. Zhang, and D. R. Reichman, "Finite-temperature auxiliary-field quantum Monte Carlo technique for Bose-Fermi mixtures," *Phys. Rev. A*, vol. 86, p. 053606, Nov. 2012.

[41] T. Schoof, S. Groth, J. Vorberger, and M. Bonitz, "Ab initio thermodynamic results for the degenerate electron gas at finite temperature," *Phys. Rev. Lett.*, vol. 115, p. 130402, Sept. 2015.

[42] K. Takai, K. Ido, T. Misawa, Y. Yamaji, and M. Imada, "Finite-temperature variational Monte Carlo method for strongly correlated electron systems," *J.*

Phys. Soc. Jpn., vol. 85, p. 034601, Feb. 2016.

[43] J. Claes and B. K. Clark, "Finite-temperature properties of strongly correlated systems via variational Monte Carlo," *Phys. Rev. B*, vol. 95, p. 205109, May 2017.

[44] Y. Liu, M. Cho, and B. Rubenstein, "Ab initio finite temperature auxiliary field quantum Monte Carlo," *J. Chem. Theory Comput.*, vol. 14, pp. 4722–4732, Sept. 2018.

[45] Y.-Y. He, M. Qin, H. Shi, Z.-Y. Lu, and S. Zhang, "Finite-temperature auxiliary-field quantum Monte Carlo: Self-consistent constraint and systematic approach to low temperatures," *Phys. Rev. B*, vol. 99, p. 045108, Jan. 2019.

[46] H. R. Petras, S. K. Ramadugu, F. D. Malone, and J. J. Shepherd, "Using density matrix quantum Monte Carlo for calculating exact-on-average energies for ab initio Hamiltonians in a finite basis set," *J. Chem. Theory Comput.*, vol. 16, pp. 1029–1038, Feb. 2020.

[47] Y. Liu, T. Shen, H. Zhang, and B. Rubenstein, "Unveiling the finite temperature physics of hydrogen chains via auxiliary field quantum Monte Carlo," *J. Chem. Theory Comput.*, vol. 16, pp. 4298–4314, July 2020.

[48] F. Verstraete, J. J. García-Ripoll, and J. I. Cirac, "Matrix product density operators: Simulation of finite-temperature and dissipative systems," *Phys. Rev. Lett.*, vol. 93, p. 207204, Nov. 2004.

[49] A. E. Feiguin and S. R. White, "Finite-temperature density matrix renormalization using an enlarged Hilbert space," *Phys. Rev. B*, vol. 72, p. 220401, Dec. 2005.

[50] E. M. Stoudenmire and S. R. White, "Minimally entangled typical thermal state algorithms," *New J. Phys.*, vol. 12, no. 5, p. 055026, 2010.

[51] S. Pittalis, C. R. Proetto, A. Floris, A. Sanna, C. Bersier, K. Burke, and E. K. U. Gross, "Exact conditions in finite-temperature density-functional theory," *Phys. Rev. Lett.*, vol. 107, p. 163001, Oct. 2011.

[52] A. Nocera and G. Alvarez, "Symmetry-conserving purification of quantum states within the density matrix renormalization group," *Phys. Rev. B*, vol. 93, p. 045137, Jan. 2016.

[53] J. Ren, Z. Shuai, and G. Kin-Lic Chan, "Time-dependent density matrix renormalization group algorithms for nearly exact absorption and fluorescence spectra of molecular aggregates at both zero and finite temperature," *J. Chem. Theory Comput.*, vol. 14, pp. 5027–5039, Oct. 2018.

[54] G. Sanyal, S. H. Mandal, and D. Mukherjee, "Thermal averaging in quantum many-body systems: a non-perturbative thermal cluster cumulant approach," *Chemical Physics Letters*, vol. 192, pp. 55–61, Apr. 1992.

[55] G. Sanyal, S. H. Mandal, S. Guha, and D. Mukherjee, "Systematic nonperturbative approach for thermal averages in quantum many-body systems: The thermal-cluster-cumulant method," *Phys. Rev. E*, vol. 48, pp. 3373–3389, Nov. 1993.

[56] S. H. Mandal, G. Sanyal, and D. Mukherjee, "A thermal cluster-cumulant theory," in *Microscopic Quantum Many-Body Theories and Their Applications* (J. Navarro and A. Polls, eds.), Lecture Notes in Physics, pp. 93–117, Springer Berlin Heidelberg, 1998.

[57] S. H. Mandal, R. Ghosh, G. Sanyal, and D. Mukherjee, "A finite-temperature generalisation of the coupled cluster method: a non-perturbative access to grand partition functions," *Int. J. Mod. Phys. B*, vol. 17, pp. 5367–5377, Nov. 2003.

[58] M. R. Hermes and S. Hirata, "Finite-temperature coupled-cluster, many-body perturbation, and restricted and unrestricted Hartree–Fock study on one-dimensional solids: Luttinger liquids, Peierls transitions, and spin- and charge-density waves," *The Journal of Chemical Physics*, vol. 143, p. 102818, Sept. 2015.

[59] F. Hummel, "Finite temperature coupled cluster theories for extended systems," *J. Chem. Theory Comput.*, Oct. 2018.

[60] A. F. White and G. K.-L. Chan, "A time-dependent formulation of coupled-cluster theory for many-fermion systems at finite temperature," *J. Chem. Theory Comput.*, vol. 14, pp. 5690–5700, Nov. 2018.

[61] P. Shushkov and T. F. Miller, "Real-time density-matrix coupled-cluster approach for closed and open systems at finite temperature," *J. Chem. Phys.*, vol. 151, p. 134107, Oct. 2019.

[62] A. F. White and G. Kin-Lic Chan, "Finite-temperature coupled cluster: Efficient implementation and application to prototypical systems," *J. Chem. Phys.*, vol. 152, p. 224104, June 2020.

[63] X. He, S. Ryu, and S. Hirata, "Finite-temperature second-order many-body perturbation and Hartree–Fock theories for one-dimensional solids: An application to Peierls and charge-density-wave transitions in conjugated polymers," *J. Chem. Phys.*, vol. 140, p. 024702, Jan. 2014.

[64] H. Matsumoto, Y. Nakano, H. Umezawa, F. Mancini, and M. Marinaro, "Thermo field dynamics in interaction representation," *Prog Theor Phys*, vol. 70, pp. 599–602, Aug. 1983.

[65] G. W. Semenoff and H. Umezawa, "Functional methods in thermofield dynamics: A real-time perturbation theory for quantum statistical mechanics," *Nuclear Physics B*, vol. 220, pp. 196–212, June 1983.

[66] H. Umezawa, "Methods of quantum field theory in condensed matter physics - New perspectives, extensions and applications," *Prog Theor Phys*, vol. 80, pp. 26–39, Mar. 1984.

[67] T. S. Evans, I. Hardman, H. Umezawa, and Y. Yamanaka, "Heisenberg and interaction representations in thermo field dynamics," *Journal of Mathematical Physics*, vol. 33, pp. 370–378, Jan. 1992.

[68] G. Harsha, T. M. Henderson, and G. E. Scuseria, "Thermofield theory for finite-temperature quantum chemistry," *J. Chem. Phys.*, vol. 150, p. 154109, Apr. 2019.

[69] G. Harsha, T. M. Henderson, and G. E. Scuseria, "Thermofield theory for finite-temperature coupled cluster," *J. Chem. Theory Comput.*, vol. 15, pp. 6127–6136, Nov. 2019.

[70] G. Harsha, T. M. Henderson, and G. E. Scuseria, "Wave function methods for canonical ensemble thermal averages in correlated many-fermion systems," *J. Chem. Phys.*, vol. 153, p. 124115, Sept. 2020.

[71] G. Harsha, Y. Xu, T. M. Henderson, and G. E. Scuseria, "Thermal coupled cluster theory for SU(2) systems," *arXiv:2107.07922 [cond-mat, physics:physics]*,

July 2021.

[72] Hubbard J. and Flowers Brian Hilton, "Electron correlations in narrow energy bands," *Proceedings of the Royal Society of London. Series A. Mathematical and Physical Sciences*, vol. 276, pp. 238–257, Nov. 1963.

[73] E. Gull and A. J. Millis, "Ten years of *Nature Physics*: Numerical models come of age," *Nature Physics*, vol. 11, pp. 808–810, Oct. 2015.

[74] J. Bardeen, L. N. Cooper, and J. R. Schrieffer, "Theory of superconductivity," *Phys. Rev.*, vol. 108, pp. 1175–1204, Dec. 1957. Publisher: American Physical Society.

[75] S. T. Belyaev, "Effect of pairing correlations on nuclear properties," *Kgl. Danske Videnskab. Selskab. Mat.-Fys. Medd.*, vol. Vol: 31, No. 11, Jan. 1959. Institution: Originating Research Org. not identified.

[76] W. Ogle, S. Wahlborn, R. Piepenbring, and S. Fredriksson, "Single-particle levels of nonspherical nuclei in the region $150<A<190$," *Rev. Mod. Phys.*, vol. 43, pp. 424–478, July 1971.

[77] H. Bethe, "Zur theorie der metalle," *Z. Physik*, vol. 71, pp. 205–226, Mar. 1931.

[78] J. Arponen, "Variational principles and linked-cluster exp S expansions for static and dynamic many-body problems," *Annals of Physics*, vol. 151, pp. 311–382, Dec. 1983.

[79] T. Helgaker and P. Jørgensen, "Analytical calculation of geometrical derivatives in molecular electronic structure theory," in *Advances in Quantum Chemistry* (P.-O. Löwdin, ed.), vol. 19, pp. 183–245, Academic Press, Jan. 1988.

[80] Q. Sun, T. C. Berkelbach, N. S. Blunt, G. H. Booth, S. Guo, Z. Li, J. Liu, J. D. McClain, E. R. Sayfutyarova, S. Sharma, S. Wouters, and G. K.-L. Chan, "PySCF: the Python-based simulations of chemistry framework," *WIREs Computational Molecular Science*, vol. 8, no. 1, p. e1340, 2018.

[81] Q. Sun, X. Zhang, S. Banerjee, P. Bao, M. Barbry, N. S. Blunt, N. A. Bogdanov, G. H. Booth, J. Chen, Z.-H. Cui, J. J. Eriksen, Y. Gao, S. Guo, J. Hermann, M. R. Hermes, K. Koh, P. Koval, S. Lehtola, Z. Li, J. Liu, N. Mardirossian, J. D. McClain, M. Motta, B. Mussard, H. Q. Pham, A. Pulkin, W. Purwanto, P. J. Robinson, E. Ronca, E. R. Sayfutyarova, M. Scheurer, H. F. Schurkus, J. E. T. Smith, C. Sun, S.-N. Sun, S. Upadhyay, L. K. Wagner, X. Wang, A. White, J. D. Whitfield, M. J. Williamson, S. Wouters, J. Yang, J. M. Yu, T. Zhu, T. C. Berkelbach, S. Sharma, A. Y. Sokolov, and G. K.-L. Chan, "Recent developments in the PySCF program package," *J. Chem. Phys.*, vol. 153, p. 024109, July 2020.

[82] E. Celeghini, S. De Martino, S. De Siena, A. Iorio, M. Rasetti, and G. Vitiello, "Thermo field dynamics and quantum algebras," *Physics Letters A*, vol. 244, pp. 455–461, Aug. 1998.

[83] S. Floquet, M. A. S. Trindade, and J. D. M. Vianna, "Lie algebras and generalized thermal coherent states," *Int. J. Mod. Phys. A*, vol. 32, p. 1750015, Jan. 2017.

[84] A. Das and P. Kalauni, "Operator description for thermal quantum field theories on an arbitrary path in the real time formalism," *Phys. Rev. D*, vol. 93, p. 125028, June 2016.

[85] T. Klamroth, "Laser-driven electron transfer through metal-insulator-metal contacts: Time-dependent configuration interaction singles calculations for a jellium model," *Phys. Rev. B*, vol. 68, p. 245421, Dec. 2003.

[86] C. Huber and T. Klamroth, "Simulation of two-photon-photoelectron spectra at a jellium-vacuum interface," *Appl. Phys. A*, vol. 81, pp. 93–101, June 2005.

[87] M. Nooijen, K. R. Shamasundar, and D. Mukherjee, "Reflections on size-extensivity, size-consistency and generalized extensivity in many-body theory," *Molecular Physics*, vol. 103, pp. 2277–2298, Aug. 2005.

[88] G. Harsha, "thermal-ci." https://github.com/gauravharsha/thermal-ci.

[89] J. Zhao, *Symbolic solution for computational quantum many-body theory development*. Thesis, Rice University, Mar. 2018. Accepted: 2019-05-17T14:17:23Z.

[90] T. M. Henderson, G. E. Scuseria, J. Dukelsky, A. Signoracci, and T. Duguet, "Quasiparticle coupled cluster theory for pairing interactions," *Phys. Rev. C*, vol. 89, p. 054305, May 2014.

[91] R. M. Wilcox, "Exponential operators and parameter differentiation in quantum physics," *Journal of Mathematical Physics*, vol. 8, pp. 962–982, Apr. 1967.

[92] J. R. Dormand and P. J. Prince, "A family of embedded Runge-Kutta formulae," *Journal of Computational and Applied Mathematics*, vol. 6, pp. 19–26, Mar. 1980.

[93] E. Hairer, S. P. Nørsett, and G. Wanner, *Solving Ordinary Differential Equations I: Nonstiff Problems*. Springer Series in Computational Mathematics,

Springer Ser.Comp.Mathem. Hairer,E.:Solving Ordinary Diff., Berlin Heidelberg: Springer-Verlag, 2 ed., 1993.

[94] D. S. Kosov, M. F. Gelin, and A. I. Vdovin, "Calculations of canonical averages from the grand canonical ensemble," *Phys. Rev. E*, vol. 77, p. 021120, Feb. 2008.

[95] J. S. Andrews, D. Jayatilaka, R. G. A. Bone, N. C. Handy, and R. D. Amos, "Spin contamination in single-determinant wavefunctions," *Chemical Physics Letters*, vol. 183, pp. 423–431, Sept. 1991.

[96] M. Binder and T. Barthel, "Symmetric minimally entangled typical thermal states for canonical and grand-canonical ensembles," *Phys. Rev. B*, vol. 95, p. 195148, May 2017.

[97] K. Tanabe and H. Nakada, "Quantum number projection at finite temperature via thermofield dynamics," *Phys. Rev. C*, vol. 71, p. 024314, Feb. 2005.

[98] K. Esashika, H. Nakada, and K. Tanabe, "Effects of particle-number conservation on heat capacity of nuclei," *Phys. Rev. C*, vol. 72, p. 044303, Oct. 2005.

[99] H. Nakada and K. Tanabe, "New Bardeen-Cooper-Schrieffer-type theory at finite temperature with particle-number conservation," *Phys. Rev. C*, vol. 74, p. 061301, Dec. 2006.

[100] W. Magnus, L. Lemmens, and F. Brosens, "Quantum canonical ensemble: A projection operator approach," *Physica A: Statistical Mechanics and its Applications*, vol. 482, pp. 1–13, Sept. 2017.

[101] T. Shen, Y. Liu, Y. Yu, and B. M. Rubenstein, "Finite temperature auxiliary field quantum Monte Carlo in the canonical ensemble," *J. Chem. Phys.*, vol. 153,

p. 204108, Nov. 2020.

[102] S. Diehl, E. Rico, M. A. Baranov, and P. Zoller, "Topology by dissipation in atomic quantum wires," *Nature Physics*, vol. 7, pp. 971–977, Dec. 2011.

[103] G. Ortiz, J. Dukelsky, E. Cobanera, C. Esebbag, and C. Beenakker, "Many-body characterization of particle-conserving topological superfluids," *Phys. Rev. Lett.*, vol. 113, p. 267002, Dec. 2014.

[104] F. Iemini, L. Mazza, D. Rossini, R. Fazio, and S. Diehl, "Localized Majorana-like modes in a number-conserving setting: An exactly solvable model," *Phys. Rev. Lett.*, vol. 115, p. 156402, Oct. 2015.

[105] A. Mastellone, G. Falci, and R. Fazio, "Small superconducting grain in the canonical ensemble," *Phys. Rev. Lett.*, vol. 80, pp. 4542–4545, May 1998.

[106] A. J. Coleman, "Structure of Fermion Density Matrices. II. Antisymmetrized Geminal Powers," *Journal of Mathematical Physics*, vol. 6, pp. 1425–1431, Sept. 1965.

[107] A. Khamoshi, T. M. Henderson, and G. E. Scuseria, "Efficient evaluation of AGP reduced density matrices," *J. Chem. Phys.*, vol. 151, p. 184103, Nov. 2019.

[108] T. M. Henderson and G. E. Scuseria, "Geminal-based configuration interaction," *J. Chem. Phys.*, vol. 151, p. 051101, Aug. 2019.

[109] T. M. Henderson and G. E. Scuseria, "Correlating the antisymmetrized geminal power wave function," *J. Chem. Phys.*, vol. 153, p. 084111, Aug. 2020.

[110] R. Dutta, T. M. Henderson, and G. E. Scuseria, "Geminal replacement models based on AGP," *J. Chem. Theory Comput.*, Sept. 2020.

[111] A. Khamoshi, F. A. Evangelista, and G. E. Scuseria, "Correlating AGP on a quantum computer," *Quantum Sci. Technol.*, vol. 6, p. 014004, Nov. 2020.

[112] A. Signoracci, T. Duguet, G. Hagen, and G. R. Jansen, "Ab initio Bogoliubov coupled cluster theory for open-shell nuclei," *Phys. Rev. C*, vol. 91, p. 064320, June 2015.

[113] R. E. Peierls and J. Yoccoz, "The collective model of nuclear motion," *Proc. Phys. Soc. A*, vol. 70, pp. 381–387, May 1957.

[114] B. F. Bayman, "A derivation of the pairing-correlation method," *Nuclear Physics*, vol. 15, pp. 33–38, Feb. 1960.

[115] P. Ring and P. Schuck, *The Nuclear Many-Body Problem.* Theoretical and Mathematical Physics, The Nuclear Many-Body Problem, Berlin Heidelberg: Springer-Verlag, 1980.

[116] T. Duguet, "Symmetry broken and restored coupled-cluster theory: I. Rotational symmetry and angular momentum," *J. Phys. G: Nucl. Part. Phys.*, vol. 42, p. 025107, Dec. 2014.

[117] T. Tsuchimochi and S. Ten-no, "Communication: Configuration interaction combined with spin-projection for strongly correlated molecular electronic structures," *J. Chem. Phys.*, vol. 144, p. 011101, Jan. 2016.

[118] T. Duguet and A. Signoracci, "Symmetry broken and restored coupled-cluster theory: II. Global gauge symmetry and particle number," *J. Phys. G: Nucl.*

Part. Phys., vol. 44, p. 015103, Dec. 2016.

[119] Y. Qiu, T. M. Henderson, J. Zhao, and G. E. Scuseria, "Projected coupled cluster theory," *The Journal of Chemical Physics*, vol. 147, p. 064111, Aug. 2017.

[120] Y. Qiu, T. M. Henderson, T. Duguet, and G. E. Scuseria, "Particle-number projected Bogoliubov-coupled-cluster theory: Application to the pairing Hamiltonian," *Phys. Rev. C*, vol. 99, p. 044301, Apr. 2019.

[121] M. Degroote, T. M. Henderson, J. Zhao, J. Dukelsky, and G. E. Scuseria, "Polynomial similarity transformation theory: A smooth interpolation between coupled cluster doubles and projected BCS applied to the reduced BCS Hamiltonian," *Phys. Rev. B*, vol. 93, p. 125124, Mar. 2016.

[122] J. M. Wahlen-Strothman, T. M. Henderson, M. R. Hermes, M. Degroote, Y. Qiu, J. Zhao, J. Dukelsky, and G. E. Scuseria, "Merging symmetry projection methods with coupled cluster theory: Lessons from the Lipkin model Hamiltonian," *The Journal of Chemical Physics*, vol. 146, p. 054110, Feb. 2017.

[123] M. R. Hermes, J. Dukelsky, and G. E. Scuseria, "Combining symmetry collective states with coupled-cluster theory: Lessons from the Agassi model Hamiltonian," *Phys. Rev. C*, vol. 95, p. 064306, June 2017.

[124] S.-C. T. Choi, C. C. Paige, and M. A. Saunders, "MINRES-QLP: A Krylov Subspace Method for Indefinite or Singular Symmetric Systems," *SIAM J. Sci. Comput.*, vol. 33, pp. 1810–1836, Jan. 2011.

[125] S.-C. T. Choi and M. A. Saunders, "Algorithm 937: MINRES-QLP for symmetric and Hermitian linear equations and least-squares problems," *ACM Trans.*

Math. Softw., vol. 40, pp. 16:1–16:12, Mar. 2014.

[126] P. Pfeuty, "The one-dimensional Ising model with a transverse field," *Annals of Physics*, vol. 57, pp. 79–90, Mar. 1970.

[127] H. J. Lipkin, N. Meshkov, and A. J. Glick, "Validity of many-body approximation methods for a solvable model: (I). Exact solutions and perturbation theory," *Nuclear Physics*, vol. 62, pp. 188–198, Feb. 1965.

[128] N. Meshkov, A. J. Glick, and H. J. Lipkin, "Validity of many-body approximation methods for a solvable model: (II). Linearization procedures," *Nuclear Physics*, vol. 62, pp. 199–210, Feb. 1965.

[129] A. J. Glick, H. J. Lipkin, and N. Meshkov, "Validity of many-body approximation methods for a solvable model: (III). Diagram summations," *Nuclear Physics*, vol. 62, pp. 211–224, Feb. 1965.

[130] R. F. Bishop, "An overview of coupled cluster theory and its applications in physics," *Theoret. Chim. Acta*, vol. 80, pp. 95–148, Mar. 1991.

[131] J. Rosenfeld, N. E. Ligterink, and R. F. Bishop, "Extended coupled-cluster treatment of correlations in quantum magnets," *Phys. Rev. B*, vol. 60, pp. 4030–4042, Aug. 1999.

[132] J. Rosenfeld and N. E. Ligterink, "Phase transition in the transverse Ising model using the extended coupled-cluster method," *Phys. Rev. B*, vol. 62, pp. 308–315, July 2000.

[133] R. F. Bishop, N. Ligterink, and N. R. Walet, "Towards a coupled-cluster treatment of su(n) lattice gauge field theory," *Int. J. Mod. Phys. B*, vol. 20, pp. 4992–

5007, Dec. 2006.

[134] G. Harsha, T. Shiozaki, and G. E. Scuseria, "On the difference between variational and unitary coupled cluster theories," *The Journal of Chemical Physics*, vol. 148, p. 044107, Jan. 2018.

[135] R. F. Bishop, P. H. Y. Li, O. Götze, and J. Richter, "Frustrated spin-$\frac{1}{2}$ Heisenberg magnet on a square-lattice bilayer: High-order study of the quantum critical behavior of the J_1–J_2–$J_1^{\perp}$ model," *Phys. Rev. B*, vol. 100, p. 024401, July 2019.

[136] A. Khamoshi, G. P. Chen, T. M. Henderson, and G. E. Scuseria, "Exploring non-linear correlators on AGP," *J. Chem. Phys.*, vol. 154, p. 074113, Feb. 2021.

[137] M. Suzuki, "Thermo field dynamics of quantum spin systems," *J Stat Phys*, vol. 42, pp. 1047–1070, Mar. 1986.

[138] T. Hatsuda, "Mean field theory and boson expansion at finite temperature on the basis of the thermo field dynamics," *Nuclear Physics A*, vol. 492, no. 2, pp. 187–204, 1989.

[139] N. R. Walet and A. Klein, "Thermal boson expansions and dynamical symmetry," *Nuclear Physics A*, vol. 510, pp. 261–284, Apr. 1990.

[140] P. Virtanen, R. Gommers, T. E. Oliphant, M. Haberland, T. Reddy, D. Cournapeau, E. Burovski, P. Peterson, W. Weckesser, J. Bright, S. J. van der Walt, M. Brett, J. Wilson, K. J. Millman, N. Mayorov, A. R. J. Nelson, E. Jones, R. Kern, E. Larson, C. J. Carey, İ. Polat, Y. Feng, E. W. Moore, J. VanderPlas, D. Laxalde, J. Perktold, R. Cimrman, I. Henriksen, E. A. Quintero, C. R. Harris, A. M. Archibald, A. H. Ribeiro, F. Pedregosa, P. van Mulbregt, and SciPy

1.0 Contributors, “SciPy 1.0: Fundamental lgorithms for cientific omputing in ython,” *Nature Methods*, vol. 17, pp. 261–272, 2020.

[141] G. Ortiz, R. Somma, J. Dukelsky, and S. Rombouts, “Exactly-solvable models derived from a generalized Gaudin algebra,” *Nuclear Physics B*, vol. 707, pp. 421–457, Feb. 2005.

[142] S. Lerma H. and J. Dukelsky, “The Lipkin–Meshkov–Glick model as a particular limit of the SU(1,1) Richardson–Gaudin integrable models,” *Nuclear Physics B*, vol. 870, pp. 421–443, May 2013.